TR 86

AD 620 956

Technical Report 86
EXPLOSIONS IN SNOW

by

Clifton W. Livingston

MAY 1968

U.S. ARMY MATERIEL COMMAND
COLD REGIONS RESEARCH & ENGINEERING LABORATORY
HANOVER, NEW HAMPSHIRE
Aerodynamics Inc.

JUL 28 1968

AD 672 056

Technical Report 86
EXPLOSIONS IN SNOW

by

Clifton W. Livingston

MAY 1968

U.S. ARMY MATERIEL COMMAND
COLD REGIONS RESEARCH & ENGINEERING LABORATORY
HANOVER, NEW HAMPSHIRE

Barodynamics Inc.
Contract DA-11-190-ENG-33

This document has been approved for public release and sale, its distribution is unlimited.

Best
Available
Copy

PREFACE

The investigation reported herein was performed during the summer of 1958 under contract DA-11-190-Eng-33 with Barodynamics, Inc. The purpose of the investigation was to acquire information for the development of criteria for the destruction and protection of structures in or on snow.

Design and planning of the project were accomplished under the direction of W. K. Boyd, then Chief, Frozen Ground Applied Research Branch, Snow, Ice and Permafrost Research Establishment* (now Chief Engineer, U. S. Army Cold Regions Research and Engineering Laboratory). Cratering aspects of the work were performed by USA SIPRE under the direction of Robert Benert; instrumentation was performed by U. S. Army Waterways Experiment Station under the direction of Francis Hanes; and supervision and analysis were performed by Barodynamics, Inc.

The report was written by Clifton W. Livingston with the assistance of H. L. Waldron, C. E. Knapp, and R. W. Livingston.

USA CRREL is an Army Materiel Command laboratory.

*Combined in 1961 with the Arctic Construction and Frost Effects Laboratory, Corps of Engineers, U. S. Army to form the U. S. Army Cold Regions Research and Engineering Laboratory.

CONTENTS

	Page
Preface	ii
Summary	vi
Symbols	viii
Equations	xi
General plan of the tests	1
The problem	1
Description of the tests	1
Test site	2
Field procedure on uninstrumented shots	2
Instrumentation	10
Evaluation of the data	18
Crater and cavity nomenclature	18
Variation in crater shape with charge depth	23
Typical undersnow pressure records	23
Typical acceleration records	23
Typical seismic records	23
The failure process	28
Mechanics of viscous-damping failure	33
Constant quantities and energy utilization	35
Introduction	35
Evaluating the strain-energy factor	36
Determining the depth ratio at optimum depth	37
Evaluating the materials-behavior index	39
The energy-utilization number A	39
Crater evaluation	44
Apparent crater	44
Evaluating dimensions within limits of complete rupture	45
The N-scaled crater depth K_h	49
The complete-rupture shape factor K_s	49
The N-scaled complete-rupture radius K_r	50
A correlation of complete-rupture and extreme-rupture limits	50
Dimensions of the cavity	56
Ranges of similar behavior in snow	57
The effect of materials type upon the relation A vs Δ	58
Conclusions and recommendations	58
Literature cited	59

ILLUSTRATIONS

Figure		
1.	Surface blasts, Atlas 60%	3
2.	Surface blasts, military explosive C-4	3
3.	Surface blasts, Coalite 7S	4
4.	Trench blasts, Atlas 60%	4
5.	Trench blasts, Coalite 7S	5
6.	Air blasts and contact blasts, Atlas 60%	5
7.	Air blasts and contact blasts, military explosive C-4	6
8.	Air blasts and contact blasts, Coalite 7S	6
9.	Test site	7
10.	Weather data	7
11.	Density profile, undisturbed snow	8

CONTENTS (Cont'd)

Figure		Page
12.	Recording fracture pattern and displacement of colored columns	11
13.	Snow texture along crater cross section as revealed using smudge technique	11
14.	Drilling and recovering cores along density-sample profile lines	12
15.	Miller recording unit	12
16.	Pencil gage	13
17.	Baffle and water-shock gages	13
18.	Statham accelerometer	14
19.	VibraShock accelerometer	14
20.	Standard gage layout, depth of charge = 3.0λ	16
21.	Standard gage layout, depth of charge = 1.0λ	16
22.	Standard gage layout, contact burst	17
23.	Standard gage layout, height of charge = 0.5λ	17
24.	Standard gage layout, height of charge = 1.0λ	18
25.	Crater limits and column displacement	21
26.	Crater nomenclature	21
27.	Cavity fracture limits and column displacement	22
28.	Cavity nomenclature	22
29.	Apparent- and true-crater shapes at increasing depth ratios	24
30.	Complete and extreme rupture limits at increasing depth ratios	24
31.	Typical variation of undersnow pressure with distance	25
32.	Comparison of void pressure and undersnow pressure	25
33.	Typical undersnow-acceleration records	26
34.	Typical seismic records, longitudinal component	26
35.	Typical seismic records, vertical component	27
36.	Typical seismic records, transverse component	27
37.	Viscous-damping failure	29
38.	Shearing failure in 0.45 g/cm³ density trench snow	29
39.	Sequence of events at the explosion cavity	31
40.	Implosion and related events	32
41.	Vortex and scouring action	34
42.	Energy-utilization no., surface snow, Atlas 60	41
43.	Energy-utilization no., surface snow, C-4	41
44.	Energy-utilization no., surface snow, Coalite 7S	41
45.	Energy-utilization no., trench snow, Atlas 60	41
46.	Energy-utilization no., trench snow, Coalite 7S	42
47.	Apparent crater V/W vs Δ, surface snow, Atlas 60	45
48.	Apparent crater V/W vs Δ, surface snow, C-4	45
49.	Apparent crater V/W vs Δ, surface snow, Coalite 7S	46
50.	N-scaled apparent-crater depth, surface snow, Atlas 60	46
51.	N-scaled apparent-crater depth, surface snow, C-4	46
52.	N-scaled apparent-crater depth, surface snow, Coalite 7S	46
53.	N-scaled apparent-crater radius, surface snow, Atlas 60	47
54.	N-scaled apparent-crater radius, surface snow, C-4	47
55.	N-scaled apparent-crater radius, surface snow, Coalite 7S	47
56.	N-scaled complete-rupture depth, surface snow, Atlas 60	47
57.	N-scaled complete-rupture depth, surface snow, C-4	48
58.	N-scaled complete-rupture depth, surface snow, Coalite 7S	48

CONTENTS (Cont'd)

Figure		Page
59.	N-scaled complete-rupture depth, trench snow, Atlas 60	48
60.	N-scaled complete-rupture depth, trench snow, C7S	48
61.	Crater-shape factor, surface snow, Atlas 60	51
62.	Crater-shape factor, surface snow, C-4	51
63.	Crater-shape factor, surface snow, Coalite 7S	51
64.	Crater-shape factor, trench snow, Atlas 60	51
65.	Crater-shape factor, trench snow, Coalite 7S	52
66.	K_r vs Δ, surface snow, Atlas 60	52
67.	K_r vs Δ, surface snow, C-4	52
68.	K_r vs Δ, surface snow, Coalite 7S	52
69.	K_r vs Δ, trench snow, Atlas 60	53
70.	K_r vs Δ, trench snow, Coalite 7S	53
71.	$C_r/\sqrt[3]{W}$ vs λ_c, surface snow, Atlas 60, complete rupture	54
72.	$C_e/\sqrt[3]{W}$ vs λ_c, surface snow, Atlas 60, extreme rupture	54
73.	$C_r/\sqrt[3]{W}$ vs λ_c, surface snow, C-4, complete rupture	54
74.	$C_e/\sqrt[3]{W}$ vs λ_c, surface snow, C-4, extreme rupture	54
75.	$C_r/\sqrt[3]{W}$ vs λ_c, surface snow, Coalite 7S, complete rupture	55
76.	$C_e/\sqrt[3]{W}$ vs λ_c, surface snow, Coalite 7S, extreme rupture	55
77.	$C_r/\sqrt[3]{W}$ vs λ_c, trench snow, Atlas 60, complete rupture	55
78.	$C_e/\sqrt[3]{W}$ vs λ_c, trench snow, Atlas 60, extreme rupture	55
79.	$C_r/\sqrt[3]{W}$ vs λ_c, trench snow, Coalite 7S, complete rupture	56
80.	$C_e/\sqrt[3]{W}$ vs λ_c, trench snow, Coalite 7S, extreme rupture	56
81.	Ranges of similar behavior in 1958 surface snow	57
82.	Energy-utilization number A vs Δ in snow, ice, frozen ground	58

TABLES

Table		
I.	Variation in density, incompressibility, and rigidity with depth below the 1954 snow surface	9
II.	Properties of the test explosives	9
III.	Dimensions of explosive spheres	9
IV.	Horizontal- and vertical-compressional-wave velocity	15
V.	Suggested test conditions for analysis of undersnow shock	15
VI.	Constants for charges of spherical shape	38

SUMMARY

Studies were made to establish means of predicting and optimizing the results of blasts in snow of the Greenland Ice Cap. A total of 141 test blasts were fired above and at various depths below the snow surface using three types of explosives. Seismic measurements were taken of all shots, and 32 were instrumented for measurement of airblast and/or undersnow shock pressure.

Vertical holes were drilled in a plane through the charge center, and adjacent holes were filled with snow dyed different colors. The explosive charge was detonated electrically. During the blast, motion pictures recorded flyrock travel, surface movements and displacement.

Following the blast, crews excavated snow to expose a vertical wall through the blast center. Crater cross sections were then mapped to beyond the limits of complete rupture. The change in texture of the snow was studied by a technique of smudging the exposed wall. Density samples of the disturbed and undisturbed snow were taken in a regular pattern using core-sample augers.

The failure process in snow differs from that in glacier ice, frozen ground, rock, and certain types of soil. Characteristic features of this failure (referred to here as "viscous-damping failure") are: 1) damping of the disturbance during the rise to peak pressure, and 2) substantial recovery of stored potential energy during unloading. Both features result because air in substantial quantity is trapped within the voids in snow. The sequence of a blast in snow has been determined by applying the theory of relative behavior of materials, wherein a change that is accomplished in time is analogous to a change in energy density as measured by the depth ratio. Earlier events begin at a high value of the depth ratio and these may be traced to their conclusion by observing the end product of a blast at lower values of the depth ratio. Thus "early" may refer here to deep, and "late" to shallow.

The snow is first compacted and driven outward as the gas bubble expands, and a primary cavity is formed. Melting at the cavity wall converts the skin of the compacted, fractured, and expanding zone to ice. The next event is implosion and disturbance of the original cavity. The walls of the primary cavity are displaced inward, and both the zone of skin-surface melting and the zone of compaction are destroyed. A sensitively balanced transition condition appears to exist at critical depth. The balance determines under what conditions fractures during the rise of pressure and the outward expansion of the gas bubble predominate over fractures formed as a result of implosion. Implosion is closely followed by a vortex motion within the snow and scouring action as the gas bubble emerges from the rising column defined by the vortex. This scouring motion largely determines the final shape of the apparent crater.

Viscous-damping failure differs markedly from shock-type failure, which is characteristic of brittle materials, and from shear-type failure, which is characteristic of more plastic materials. During loading of the snow, a substantial proportion of the energy of the explosion is expended to compact and deform the material; during unloading, much of the energy expended to compress air in the voids is recovered and re-expended in both fracture and flow.

SUMMARY (Cont'd)

Tables, curves, equations, and example problems presented in the report make it possible, within the range of the experiments, to accurately predict any desired dimensions of the limit of complete rupture. Limits of complete rupture and limits of extreme rupture in snow are correlated empirically using cube-root scaling as a first approximation. Ranges of similar behavior and transition limits between ranges for blasts with small HE charges in 1958 surface snow are discussed. At charge depths greater than critical depth, more of the energy of the explosion is required for seismic effects and for deformation of the snow without loss of cohesion. At charge depth less than that at which maximum scouring occurs, more of the energy of the explosion is expended in the atmosphere and less is available to the snow. An apparent crater, as defined in the report, occurs in the air-blast range and the secondary zone of the fragmentation range. The volume of apparent crater per pound of explosive is maximum at the transition limit between the two ranges, where scouring is maximum. The energy-utilization number depends upon the explosive and the material and, where V/W of the apparent crater in snow is maximum, varies from 0.4 to 0.7. Dimensions of the apparent crater are neither predictable with accuracy using conventional cube-root scaling nor usable as a basis for predicting undersnow damage because 1) the energy-utilization number is a relative measure of the proportion of the energy of the explosive partitioned to loading the snow, and 2) the apparent crater in snow occurs subsequent to loading and is the result of the scouring action of the vented gas bubble. The effect of the type of material upon the relation of energy utilization number $\underline{A}$ and depth ratio Δ is summarized for snow, ice, and frozen ground. In extrapolations beyond the range of the experiments: 1) the observed variation in the strain-energy factor E with physical properties of the snow and with the type of explosive, 2) the observed variation of the materials-behavior index B with the weight of the charge, and 3) the interdependence of physical properties of the material and the energy-utilization number should prove useful.

SYMBOLS

A — Energy-utilization number: a dimensionless ratio of volumes determined by the limits of complete rupture. A, which stands for available, is a variable function of the depth ratio Δ and reaches a maximum of 1.0 at optimum depth.

$$A = \frac{V}{V_0}.$$

B — Materials-behavior index: a constant for a given explosive, a given material, and a given weight of charge, it is a dimensionless number that may be thought of as a ratio of volumes at two different energy levels. B stands for behavior.

$$B = \frac{V_0}{N^3}.$$

C — Stress-distribution number: a dimensionless ratio of energy levels in single-shot or multiple-shot blasting. C stands for charge shape, one of the principal factors affecting stress distribution. The stress geometry was so controlled that C equalled 1.0 in the tests described herein.

C_a — Slant distance of apparent crater, feet, from the center of gravity of the explosive charge to the limit of the apparent crater at the surface.

C_r — Slant distance, ft, from the center of gravity of the explosive charge to the limit of complete rupture at the surface.

d_c — Depth of charge: depth, ft, from the surface to the center of gravity of the explosive charge.

d_0 — Optimum depth of charge: depth of charge at which a given weight of explosive breaks a maximum volume of material per pound of explosive (at which V/W is a maximum).

E — Strain-energy factor: a variable factor dependent upon the explosive and the material (dimensionless when cube-root scaling is assumed). It is defined by the equation

$$N = E\sqrt[3]{W}.$$

h or h_r — Depth of crater, ft, from the surface to the limits of complete rupture (see Fig. 26, 28).

h_a — Depth of apparent crater, ft, from the surface to the bottom of the apparent crater.

K — N-scaled crater volume, dimensionless:

$$K = \frac{V}{N^3}.$$

It can also be shown that

$$K = ABC = \pi K_s (K_r)^2 K_h.$$

SYMBOLS (Cont'd)

K_h N-scaled crater depth to the limits of complete rupture, dimensionless:

$$K_h = \frac{h}{N}.$$

$K_h{}^1$ N-scaled depth of the apparent crater, dimensionless:

$$K_h{}^1 = \frac{h_a}{N}.$$

K_r N-scaled crater radius to the limits of complete rupture, dimensionless:

$$K_r = \frac{r}{N}.$$

$K_r{}^1$ N-scaled radius of the apparent crater, dimensionless:

$$K_r{}^1 = \frac{r_a}{N}.$$

K_s Complete rupture shape factor, $K_s = V/\pi r^2 h$.

N Critical depth: the minimum depth, ft, at which displacement of the surface above an explosive charge of spherical shape does not exceed a specified limit on a blast with a given type and weight of explosive in a given homogeneous material beneath a horizontal surface of semi-infinite lateral extent. The limiting displacement is that at which fracture begins.

r or r_r Average radius, ft, to the limits of complete rupture as measured at the surface (see Fig. 26, 28).

r_a Average radius of apparent crater, ft, as measured at the surface.

R Gage slant distance from the center of gravity of the charge.

V or V_r Volume, ft^3, within the limits of complete rupture (see Fig. 26, 2[illegible]).

V_a Volume, ft^3, of the apparent crater.

V_0 Optimum volume: the volume, ft^3, within limits of complete rupture at d_0.

V_{px} Volume of the crater under prototype conditions: the volume in cubic feet within the limits of complete rupture at any given depth ratio Δ_x relative to the horizontal free surface. Geometry, detonation conditions, and charge shape as for prototype conditions.

V_x Volume, ft^3, of the crater to the limits of complete rupture at a depth ratio Δ_x relative to the nearest free face. Geometry, detonation conditions, and charge shape as in practice.

SYMBOLS (Cont'd)

W, w — Weight, lb, of the explosive charge.

x — Gage distance: horizontal distance, ft, from the center of gravity of the charge to the gage position.

Z — Gage depth: depth, ft, from the horizontal surface to the gage position.

Δ — Depth ratio: ratio of depth of charge to critical depth of charge,

$$\Delta = \frac{d_c}{N}.$$

Δ_0 — Optimum depth ratio: d_0/N.

λ — Cube root of charge weight: a distance in feet equal to the cube root of the charge weight in pounds.

Note concerning subscripts: the following subscripts may be used with any given crater dimension. For example, if $\underline{r}$ is the crater radius, r_a is the radius of the apparent crater. If no subscript is used, the dimension concerns the limit of complete-rupture; in other words $\underline{r}$ and r_r have identical meanings (see Fig. 26, 28).

- a apparent crater
- e extreme-rupture limit
- r complete-rupture limit (absence of any subscript also indicates the dimension is to the limit of complete-rupture)
- t true crater.

EQUATIONS

	Page
Breakage-process equation	19
$\frac{V}{W} = E^3 ABC$	
Strain-energy equation	36
$N = E \sqrt[3]{W}$	
General equation	37
$d_0 = \Delta_0 \; E \sqrt[3]{W}$	
Optimum-depth-ratio equation	37
$\Delta_0 = \frac{d_0}{N}$	
Materials-behavior-index equation	39
$B = \frac{V_0}{N^3}$	
Energy-utilization-number equation	40
$A = \frac{V}{V_0}$	
Equation of interdependence of linear and volume dimensions	45
$K = ABC = \pi K_s (K_r)^2 \; K_h$	
Crater-volume equations	49
$V = K_s \pi r^2 h$	
$V = KN^3$	
Stress-distribution-number equation	(Livingston, 1960a)
$C = \frac{V_x}{V_{px}}$	

EXPLOSIONS IN SNOW

by

Clifton W. Livingston

GENERAL PLAN OF THE TESTS

The problem

The investigation of the effects of explosions upon snow, ice, and frozen ground began with small-scale cratering studies in shallow frozen ground and later was extended to include deep frozen ground. The work was continued using small-scale cratering blasts in ice aided by a moderate instrumentation program. As a result of these studies, evidence bearing upon failure criteria was accumulated and a theory known as the theory of relative behavior of materials evolved.

By the time of completion of "Explosions in Ice" (Livingston, 1960b), it appeared that the shock wave-reflection theory, which is generally regarded as explaining the mechanism of failure in blasting, was not applicable to all materials. Shock failure is characteristic of brittle substances, but, as the ductility of the material increases, the failure gradually changes to a shearing type. In blasts of glacier ice, shearing failure predominates over shock failure.

Snow that falls in the interior of Greenland eventually metamorphoses to ice, changing from a cohesionless substance to one possessing snear strength. Butkovich (1956) has shown that strength properties are related to the density of the snow, and that when the density approaches 0.37 g/cm^3, snow possesses measurable strength in shear. Hence, during blasts in snow the failure process can be expected to approach as a limit the shearing-type failure observed when blasting in glacier ice. Accordingly, the field work was planned to allow observation of the effect upon the failure process as the shear strength of snow increases with depth.

This report describes the field work, presents the compiled data, and deals with cratering aspects of the problem. The instrumentation data are referred to here only in connection with the mechanics of the breakage process.

Description of the tests

The 1958 explosion tests in snow were conducted during the period 25 June to 16 August at Camp Fistclench on the interior of the Greenland Ice Cap. Three test explosives were used: Atlas 60-percent straight gelatin, military explosive C-4, and Atlas Coalite 7S. The blast charges weighed from 1 to 40 lb, and most were spherical in shape. In addition to the charges of spherical shape, three instrumented, 160-lb, cylindrical charges (one of each type of explosive) were detonated in 14-in.-diam boreholes.

Fifteen blasts were fired a short distance above, or in contact with, the snow surface. Ninety-one were fired at various depths below the 1958 snow surface, and 28 were fired in snow having a density of 0.4 g/cm^3 or greater. The high-density snow blasts, referred to here as trench blasts, were fired in wide, 12-ft-deep trenches excavated with a Peter plow.

Seven preliminary shots were fired either to zero-in the shock gages or to investigate some feature of the shock-gage instrumentation. Thirty-two of the total of 141 shots were instrumented so as to measure the air-blast and/or undersnow shock pressure. Positive-displacement seismic measurements

were taken at three different standard scaled distances on all except the preliminary instrumentation shots. Acceleration was measured at one gage position and at a constant scaled slant distance from each undersnow instrumented shot.

Figures 1 through 8 give the test geometry, type of explosive and charge weight. For some shots, only seismic measurements were taken: for others both shock and seismic measurements were taken.

Test site

The test site (Fig. 9) was located at Camp Fistclench about 220 miles east of Thule, Greenland, near 78° N latitude and at an elevation of approximately 7000 ft above sea level. The temperature during the test season ranged from -5 F to 32 F. The daily average velocity of the wind ranged from 4 to 20 knots. Weather data recorded at the test site are summarized in Figure 10.

Many of the physical and elastic properties of the snow have been found to be a function of the density. Although the correlation between physical properties and blast effects is beyond the scope of the present work, density profiles were measured throughout the test season so that such correlation could be made later. The density of undisturbed snow before blasting and of the disturbed snow after blasting was determined. Density samples were taken at various positions relative to the walls of the crater and to the walls of the explosion cavity.

Figure 11 summarizes the variation in density with depth below the 1958 surface. The variation does not differ greatly from that found earlier with respect to the 1954 surface (Table I). However, a substantial dispersion in density occurs at any given depth. When Figure 11 is used in connection with Figures 1-5, the approximate mean density of the undisturbed snow at the charge elevation may be estimated for any blast.

Table I summarizes (using data from Bentley, Pomeroy, and Dorman, 1957) the variation in density with depth below the 1954 snow surface as measured at the walls of the SIPRE test shaft. The table also records the relation between density, incompressibility, and rigidity.

Field procedure on uninstrumented shots

Those shots not instrumented for air-blast or undersnow shock are referred to as uninstrumented. However, both seismic measurements and motion pictures were taken of flyrock and ground motion. The uninstrumented shots were fired both before preparing the snow surface and after excavating and preparing a smooth trench bottom in high-density snow with the Peter plow. Because of the texture of the snow, the snow surface was not greatly damaged by equipment or men (see Fig. 9).

Placement of colored columns and auger drilling. The colored-column technique was used to determine the limits of the true crater, complete rupture, and extreme rupture. An A-rod was forced into the snow using the pull-down feed mechanism of a track-mounted drill rig. Holes spaced at a distance in feet equal to the cube root of the charge weight in pounds were punched to a depth exceeding the depth of complete rupture for the specified weight of charge. Holes were then backfilled with snow mixed with dyes of different colors. Charge holes of either 5, 7, 9, 11 or 13 in. diam were then augered to the proper depth.

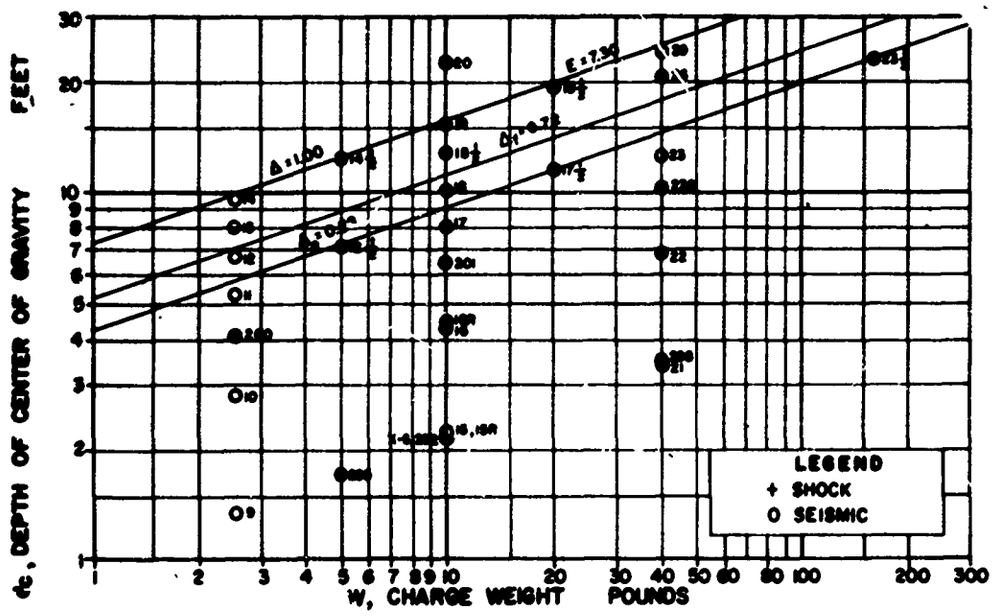

Figure 1. Surface blasts, Atlas 60%.

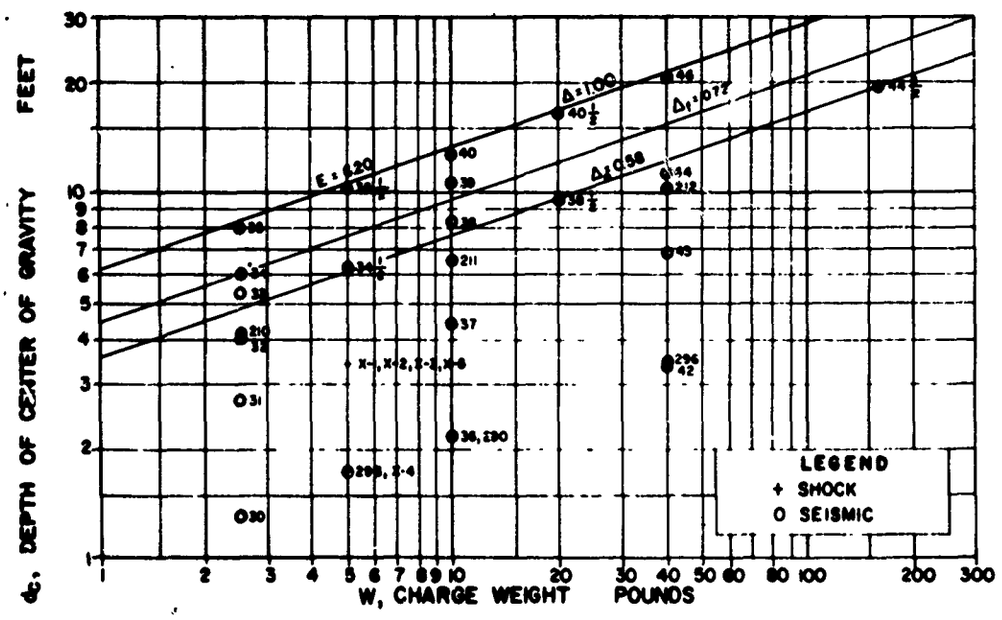

Figure 2. Surface blasts, military explosive C-4.

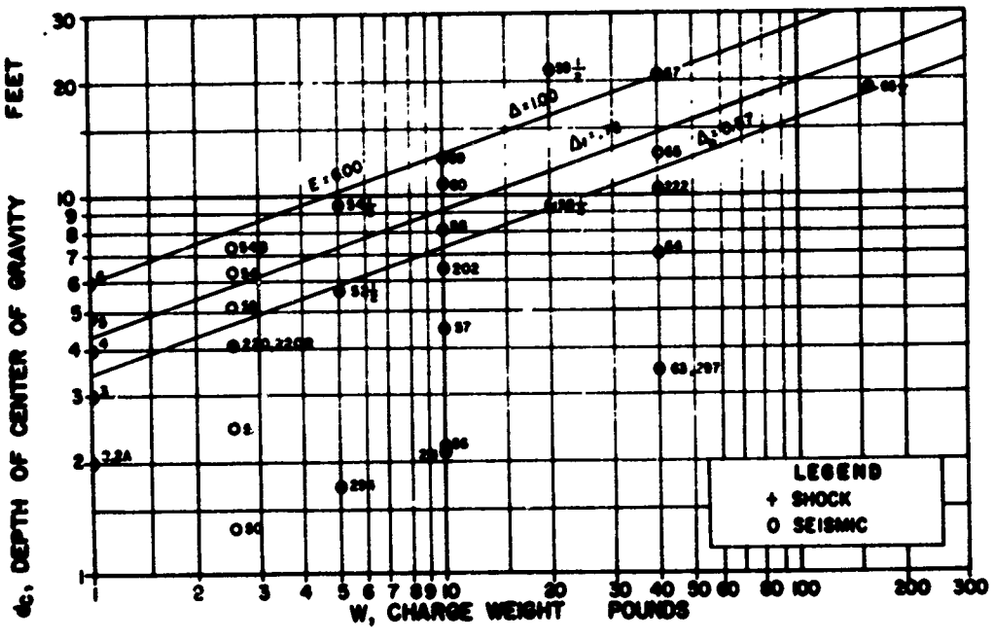

Figure 3. Surface blasts, Coalite 7S.

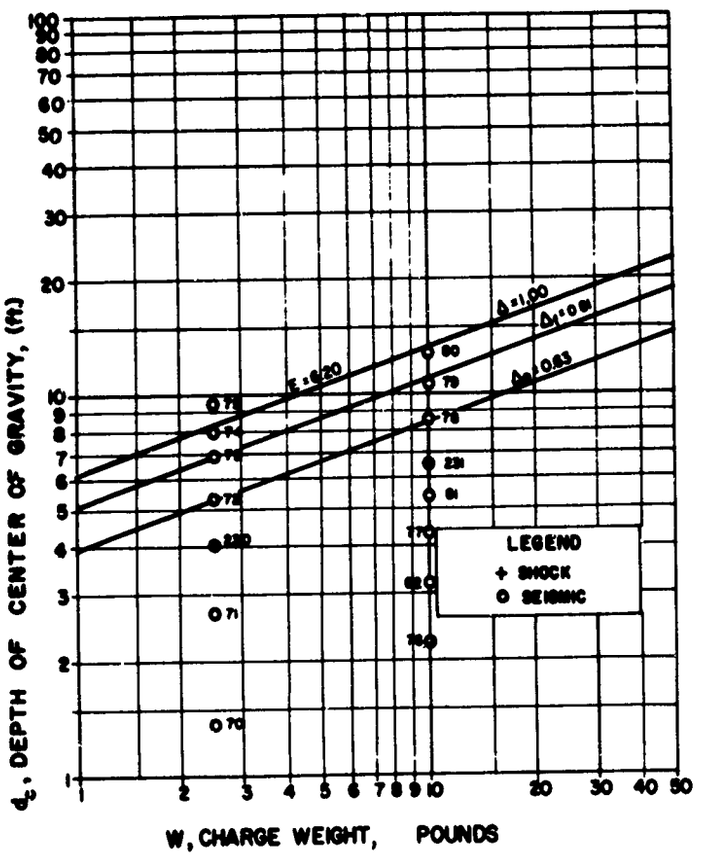

Figure 4. Trench blasts, Atlas 60%.

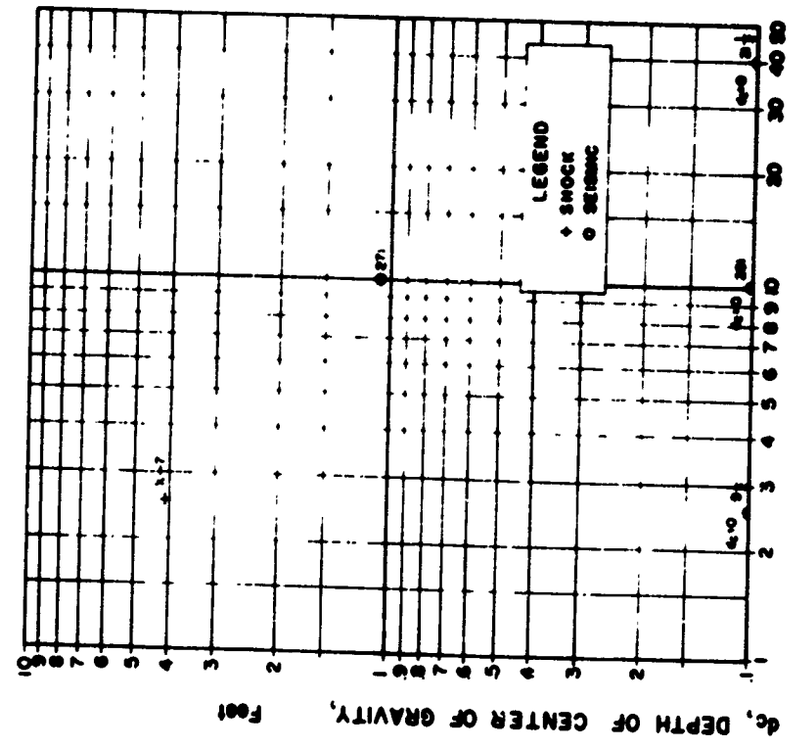

Figure 6. Air blasts and contact blasts, Atlas 60%.

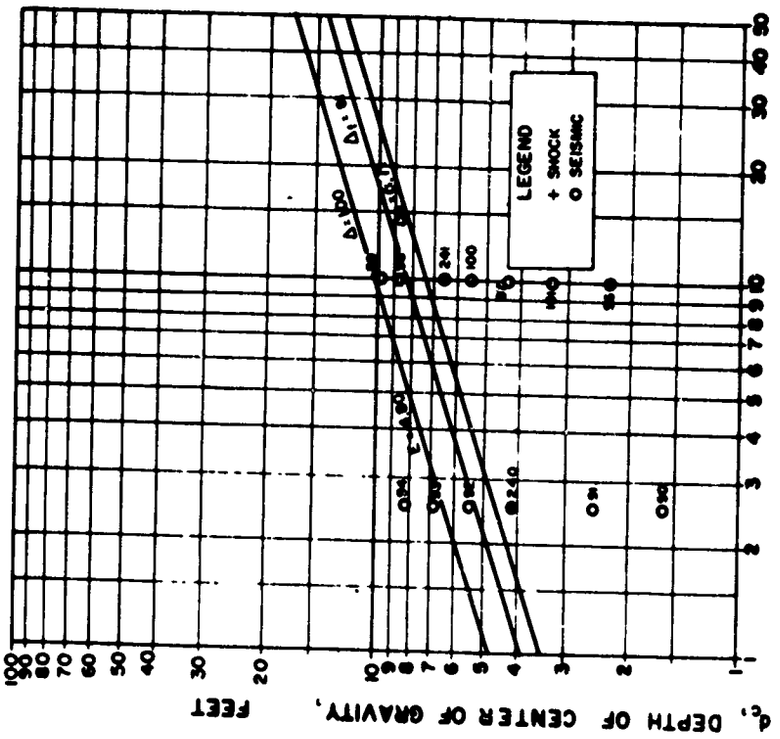

Figure 5. Trench blasts, Coalite 7S.

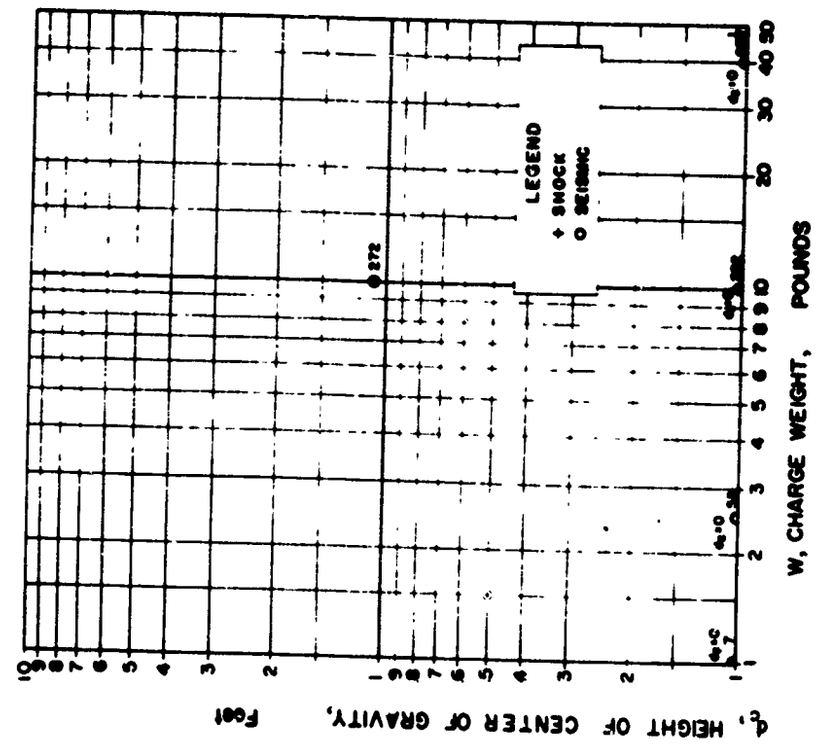

Figure 8. Air blasts and contact blasts, Coalite 7S.

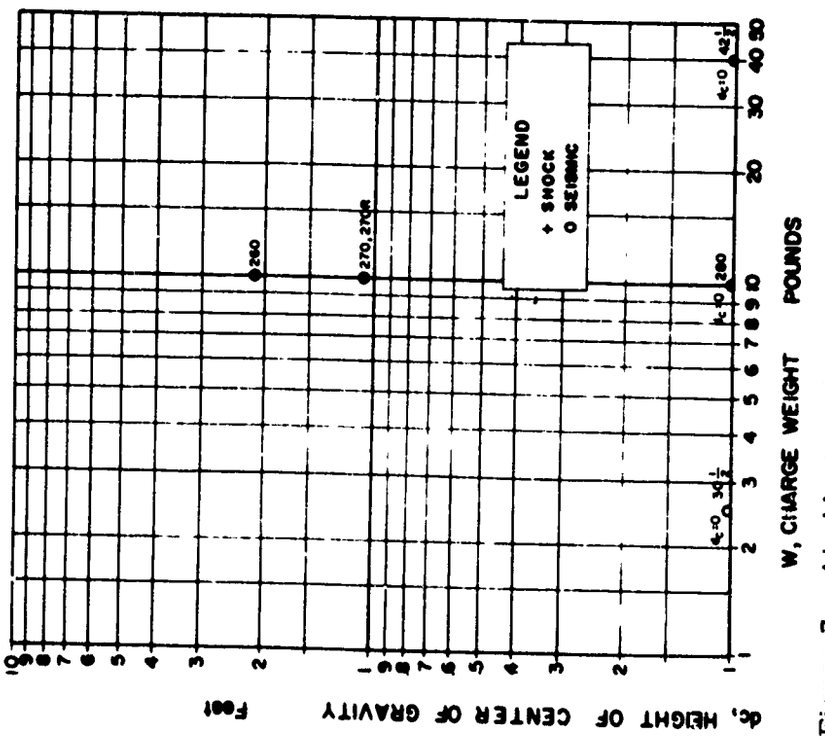

Figure 7. Air blasts and contact blasts, military explosive C-4.

Figure 9. Test site.

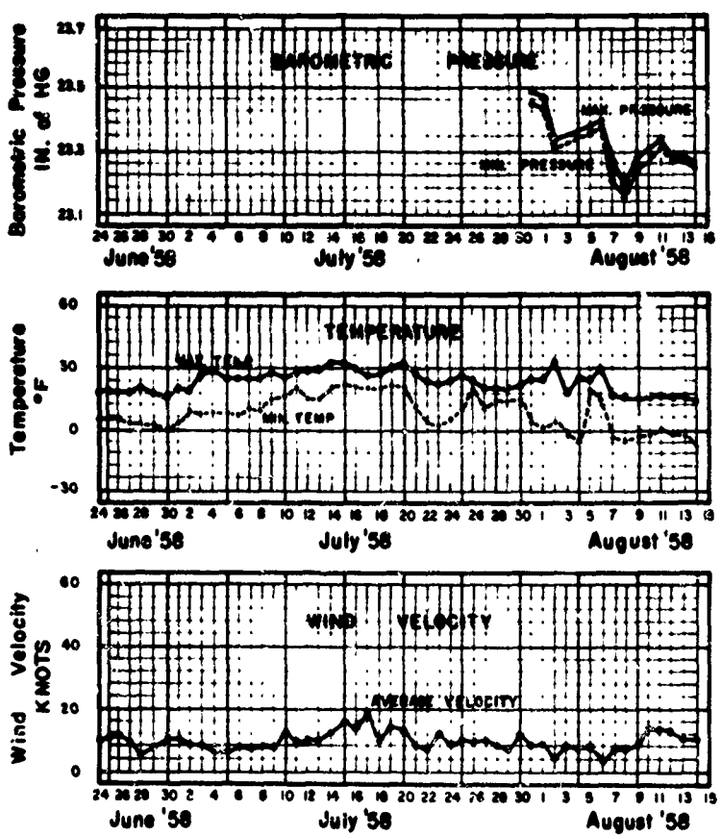

Figure 10. Weather data.

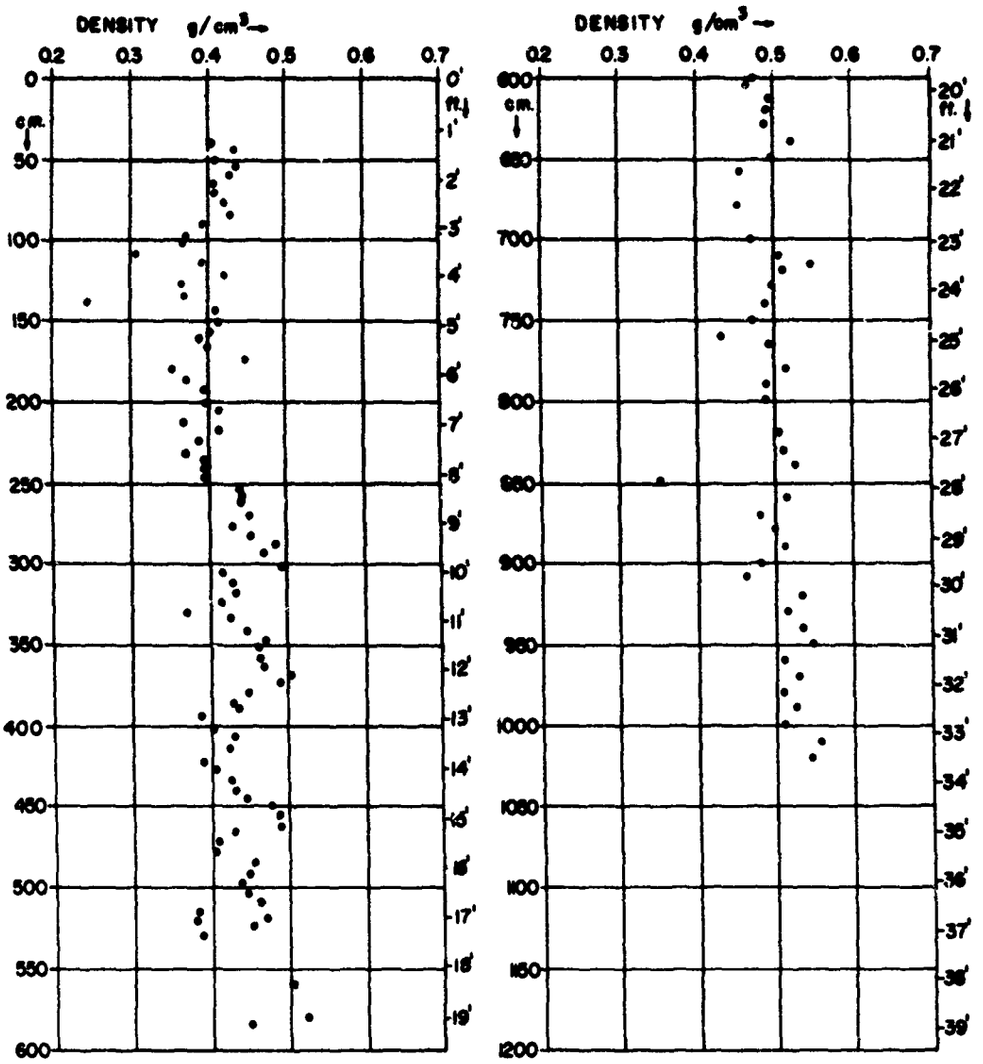

Figure 11. Density profile, undisturbed snow.

Explosives. Explosives were molded into plastic spheres and detonated using electric blasting caps. A booster sleeve was placed over the cap to insure proper detonation of the C-4. Halves of the plastic spheres were taped together with electrician's tape, and a copper wire was wrapped around the outside of the sphere to lower the charge into the hole and to serve as a means of determining the instant of detonation. After the charge had been placed and its depth measured, the hole was filled with snow, which was compacted with a bamboo loading stick as the hole was being filled. Contact bursts were placed so that the plastic sphere was half buried in the snow, and the center of gravity of the charge was at the surface. Air bursts were suspended at the proper distance above the surface using a tripod. Properties of the test explosives are summarized in Table II, and the dimensions of the explosive spheres are summarized in Table III.

Table I. Variation in density, incompressibility, and rigidity with depth below the 1954 snow surface.

Depth (m)	Density (g/cm^3)	Incompressibility (10^6 dynes/m^2)	Rigidity (10^6 dynes/m^2)
0	0.35	0	0
5	0.47	0.72	0.31
10	0.53	1.52	0.69
15	0.57	2.12	1.02
20	0.60	2.52	1.28
25	0.63	3.00	1.43
30	0.65	3.43	1.62
35	0.67	3.83	1.78
40	0.70	4.28	1.93

Table II. Properties of the test explosives.

Explosive	Classification	Energy (cal/g)	Explosion pressure (psi)	Detonation velocity* (ft/sec)	Specific volume† (in.^{3}/lb)
C-4	Military	1235	--	24,000	16.9
Atlas 60	Straight gelatin	1249	13,018	20,000	16.5
Coalite 7S	Ammonia permissible	916	14,913	10,000	25.0

*confined
†packed in spheres

Table III. Dimensions of explosive spheres.

Explosive	Inside radius (ft) 1.0-lb	2.5-lb	5.0-lb	10.0-lb	20.0-lb	40.0-lb
C-4	--	0.179	0.240	0.291	0.375	0.458
Atlas 60	--	0.179	0.240	0.291	0.375	0.458
Coalite 7S	0.135	0.213	0.276	0.326	0.436	0.542

Flyrock travel and preliminary measurements. Before a shot was fired, stakes were placed along the extension of the lines of colored columns to guide the plows during excavation. Flags were placed to serve as a ground scale for motion pictures, and camera and seismograph positions were specified, spotted, and prepared. At the time of the blast, a preliminary estimate of flyrock travel was made visually using the view finder and the ground scale. The approximate depth and diameter of the apparent crater were recorded, as also were the cracking radius at the surface, the magnitude of uplift or doming of the snow surface, and the range of sizes and predominant size of particles.

Excavation, field analysis, and crater surveys. Depending upon space limitations and the availability of equipment, either the Peter plow, the clamshell, or the dragline excavator was used to expose a wall parallel to and within one foot of the vertical plane containing the charge and the row of

colored columns. Hand tools such as saws, axes, and sharpened shovels were used to expose a vertical cross section through the axes of the colored columns to a depth greater than the limit of extreme rupture. Crater cross sections were then constructed to record the fracture pattern and the displacement of the colored columns (Fig. 12). The measurements were supplemented by black-and-white and color photography. After the colored columns had served their purpose, a smudging technique was used to determine the true crater. This technique brought out in sharp contrast the difference between the texture of snow in the walls beyond the crater and that in the region of elastic rebound and in the region of fall-back (Fig. 13). Standard density-sampling profiles were established for various types of shots (Fig. 25, 27). The samples were taken with a core-sample auger (Fig. 14). Throughout the period of field work, an analysis was carried forward daily to test various concepts suggested by evidence being accumulated. The field analysis served to direct the field work so as either to support or disprove the concept.

Seismic measurements. Three seismographs were available for the tests: a Leet 50-magnification positive-displacement meter, a Sprengnether 100-magnification seismograph, and a Sprengnether 200-magnification seismograph. All three instruments measure the three components of vibration, but because of slow camera speed are not intended for extremely accurate measurements of seismic velocity. Table IV summarizes the observed variation in horizontal and vertical compressional-wave velocity with depth below the 1954 snow surface in the vicinity of the SIPRE test pit. Because of the high shock-damping capacity of snow it was found possible to place the seismographs much closer to the charge in snow than in ice. The position of the nearest seismograph depended upon the depth of the charge and the type of snow. If the depth of the charge exceeded the critical depth, displacement was measured with a remotely controlled Leet seismograph placed at a scaled distance as close as 12 λ (λ = cube root of the charge weight, lb). The normal range of scaled distances was from 12 to 100λ. Because it is difficult to level a seismograph on soft snow, the procedure finally adopted was to excavate pits 2 ft deep by 4 ft square at each seismograph position.

Instrumentation

Gage signals were recorded using a Miller recording unit (Fig. 15) containing eight dual-beam cathode-ray oscilloscopes and a rotating-drum camera. One of the 16 channels was used for zero-time, another to measure the time of ground rise, and the remaining one to measure either undersnow pressure or pressure in the air. Three types of gage were used. Pencil gages (Fig. 16) containing barium titanate elements were used to measure pressures in the range 0.4 to 6 psi. "Baffle" gages with tourmaline-crystal elements 1-5/8 or 2-1/4 in. in diam (Fig. 17, left) were used to measure pressures in the range 5 to 30 psi; and water-shock gages with tourmaline gage elements 1/4, 3/8, or 1/2 in. in diam (Fig. 17, right) were used to measure pressures in the range 30 to 3000 psi. Statham accelerometers (Fig. 18) were used to measure acceleration in the range 0 to 20 G; and VibraShock accelerometers (Fig. 19) were used to measure acceleration in the range 20 G to 2000 G. The shock-damping capacity of the snow when charge and gage were at a shallow depth below the 1958 snow surface was found to be such that the water gages were capable of recording pressures within the ranges $1\lambda < R < 10\lambda$. The baffle gages were used in the range $1.5\lambda < R < 5\lambda$, and the pencil gages were used in the range $2\lambda < R < 10\lambda$. The shock-damping capacity of the trench snow proved lower than that of the 1958 surface snow, but the difference was not great enough to affect the choice or layout of the gages.

Figure 12. Recording fracture pattern and displacement of colored columns.

Figure 13. Snow texture along crater cross section as revealed using smudge technique.

Figure 14. Drilling and recovering cores along density-sample profile lines.

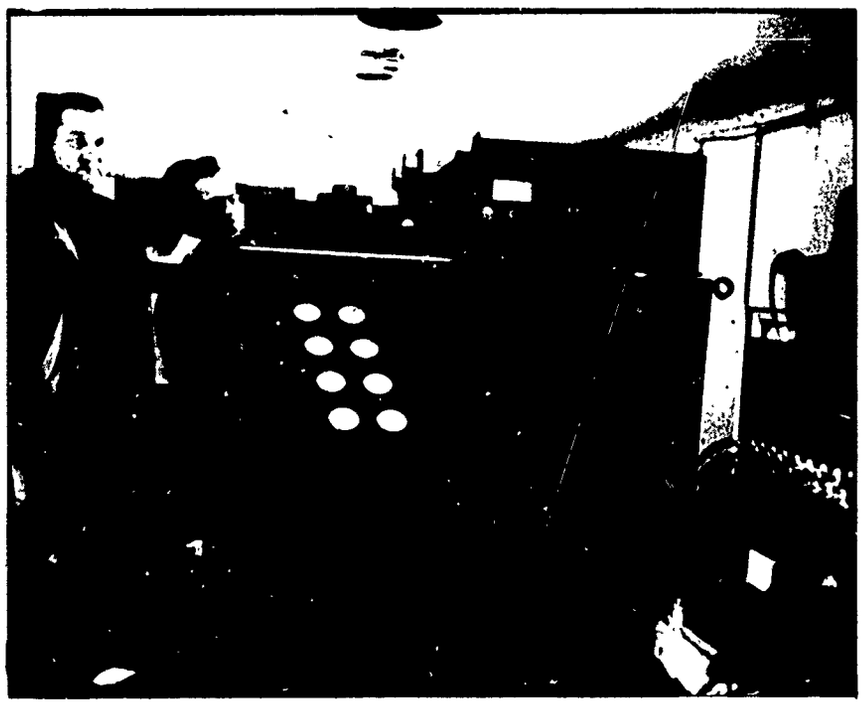

Figure 15. Miller recording unit.

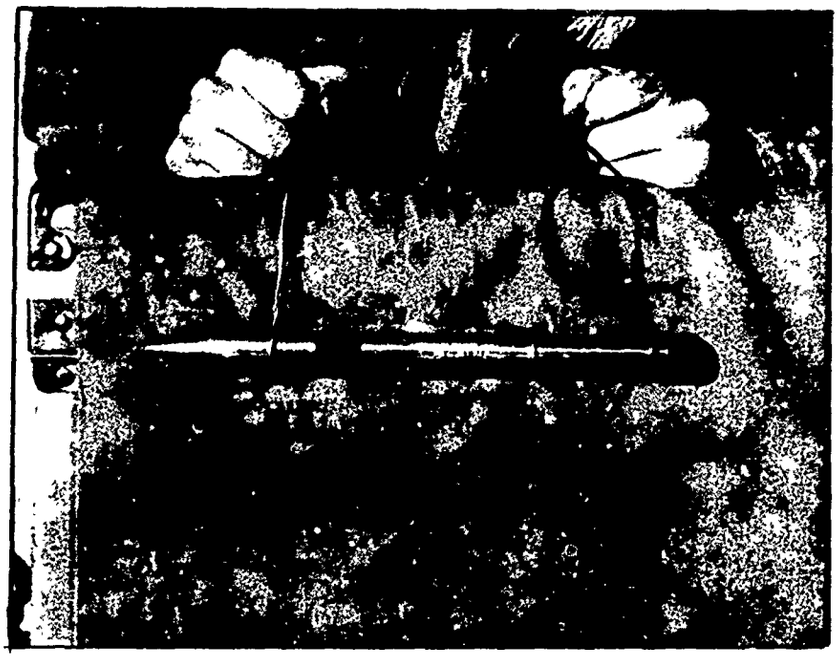

Figure 16. Pencil gage.

Figure 17. Baffle and water-shock gages.

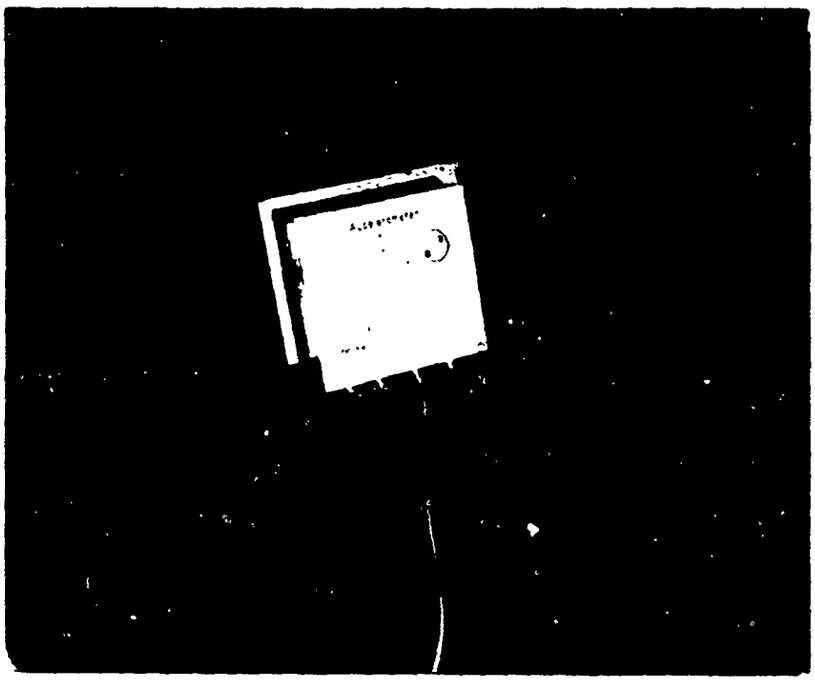

Figure 18. Statham accelerometer.

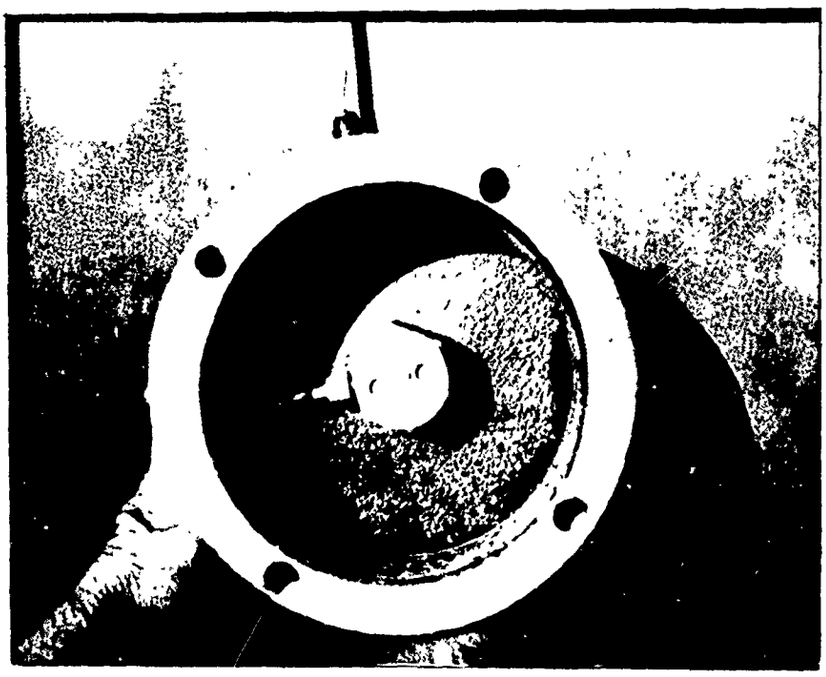

Figure 19. VibraShock accelerometer.

Table IV. Horizontal- and vertical-compressional-wave velocity. (From Bentley, et al., 1957).

Depth (m)	Horizontal compressional-wave velocity (m/sec)	Vertical compressional-wave velocity (m/sec)	Density (g/cm³)
0	700	700	0.35
5	--	1600	0.47
10	1400	2150	0.53
15	--	2400	0.57
20	2700	2650	0.60
25	--	2800	0.63
30	--	2900	0.65
40	3150	--	0.70
60	3400	--	--
80	3600	--	--
100	3700	--	--
120	3800	--	--
140	3850	--	--
200	3865 (max)	--	--

Standard gage layouts were planned so as to maintain geometric similarity, and were independent of the type of explosive and of physical properties of the material. The cube root of the charge weight was used as a scaling parameter. Figures 20 and 21 illustrate standard gage layouts for charges detonated at 3.0λ and 1.0λ below the surface. Figures 22, 23, and 24 illustrate standard gage layouts for contact and air bursts above the 1958 snow surface. Because of time limitations it was not possible to fire similar shots in contact with and above the higher-density, trench-bottom snow.

Because 1) the physical properties of the snow change as the density changes, and 2) the explosive and the material are not separate and independent variables, it seems desirable when analyzing the shock data to consider separately for each type of explosive the test conditions enumerated in Table V.

Table V. Suggested test conditions for analysis of undersnow shock.

Test condition		Scaled charge depth	Scaled gage depth
Case I	(Undersnow)	-1λ	1λ
Case II	(Undersnow)	-3λ	1.5λ
Case III	(Undersnow)	-3λ	3λ
Case IV	(Contact burst)	0	2.3 to 4.5λ
Case V	(Air burst)	+0.5λ	1.8 to 3.2λ
Case VI	(Air burst)	+1.0λ	1.3 to 2.7λ

Compilation of data

The crater data gathered during this investigation are summarized in the Appendix. Shock, design, charge, camera and seismic data have not been published but are compiled in USA CRREL Internal Report 37, which

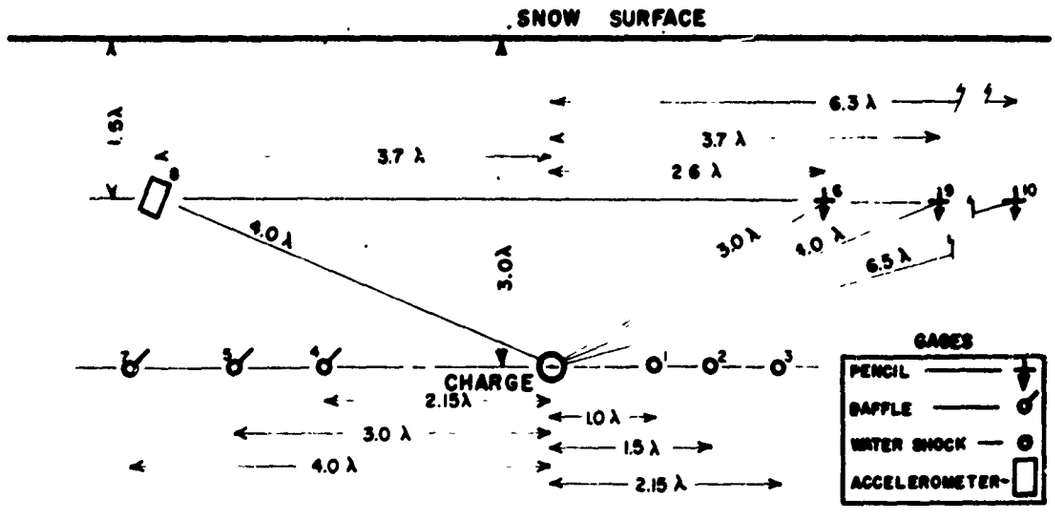

Figure 20. Standard gage layout, depth of charge = 3.0λ.

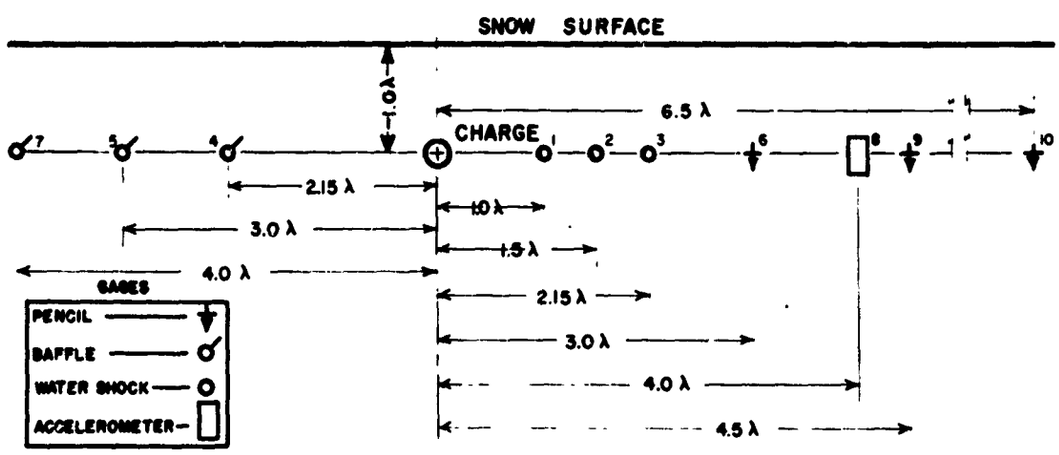

Figure 21. Standard gage layout, depth of charge = 1.0λ.

is on file at the U.S. Army Cold Regions Research and Engineering Laboratory, Hanover, New Hampshire. Also included in Internal Report 37 are 114 crater cross sections (similar to Fig. 25 and 27) with overlays showing displacement of the colored columns (see p. 2).

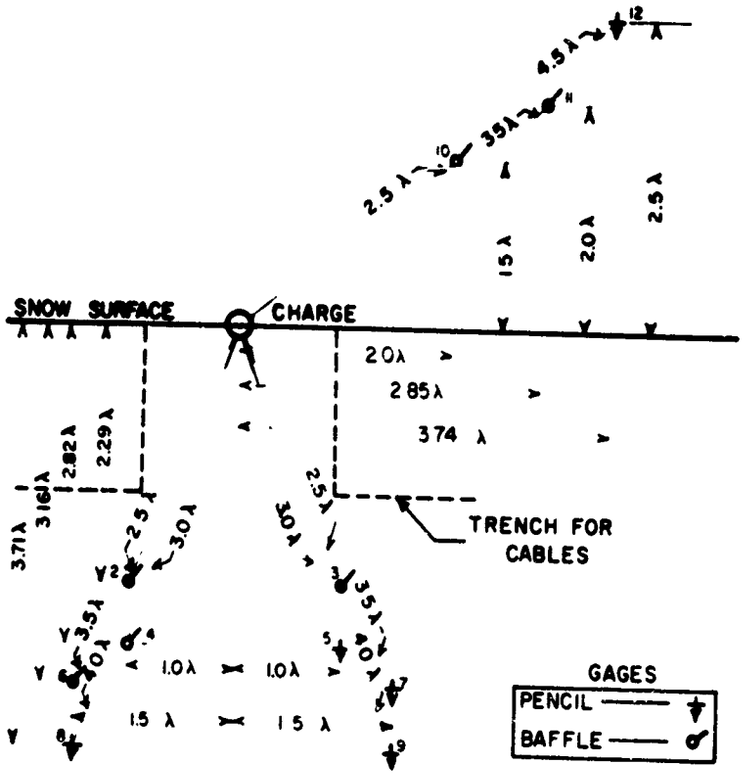

Figure 22. Standard gage layout, contact burst.

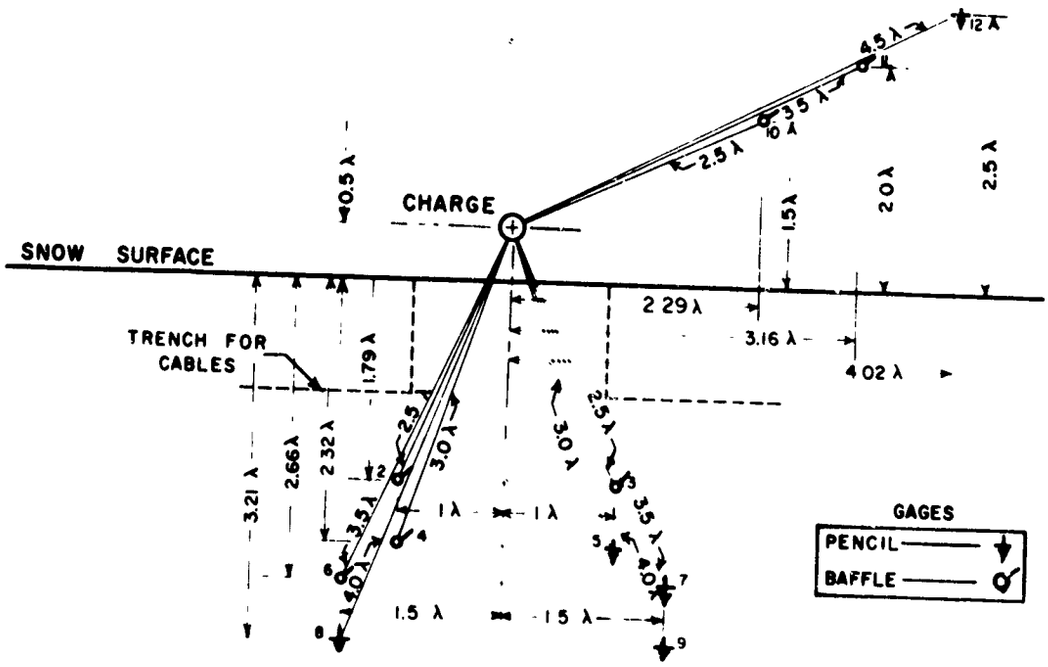

Figure 23. Standard gage layout, height of charge = 0.5λ.

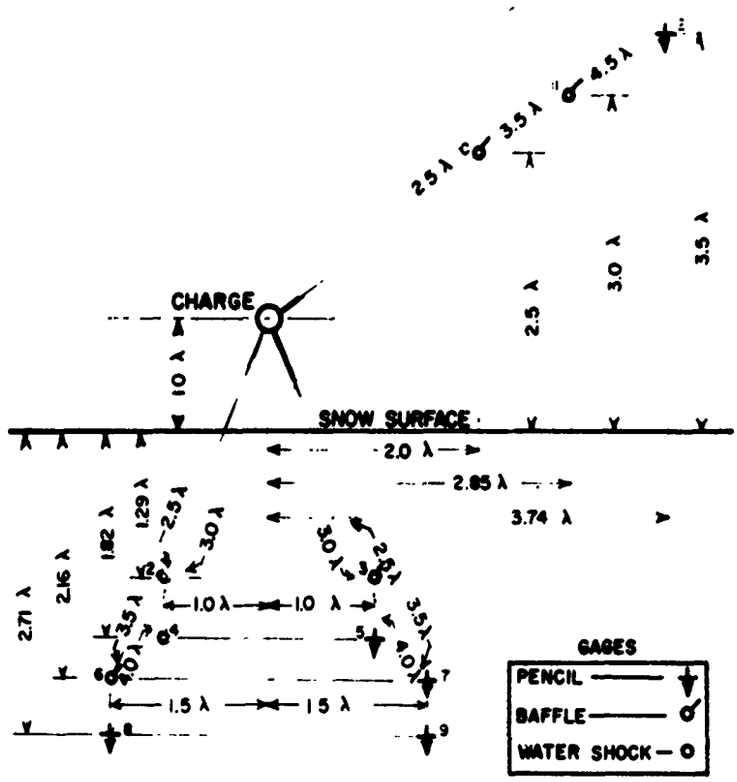

Figure 24. Standard gage layout, height of charge = 1.0λ.

EVALUATION OF THE DATA

Crater and cavity nomenclature

Snow does not occur as a homogeneous mass, but accumulates and metamorphoses as a layered system (See Fig. 13). It may be thought of as a composite substance that consists of a brittle-acting elastic solid and air. Within the range of charge depths covered by the experiments, the snow is both porous and permeable, but its physical properties (Bader et al, 1939; Butkovich, 1956) change gradually with depth below the surface. In the test blasts, several factors contributed to the variable behavior of snow. Both the air within the voids and the solid matrix affect the failure process, and the proportions of these two varied. Even if proportions had remained constant, behavior of the snow would have changed with changes in texture and permeability. Certain of the blasts were fired in near-surface snow with little cohesion; others were fired in deeper snow with greater cohesion and with shear strength. The geometry varied from blast to blast.

Although the effect of the air in the voids is much more apparent during blasts in snow than in noncohesive, porous soils, the effect observed probably exists in porous and permeable soils to a lesser degree. The air within the voids is affected during both rise to and decline from peak pressure, but the effect occurring during the decline may be apparent in low-density, high-porosity materials. The failure process resulting from blasts in snow differs

from that in most rocks and in cohesive soils. Because of its air-filled voids, snow that is permeable and highly porous behaves quite differently than glacier ice; the failure of such snow is here classified as viscous damping. In snow, this viscous-damping failure changes with increasing depth so as to approach the shear failure observed in glacier ice. A distinction, therefore, is made here between failure processes 1) in brittle-acting solids, 2) in more plastic-acting materials such as loess, clay, and ice, and 3) in composite substances such as snow in which the air-filled voids affect the stress-strain relations during both loading and unloading.

In the attempt to fix various limits of the crater and of the camouflet using terminology generally employed for blasts in soils, and on a somewhat modified basis for blasts in rocks, a conflict arises that is difficult to resolve. It is due in part to the fact that heretofore only one type of failure in blasting has been generally recognized, and in part to the fact that present terminology is an outgrowth of experiments conducted within a specific and limited range of charge depths. The colored-column technique, which made the differentiation between limits possible, has been applied primarily in soils, and is less practical (because of difficulties during excavation) to apply to rocks, frozen ground and ice. The definition of the true crater as generally applied to craters in rocks and as recently applied to frozen ground and to ice appears to coincide with the limit of complete rupture as applied to soils.

The generally held definition of the true crater is the excavation as it would appear to an observer after removing material that has been lifted from its original position by the force of the blast, but has fallen back into the excavation. The definition implies a separation and removal of material from its surroundings. The limit of the true crater is a surface between material that has been isolated and material that remains attached. The limit visualizes the failure process occurring during loading by fracture rather than as in snow during both loading and unloading by a complex combination of compaction, scouring, flowage, slumping, and rebound. Because of the complexity of the failure process and because the experiments of this report include test conditions ranging from air-burst to deep undersnow shots, the true-crater limit in snow is difficult to find and has little meaning relative to failure.

Although limits of the true crater are marked on the snow-crater cross sections and all data necessary to a conventional analysis have been summarized in the data sheets, the complete-rupture limit and the extreme-rupture limit more accurately describe the failure process. The parameters of the breakage-process equation:

$$\frac{V}{W} = E^3 ABC$$

are determined by the limits of complete rupture and extreme rupture. They describe: 1) the beginning, and 2) the completion of failure by fracture.

The following definition of the term "apparent crater" is adopted here: The excavation as it appears to an observer immediately after a blast at a depth sufficiently shallow so that a crater is formed and is not filled with fly-rock beyond the level of the original ground surface. The term does not apply to charges that dome up rather than break the surface. An apparent crater ceases to exist as the depth of the charge increases so as to approach the optimum depth, Δ_0. Inasmuch as an apparent crater does not exist in the range where the energy of the explosion is partitioned exclusively to loading the material, the dimensions of the apparent crater bear little direct relationship to the parameters of the breakage-process equation.

Limits of significance to the primary fracture process in snow are:

1) the limit of compaction, flowage, and fracture that determines the size and shape of the cavity caused by an explosion

2) the limit of complete rupture

3) the limit of extreme rupture.

The limit of complete rupture coincides with the limits of the camouflet as the charge depth increases from that at which a crater is formed to that at which a camouflet is formed. Although the zone between the limit of complete rupture and the limit of extreme rupture is fractured, it is not isolated and, in snow, both the original bedding and texture are retained.

The following definitions of the limits of complete rupture and of extreme rupture are proposed and have been adopted here.

The limit of complete rupture is a surface which divides material isolated from its surroundings and material not isolated from its surroundings.

The limit of extreme rupture is a surface running through the ends of fractures farthest from the center of the explosion. The extreme-rupture surface is always beyond the complete-rupture surface. The limit of extreme rupture exists both when a crater is formed and when a camouflet is formed.

Figure 25 illustrates the open-void fracture pattern and column displacement that is typical of failure resulting from blasts in surface and near-surface snow of the Greenland Ice Cap and the various crater limits according to terminology used here.

The texture of the snow within the true crater (see Fig. 13) differs from that beyond it, but the difference is not readily apparent before use of the smudge technique. A zone of open voids lies between the true-crater limit and the limit of complete rupture. Between the complete-rupture limit and the extreme-rupture limit the original bedding is retained, but fractures caused by the explosion are present. The observed relations suggest that the fractures were formed before the open cavities were formed and during the interval of time when the undersnow pressure rose to its peak at any given position. The limit of the true crater is difficult to determine, and has been placed with least certainty. The uncertainty is not due to definition or observation alone, but arises because various complex phenomena occur, to an extent which differs depending upon the depth ratio.

Figure 26 illustrates crater nomenclature and identifies dimensions and symbols relating to each of the crater limits. The letters h, d, Z, x, R, r, and C refer to crater depth, charge depth, gage depth, gage distance, gage slant distance, crater radius, and crater slant distance respectively. The subscripts a, t, r, and e define respectively the apparent-, true- complete-, and extreme-rupture limits.

Figure 27 illustrates the pattern of fracturing and the displacement of colored columns typical of a specific phase of cavity growth in snow. The limit of extreme rupture marks the terminus of fractures which occurred during pressure rise and outward displacement of the snow. The limit defined for a camouflet is identical to that defined for a crater. Figure 28 illustrates cavity nomenclature and designations.

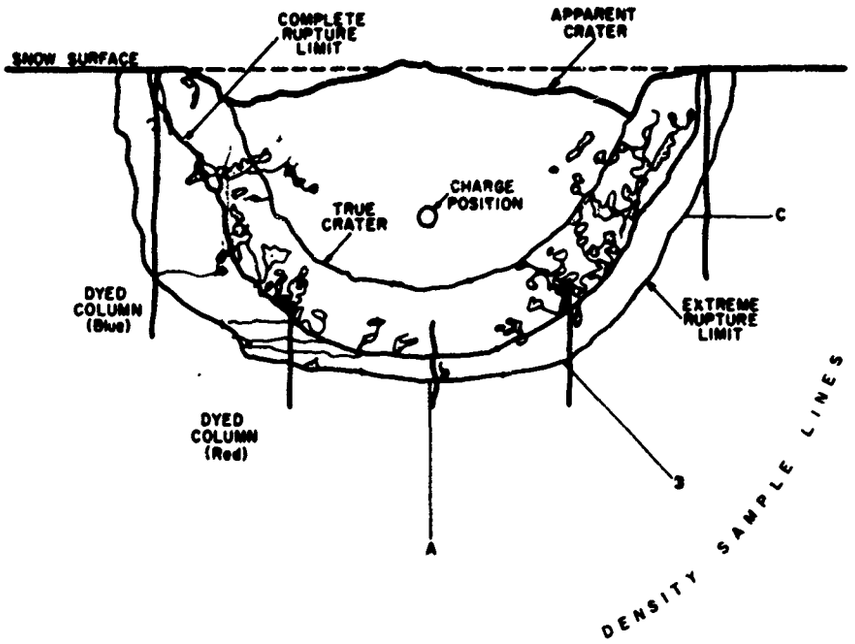

Figure 25. Crater limits and column displacement.

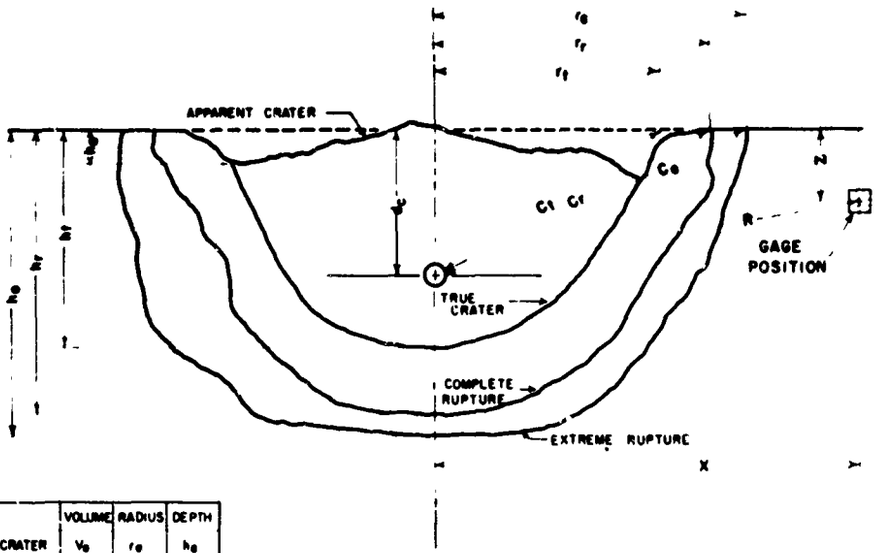

LIMIT	VOLUME	RADIUS	DEPTH
APPARENT CRATER	V_a	r_a	h_a
TRUE CRATER	V_t	r_t	h_t
COMPLETE RUPTURE	V_r	r_r	h_r
EXTREME RUPTURE	V_e	r_e	h_e

Figure 26. Crater nomenclature.

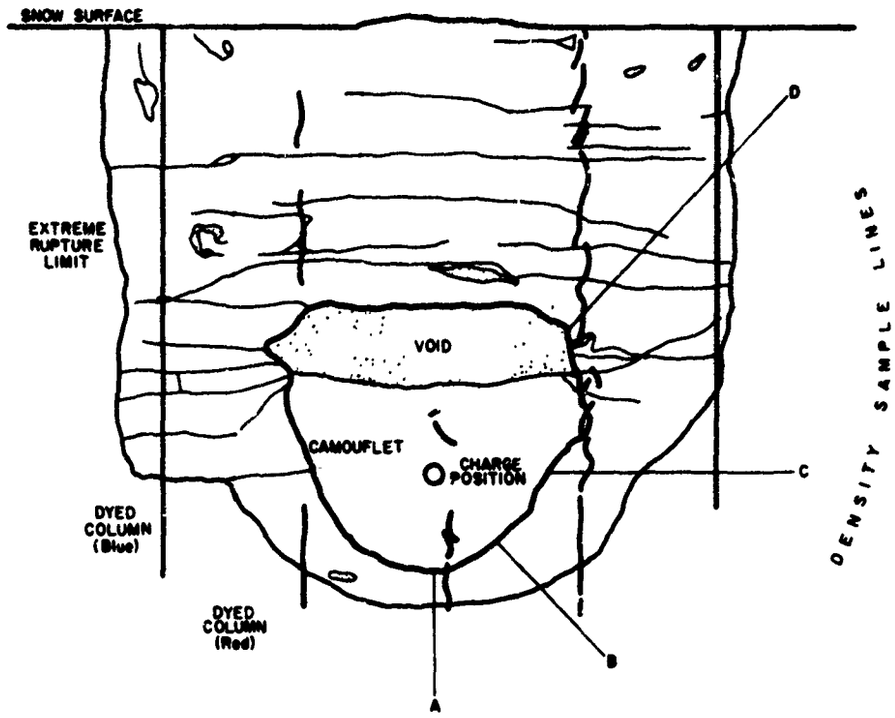

Figure 27. Cavity fracture limits and column displacement.

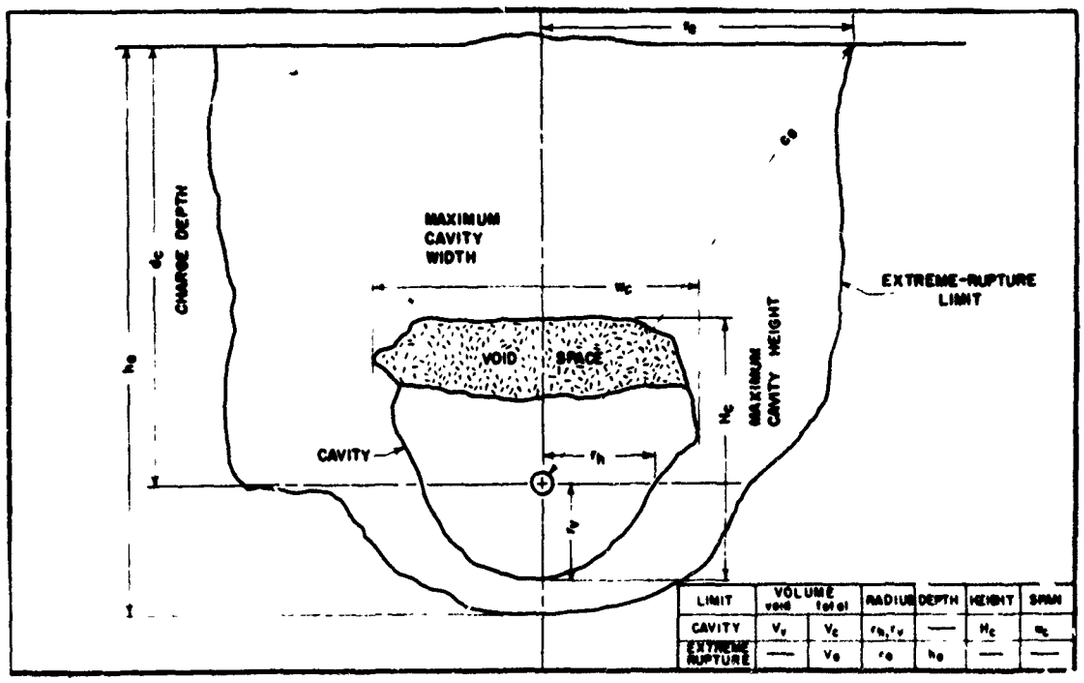

Figure 28. Cavity nomenclature.

Variation in crater shape with charge depth

Figures 29 and 30 illustrate the effect of charge depth upon size and shape of crater in 1958 surface snow. The drawings were constructed using the cube root of the charge weight as a scaling factor (λ equals the cube root of the charge weight in pounds).

Each limit increases to a maximum then decreases as the depth of the charge increases. Within the range illustrated ($-0.08 < \Delta < 0.98$) each of the limits except that of extreme rupture ceases to exist as the depth ratio increases, disappearing in this order: 1) the apparent crater, 2) the true crater, 3) complete rupture.

Typical undersnow pressure records

Figure 31 illustrates the typical variation in shape of the undersnow-pressure record with distance. In both instances the gages were placed at a depth equal to the depth of the charge, and the same type of gage was used.

The form of the pressure record differs substantially from that for water or air. The peak pressure is lower than in ice at the same scaled distance. The pressure at the front of the disturbance is small compared to the peak pressure, which at distances as small as 1.5λ arrives later. The surface of ground vertically above the charge rises after the arrival of peak pressure, which is substantially after the arrival of the disturbance. The form and the magnitude of the pressure record are affected both by the depth of the charge and the distance to the gage.

In an experiment to determine whether or not the passage of the disturbance causes an appreciable rise of pressure within the voids, the sensing element of the pencil gage (Fig. 16) was suspended in a 2-in.-diam by 2-in.-high cavity at a distance of 4λ from a 5-lb charge 2λ below the surface. The gage distance was beyond the complete-rupture limit. A baffle gage and a second pencil gage were placed in a conventional manner to measure the undersnow shock pressure at the same gage distance and at the same charge depth. After the experiment, the gage was carefully excavated, and it was found that the cavity had not been closed by the explosion.

Records from the experiment are presented in Figure 32. The form of the undersnow shock record (Fig. 32b) for the baffle gage differs somewhat from that (Fig. 32c) for the pencil gage, but both reach the same peak pressure. The air pressure within the void (Fig. 32a) rises more slowly than the undersnow pressure (Fig. 32c), but ultimately reaches a peak nearly equal to the undersnow shock pressure.

Typical acceleration records

Figure 33 illustrates typical undersnow acceleration records, for the same blasts used to illustrate the pressure record (Fig. 31). The slant distance to the accelerometers is the same for both blasts (see standard gage layouts, Fig. 20, 21), but the gage depth could not be held constant because of practical limitations. Placing an accelerometer at a substantial depth below the surface without disturbing the snow in contact with it is difficult.

Typical seismic records

The effect of the depth of the charge upon the magnitude of the displacement and upon the three components of vibration in snow is illustrated in Figures 34, 35, and 36. The direct undersnow shock is damped more rapidly

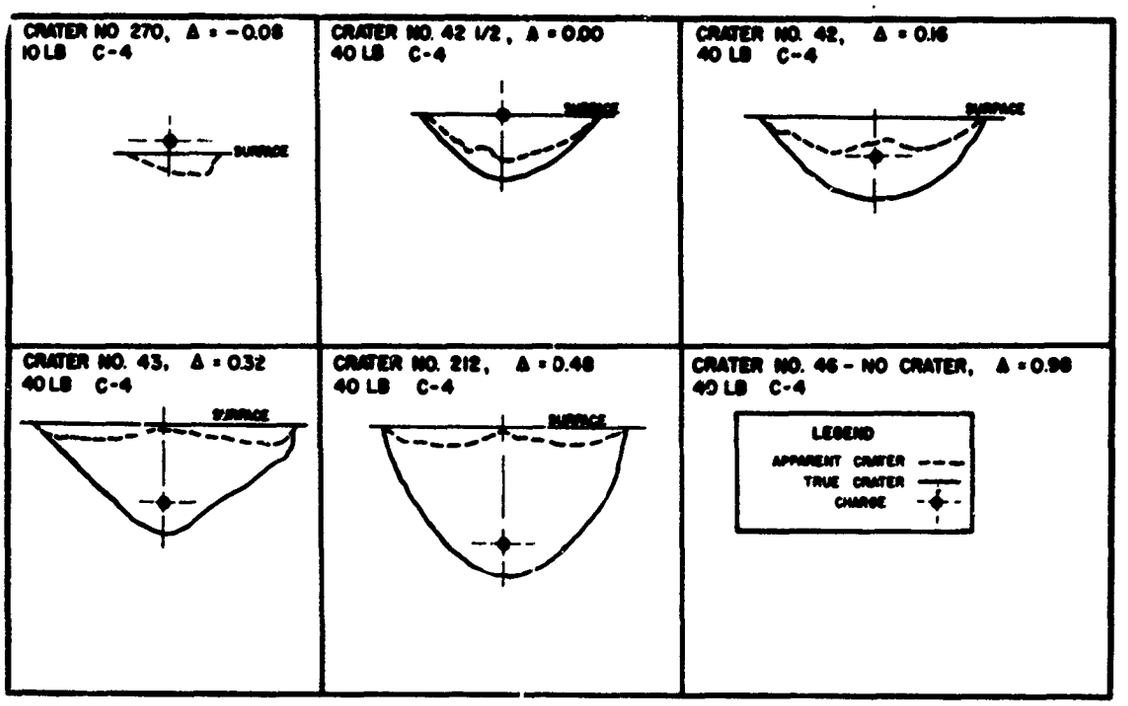

Figures 29. Apparent- and true-crater shapes at increasing depth ratios.

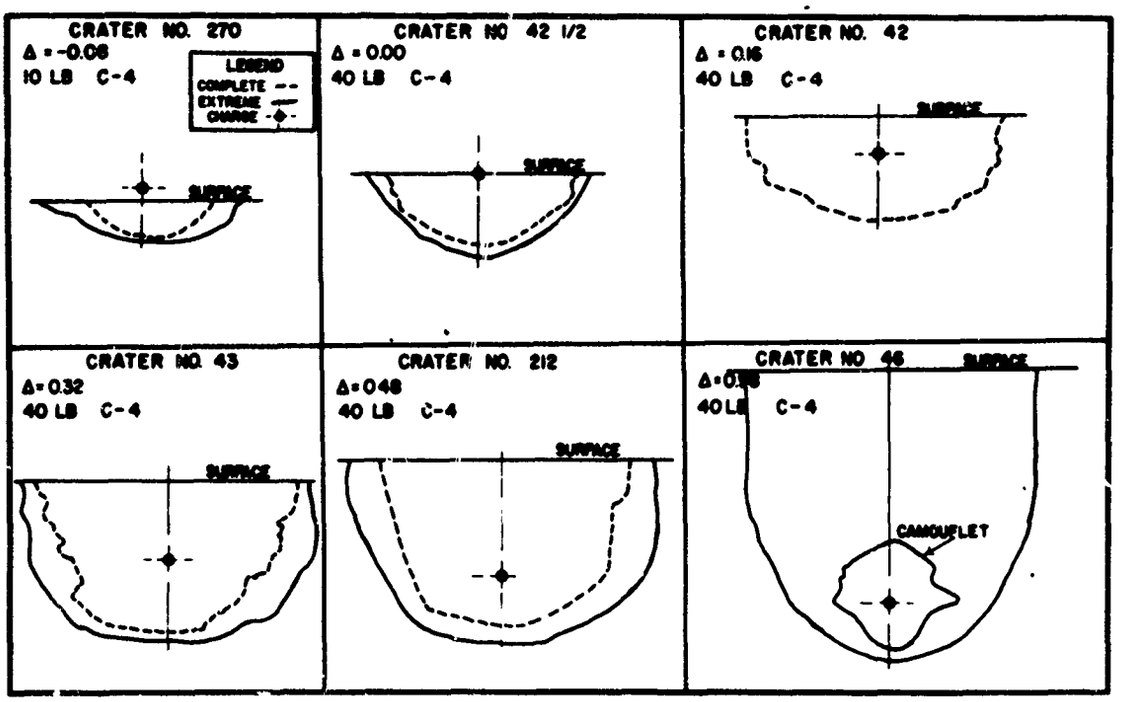

Figure 30. Complete and extreme rupture limits at increasing depth ratios.

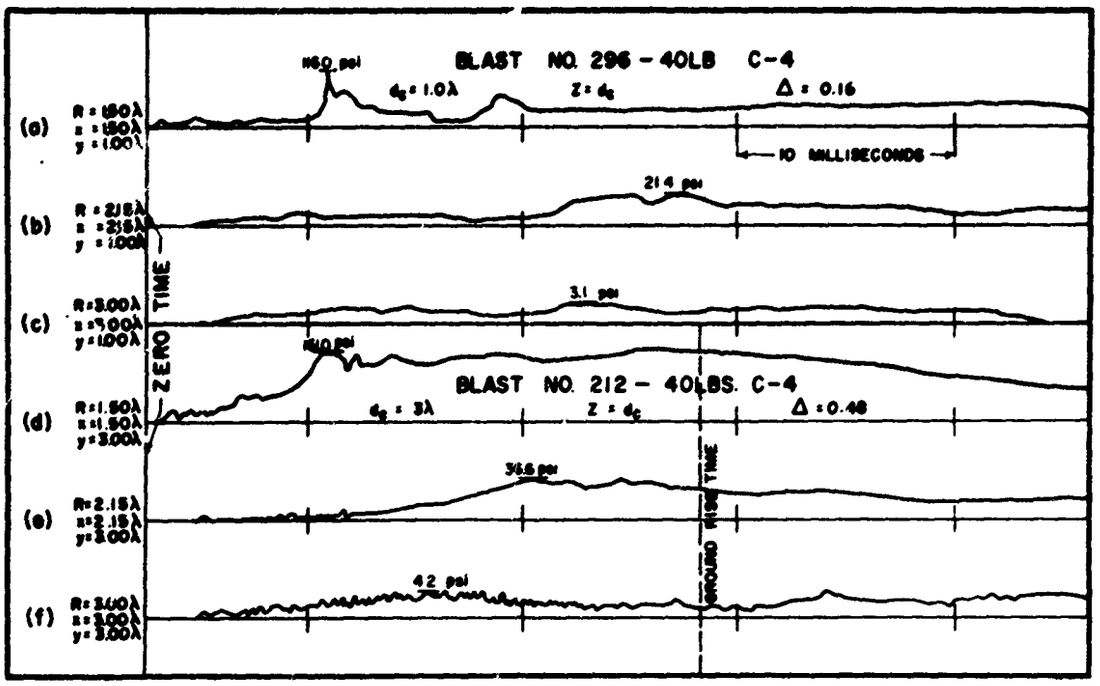

Figure 31. Typical variation of undersnow pressure with distance.

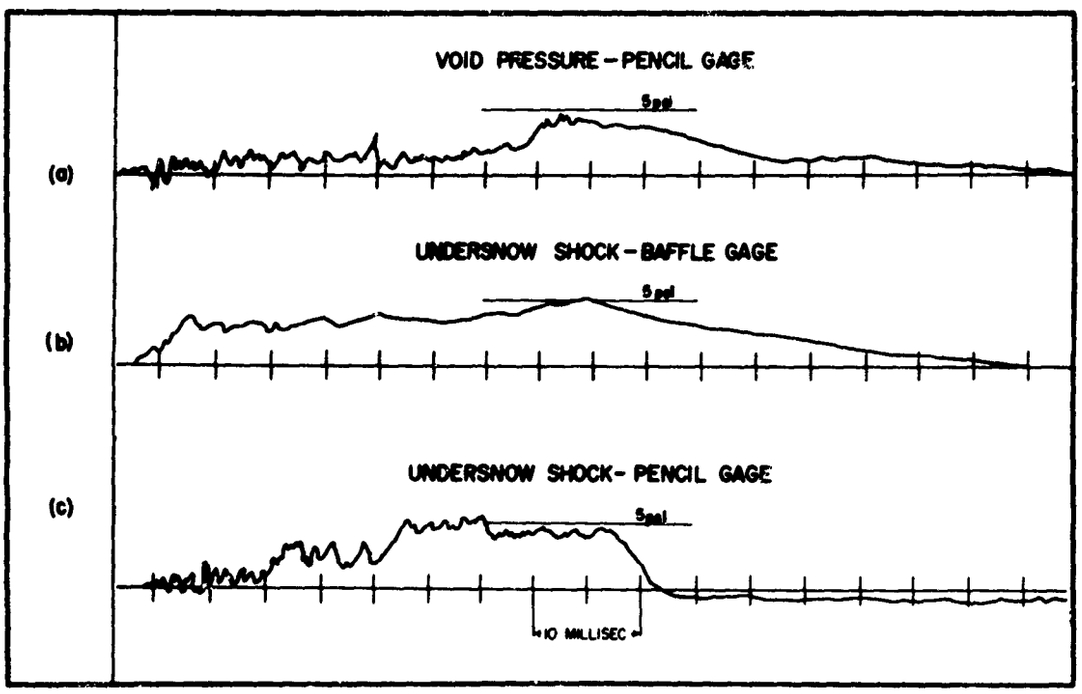

Figure 32. Comparison of void pressure and undersnow pressure.

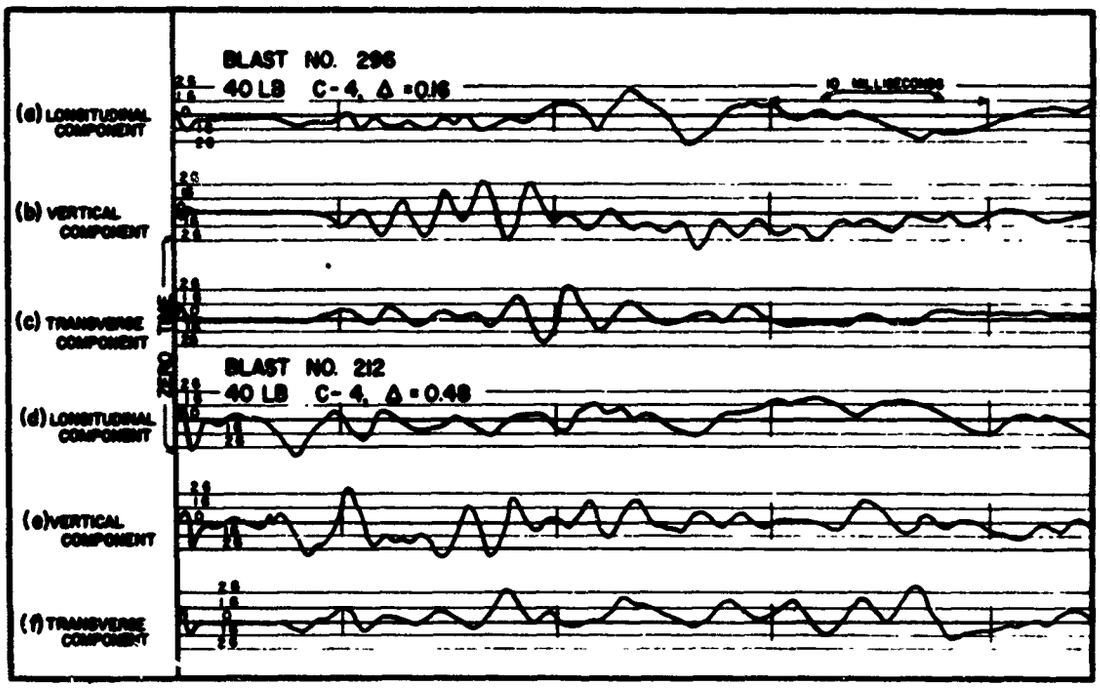

Figure 33. Typical undersnow-acceleration records.

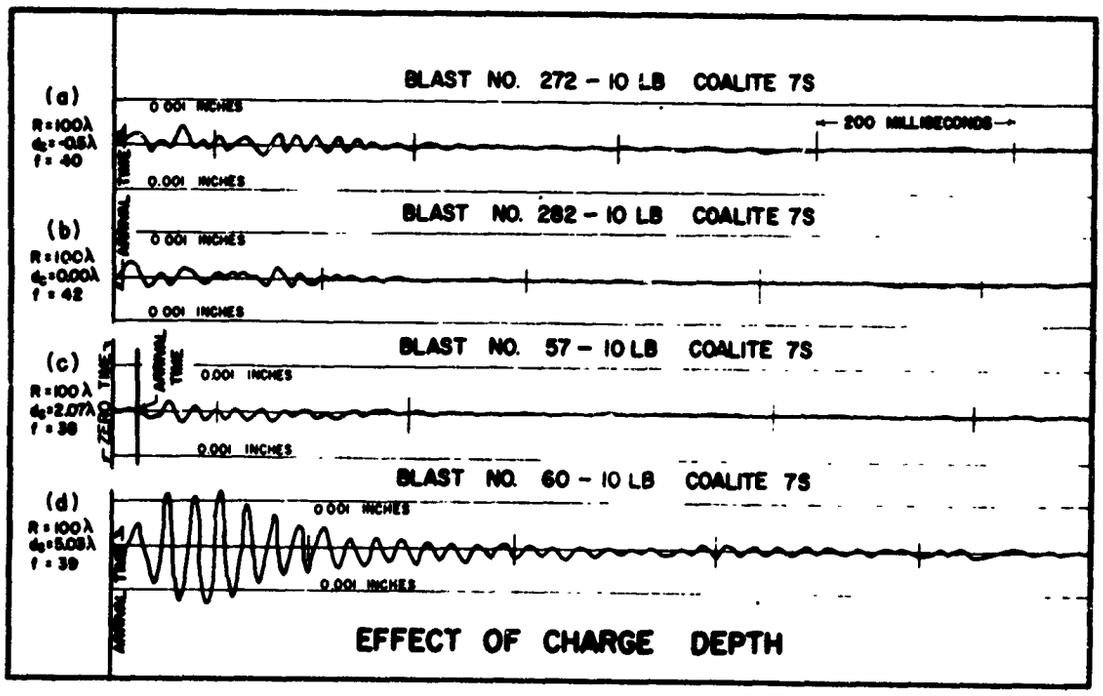

Figure 34. Typical seismic records, longitudinal component.

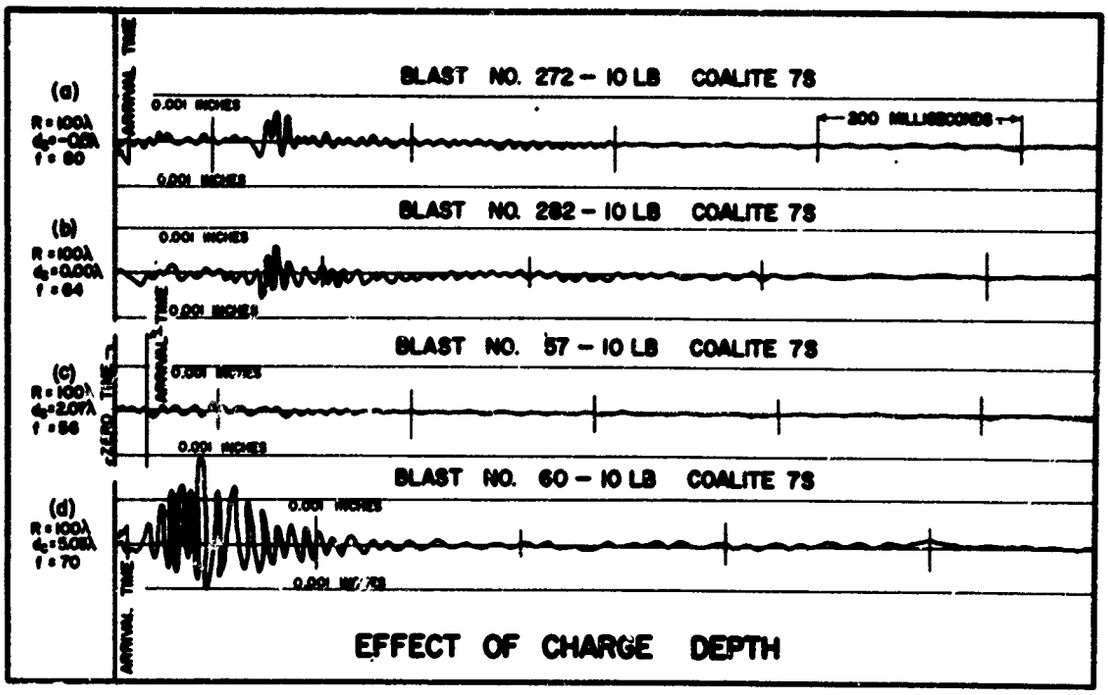

Figure 35. Typical seismic records, vertical component.

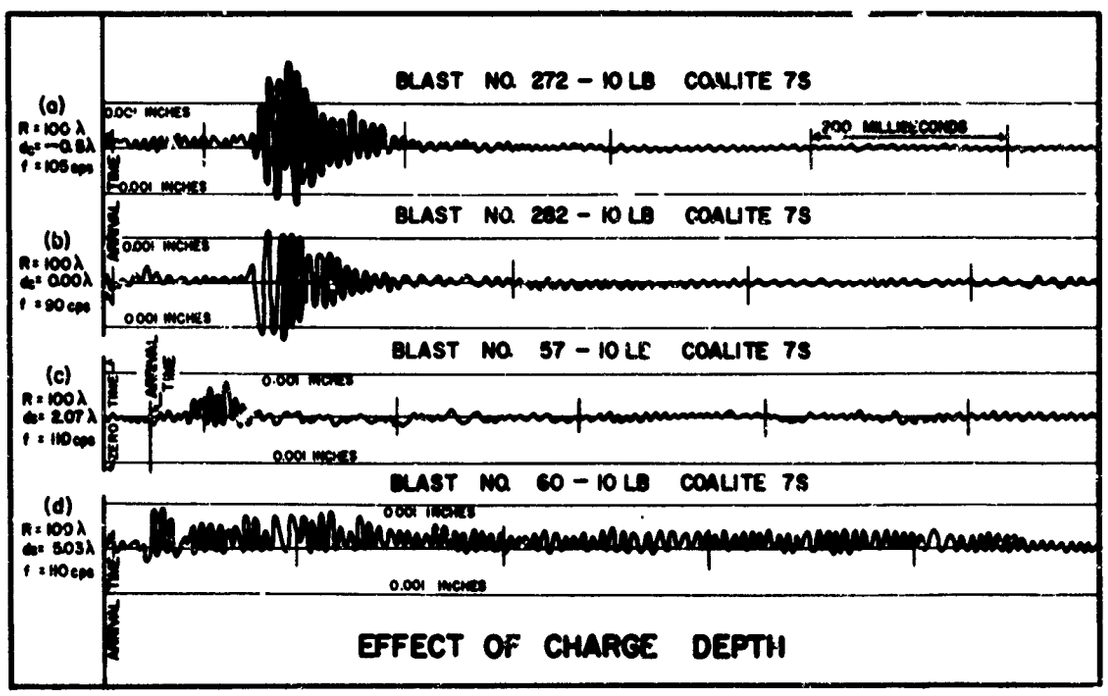

Figure 36. Typical seismic records, transverse component.

in low-density near-surface snow than in snow at greater depth. The vertical and transverse components of the air-induced undersnow shock at 100λ exceed those of the direct undersnow shock for both air bursts and contact bursts. At a charge depth of 2λ the air-induced shock is of minor consequence. As the depth of the charge increases, more of the energy of the explosion is partitioned to the material, and the displacement due to the direct shock (as measured 2 ft below the surface) increases further. The frequency of each of the three components of vibration differs, but does not vary greatly with the depth of the charge. The frequency as measured 100λ from the charge position decreases in the order:

a) transverse

b) vertical

c) longitudinal.

The damping capacity of near-surface snow is greater than that of the higher-density snow at depth. Similarly, the damping capacity of the trench snow is greater than that of glacier ice. Because of the high damping capacity of the snow, it was practical to record displacement with a Leet 50-magnification instrument at a scaled distance as small as 12λ.

The failure process

The effect observed when blasting in snow depends upon the depth ratio of the shot and upon the time and place of observation, with respect to the rise and decline of stress within the material. The "time" refers to a particular instant during the action. The "place" denotes a specific position at a given instant relative to the energy source, the disturbance, and the 1958 snow surface.

A cross section through a crater caused by an air burst reveals phenomena substantially different than those revealed by the crater of a blast at near-optimum depth. Similarly, the size and shape of the undersnow cavity, and details of fracturing beyond the cavity walls, differ depending upon the depth ratio of the blast. The behavior of the material is not independent of the scale of the experiment. At some depth below the surface, snow of the Greenland Ice Cap acquires properties of glacier ice, and failure approaches shearing failure as a limit. When blasts were in the bottom of wide, 12-ft-deep trenches, certain phenomena were observed that are indicative of the transition.

Figure 37 illustrates the type of failure referred to here as "viscous-damping." The photograph records the effect of the release of stored potential energy from the snow after venting of the gas bubble and the decline of pressure within the explosion cavity. At the stage illustrated, displacement of the columns is inward and symmetrical about the charge position. The effect illustrated in Figure 38 occurs at an earlier stage while the snow is being loaded and the stress is increasing. Shearing failure does not occur in snow that is noncohesive, but begins as the density becomes greater than 0.35 g/cm^3 (Butkovich, 1956) Figures 37 and 38 illustrate effects in 0.45 g/cm^3 density trench snow.

The cratering result viewed by an observer after an explosion is the end product of a series of events that took place during an interval measurable in milliseconds. Observation of earlier events requires suppression of later ones. Although it is beyond the power of an observer greatly to modify the duration of the action, "later" events can be suppressed by increasing the ratio of the volume of material within which the transfer is accomplished to

Figure 37. Viscous-damping failure.

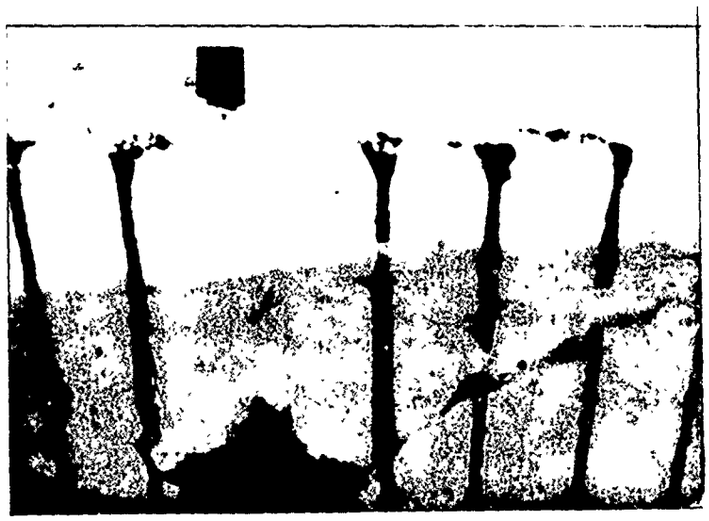

Figure 38. Shearing failure in 0.45 g/cm^3 density trench snow.

the quantity of energy to be transferred in a given interval of time. The depth ratio is a dimensionless quantity related to the failure process by definition and describing an energy-mass-time relationship fixed by the energy of the explosion, the depth of the charge, and physical properties of the material. The determination of the sequence of events during blasts in snow is made possible by applying the theory of relative behavior of materials (Livingston, 1960a) wherein a change that is accomplished in time becomes analogous to an energy-density change and is measurable by the depth ratio.

Cavity growth. Figure 39 illustrates the sequence of events at the explosion cavity when a deeply buried explosives charge is detonated in snow possessing shear strength. The snow is compacted and driven radially outward as the gas bubble expands. The displacement of the snow is greater parallel to than across the snow layers (Fig. 39a). As the snow is displaced outwardly, it is compacted. Compaction apparently does not proceed beyond some critical density, which is in the range of 0.50 to 0.60 g/cm^3. The thickness of the compacted zone in snow of a given density depends upon the shape and volume of the cavity. The walls of the explosion cavity are fractured (Fig. 39b) by stretching in a tangential direction as the cavity expands radially. Melting occurs at the cavity wall, and converts the skin of the compacted, fractured and expanding zone into ice.

Figure 39c illustrates the shape of the explosion cavity at that depth ratio where expansion ceases and fracturing begins. The roof and floor are dome-shaped, but surface uplift has proceeded sufficiently to weaken the chamber at a horizontal plane through the spring line. Weakening preferentially accelerates horizontal displacement within the zone of stretching at the charge elevation.

Cavity deformation such as illustrated is indicative of the stress distribution within the cavity during doming. Either the uplift-horizontal-stretching type of cavity deformation or the shearing illustrated in Figure 38 may occur. Which type occurs depends upon both physical properties of the material and the scale of the experiment. In either instance, failure begins at critical depth ($\Delta = 1.0$) and fracturing proceeds outwardly from the walls of the explosion cavity.

The next event (Fig. 39d) destroys the explosion cavity, and is referred to here as implosion. The walls fall inward, and both the zone of skin-surface melting and the zone of compaction are destroyed. Failure extends to a zone surrounding the collapsed opening. Limits of a zone of arching failure are shown in the figure. A transition condition and a most sensitive balance mark the beginning of implosion and the beginning of fracturing. The balance determining the extent of fracturing (shear) during the pressure rise and the extent of fracturing during the pressure decline is most delicate. The observed sensitivity is not inconsistent with variation in the form of the pressure record with charge depth and with distance such as illustrated in Figure 31.

Implosion and related events. Implosion represents a stage of failure during unloading of the material, as the undersnow pressure declines from peak pressure. Both loading and unloading depend in a complex manner upon the air within the voids and upon the texture of the snow. Implosion has an upper limit that coincides with the beginning of fracture. Whether or not it ceases at some lower limit is uncertain. The phenomenon was observed over a broader range of depth ratios in trench snow than in 1958 surface snow. The limits within which it occurs apparently depend upon the quantity of stored potential energy that is recoverable. The sequence of events leading to implosion and preliminary to venting of the gas bubble is illustrated in Figure 40.

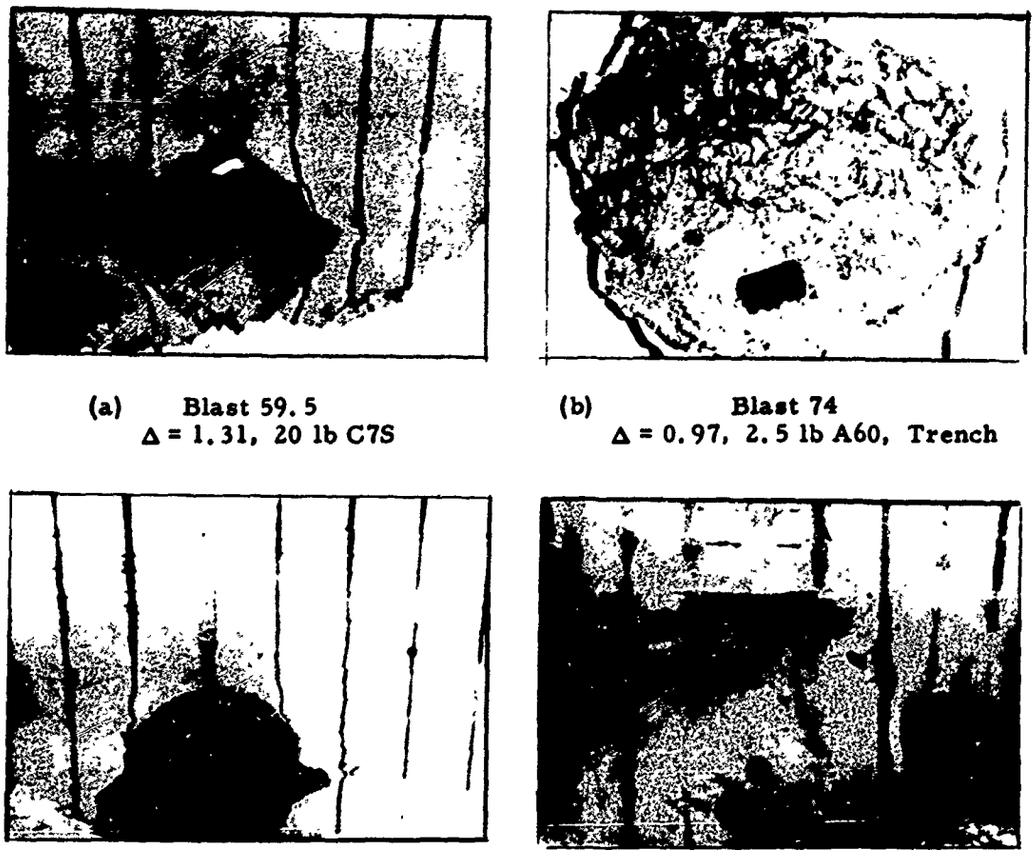

(a) Blast 59.5
Δ = 1.31, 20 lb C7S

(b) Blast 74
Δ = 0.97, 2.5 lb A60, Trench

(c) Blast 46
Δ = 0.98, 40 lb C-4

(d) Blast 54B
Δ = 0.90, 2.5 lb C-4

Figure 39. Sequence of events at the explosion cavity.

Permanent displacement of the snow during pressure rise and the variation of the displacement with distance are illustrated in Figure 40a. The columns in the figure were spaced 1 λ (3.42 ft) apart. The secondary cavity shown in Figure 40a resulted from collapse of snow possessing shear strength. It differs from the primary cavity both in shape and position. The column immediately to the right is displaced in a zigzag manner by doming and sliding along the bedding planes. The ice lens at the bottom of the photograph indicates the extent of the doming. Permanent displacement decreases with distance from the primary cavity, as is evident in the photograph. The pattern of the permanent displacement is determined to a greater extent by expansion of the gas bubble than by the preceding disturbance.

Figure 40b records that stage of implosion where the once-melted skin of the original explosion cavity explodes inward and the fragments strike each other as if they were part of the lining of a shaped charge of near-hemispherical shape. As a result of implosion, the floor below the cavity bulges upward. The bulging is greater at the centerline of the primary cavity than near the ribs. The magnitude of the bulging is indicated by the stretching of the colored column at the bottom center of the photograph.

(a) Blast 26
Δ = 0.82, 40 lb A60

(b) Blast E

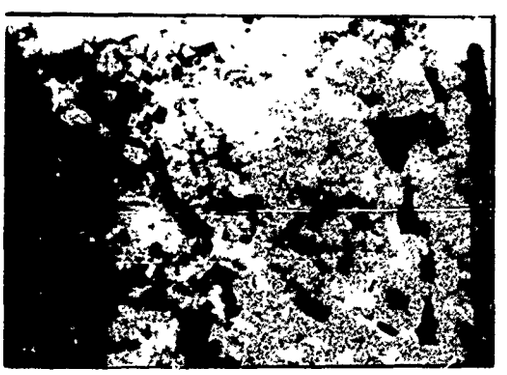

(c) Blast C

(d) Blast 34
Δ = 0.71, 2.5 lb C4

Figure 40. Implosion and related events.

Figure 40c illustrates the effect of implosion upon the wall of the cavity. The implode and collapsed cavity is to the lower left in the photograph. Displacement towards the explosion cavity leaves an open void at some distance (1.4λ in Fig. 40c), depending upon the explosive, the material, and the geometry. The void may be thought of as a tension fracture. Material beyond the void appears little affected by the implosion. A zone of voids (Fig. 25) marks the limits of the zone within which energy stored during loading is released during unloading. The entire process of implosion in snow appears analogous to elastic rebound. More energy may be recoverable from a composite of solid and air than from simple solid substances, because a lesser proportion of available energy is lost during loading and a greater proportion of the stored energy is recovered during unloading.

Figure 40d illustrates a situation after implosion and prior to venting, when shear fractures such as in Figure 38 have partly developed, but die out in the lower-density 1958 surface snow. Gases from the explosion cavity have permeated outward along the incipient shear zone, and implosion has occurred without venting of the gas bubble. A cauldron-type roof collapse such as occurs in certain large geologic structures followed implosion, and the once-domed-up snow fell back into the void that was created by compaction.

Figure 39d demonstrates that energy may be stored in and released from the roof of the explosion cavity. Because loading does not continue long after fracture or displacement begins, implosion of the roof probably diminishes as the depth of the charge decreases. The available evidence suggests that the top of the explosion cavity is isolated by a fracture process (see Fig. 38) that is accompanied by doming (see Fig. 40a). The action is in extreme contrast to that of shock-wave reflection in brittle-acting solids.

Vortex and scouring motions. As the depth of the charge decreases, a condition is reached at which loading ceases and the gas bubble vents to the atmosphere. Closely associated with implosion, a vortex motion within the snow is followed by venting, which in turn is accompanied by a scouring action caused by the motion of high-velocity gases in the air above the surface. If the energy is in excess of that transferable to the snow, events during the decline from peak pressure occur in a natural sequence (Fig. 41a-d). Since they are placed in order of decreasing depth ratio, the photographs of Figure 41 may be thought of as illustrating the motion of snow at various stages of a given blast.

Figure 41a illustrates the beginning of the vortex motion of the snow following implosion. Soot, formed by incomplete combustion of C-4, marks the path of the snow into the throat of the vortex. The displacement of the colored columns illustrates limits of the motion.

Figure 41b illustrates the upward migration of what was once the shell of the explosion cavity into the vortex. The situation occurs an instant later than that illustrated in Figure 41a. The fracture and flowage are caused by release of potential energy stored in a zone surrounding the primary cavity but within the limit of complete rupture.

Figure 41c outlines the shape of the throat an instant later and illustrates, through displacement of the one remaining colored column, the downward slumping at the crater rim that is a part of the vortex motion of the snow.

Figure 41d illustrates what is left of the roots of the vortex at the stage where scouring action predominates over the vortex action.

The vortex and scouring actions represent a sequence of events during the decline from peak pressure. The apparent crater is caused by the vortex and scouring actions, and reaches its maximum volume per pound of explosive when the scouring effect of the high-velocity gases upon the snow is maximum. Maximum velocity occurs as a result of complete conversion of the pressure head within the gas bubble to velocity head, and maximum scouring occurs at the transition depth between the fragmentation range and the air-blast range.

Mechanics of viscous-damping failure

A comprehensive analysis of the mechanics of viscous-damping failure in snow is beyond the scope of this report. The following discussion refers to the general case and does not take into account variations due to the explosive and the material. Such variations are believed consistent with and explainable by the theory of relative behavior of materials (Livingston, 1960a).

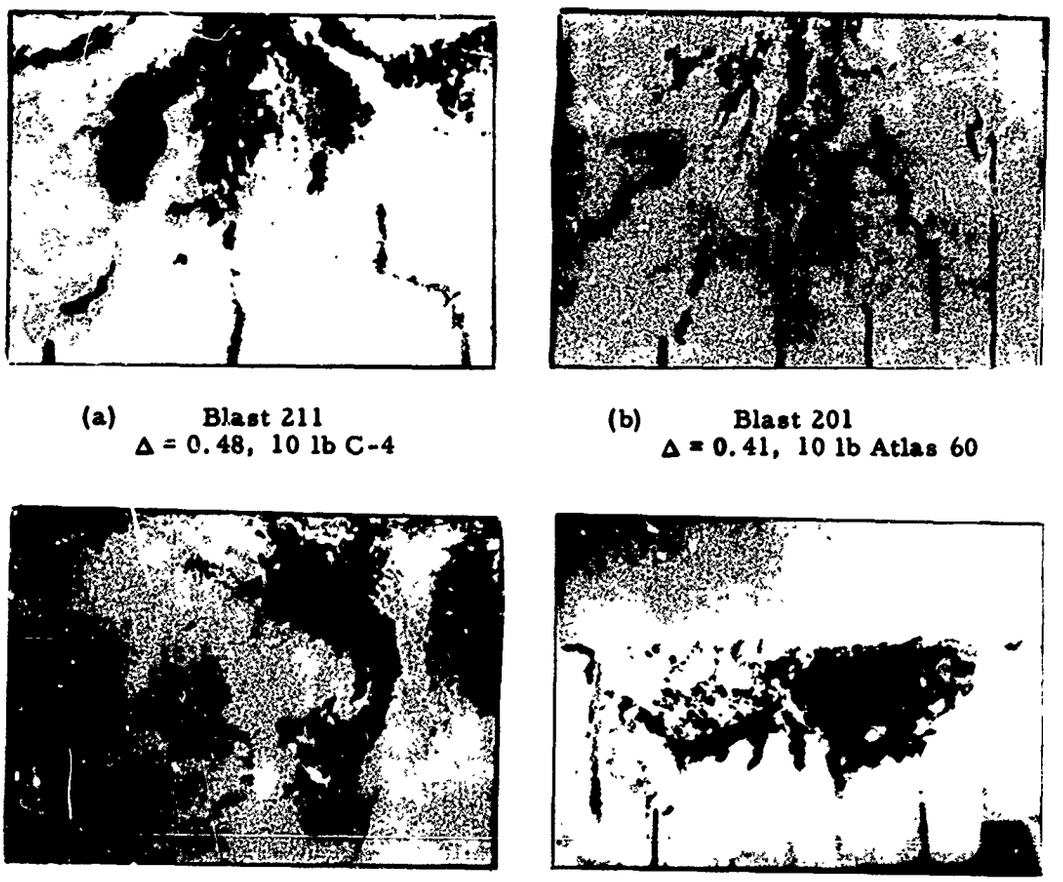

(a) Blast 211
Δ = 0.48, 10 lb C-4

(b) Blast 201
Δ = 0.41, 10 lb Atlas 60

(c) Blast 43
Δ = 0.32, 40 lb C-4

(d) Blast 36
Δ = 0.16, 10 lb C-4

Figure 41. Vortex and scouring action.

The term "viscous damping" arises from a concept of the motion of the air within the communicating voids of the snow as the material is first loaded by the force of the explosion, then unloaded. A shell of compacted snow forms as the cavity expands, and air is displaced beyond the expanding shell into the surrounding zone. The zone may be thought of as a cellular dash pot offering resistance to fluid flow. The motion of the vibrating mass is restrained by a damping force proportional to the velocity, and the action is analogous to viscous resistance in a fluid medium.

Figure 32 provides evidence of the pressure rise and of the motion of the air within the voids. Figures 39-41 provide evidence that the volume change causes motion both of the air and of the solid particles. The pressure record (Fig. 31) demonstrates that the pressure peak does not occur at the front of the disturbance, but reaches a maximum later.

The effect of the explosion upon the snow during loading depends upon the depth of the charge, the place of observation relative to the surface, and the distance to the place of observation. The loading cycle is of long duratio both because of the relatively slow propagation of the disturbance, and because

throughout the range measured the propagation velocity is greater through the solid particles than through the air in the communicating passages of the snow. The extent to which the loading cycle develops depends both upon the strength of the material and upon the depth of the charge. The extent to which it is registered depends upon the gage position. Physical properties of the snow vary with depth below the surface; but the material and the explosive are not separate and independent variables. During the loading, a substantial proportion of the energy of the explosion is required for compacting and deforming the material. Additional energy is lost to seismic effects and to fluid flow. Energy also compresses the air and stresses the solid particles.

The action differs substantially from shock failure, which is characteristic of brittle-acting substances. Failure in snow begins at the explosion cavity and proceeds outward into the material. (See Fig. 38 and 40a). Doming occurs above the charge and is accompanied by failure on radial planes which begin at the collar of the borehole and proceed outward and downward into the material. Shear displacement occurs along the bedding planes, and, as the action proceeds, the beds are domed up into concentric shells such as those observed when blasting in frozen dredge-fill silt (Livingston, 1956: p. 42-46, Fig. 53-54).

During unloading, much of the energy expended to compress air in the voids and passages of the snow is recovered and re-expended in both fracture and flow. It appears likely that a part of the energy stored in the solid snow particles also may be recovered (Livingston, 1960b, Fig. 21).

The phenomenon of implosion and the vortex and scouring actions observed in these tests relate fracture and flowage not only to loading, but also to unloading. The vortex action follows implosion, which begins at critical depth. Because more of the energy partitions to the atmosphere, effects dependent upon loading and unloading of the snow become less predominant as the depth of charge decreases. As depth decreases further to the point of transition from the fragmentation range to the air-blast range, a substantial part of the energy of explosion is partitioned to the atmosphere; at this point events dependent upon partitioning of energy to the snow become less apparent than the vortex action that begins with unloading.

CONSTANT QUANTITIES AND ENERGY UTILIZATION

Introduction

Although it is impractical to take it completely into account, the variation in physical properties of the snow with depth below the surface may be taken partly into account by treating blasts with each weight of explosive in the 1958 surface snow separately from those below the bottom of the wide, 12-ft-deep trenches.

For a given material, a given weight of charge, a given explosive, and a given set of detonation conditions, the parameters E, B and C of the Livingston crater equations (Livingston, 1960a, p. 7-21) are constants.

Within limits of accuracy determined largely by variations in physical properties which could not be evaluated, it can be shown that, at any given depth ratio Δ:

a) the volume of snow excavation within the limits of complete rupture for a given weight and type of explosive is a constant quantity (WE^3B) times the energy utilization number A

b) the volume per pound of explosive within limits of complete rupture for a given weight and type of explosive is another constant quantity ($E^3 B$) times the energy utilization number

c) the N-scaled volume of complete rupture for a given weight and type of explosive is a third constant quantity (B) times the energy-utilization number.

The materials-behavior index B appears in all three of the constant quantities and can be determined with certainty. The strain-energy factor E appears in two of the three constant quantities; it describes the beginning of fracturing and also can be determined with certainty. As E and B are measurable and W is known, the energy-utilization number A (which is a function of the depth ratio) can be evaluated to the same degree of accuracy as E or B.

Evaluating the strain-energy factor

The strain-energy equation

$$N = E \sqrt[3]{W}$$

where

N is the critical depth (determination described below)

E is the strain-energy factor, a factor that relates to the effect of the explosive on the material

W is the charge weight in pounds

describes in relative units an energy-mass-time relationship at the beginning of fracture. The relationship is that existing within the volume of material bounded by the disturbance at the instant of failure. As the effect at each element depends upon the loading and unloading conditions and varies with the radial distance from the charge, it is convenient to evaluate the average condition within the material rather than the specific condition at the element. Although the volume of material bounded by the disturbance at the instant of fracture is not known accurately, it is assumed that the material is homogeneous and that the surface of the disturbance is spherical.

Two methods of evaluating E are possible. Both assume that the disturbance at the instant of fracture is at a radial distance from the center of the charge equal to the critical depth N, and both depend upon determining the critical depth N experimentally. The first method is the maximum-radius-of-rupture method; in it the critical depth is taken as the charge depth which maximizes radial distance from charge center to limit of extreme rupture. The second method is the method of direct observation and pinpointing; in it the critical depth is defined as the depth at which fracturing begins. The depth at which fracturing begins can be distinguished from the limit to which fracturing proceeds; the difference between the two depends on the explosive and the material.

In an ideal brittle material, the disturbance is communicated to the surface at infinite velocity; and at the surface above the charge, the fracture begins when the vertical displacement is zero. In less-brittle materials, the disturbance is communicated to the surface at finite velocity, and surface uplift at failure is substantial. As the material is domed up, the maximum slant distance from the charge to the surface at the limit of extreme rupture becomes greater than the vertical distance. Shock-type failure becomes less frequent as the material becomes less brittle and as deformation without loss of cohesion occurs.

Although both methods were used here, the method of direct observation and pinpointing is more consistent with definitions and terminology adopted here, and makes possible a correlation between the limits of complete and extreme rupture. It also provides a means whereby the beginning of fracture and the beginning of doming may be related to the critical distance.

The critical depth is first approximated between some known depth at which fractures do appear at the surface and a greater depth at which they do not. The difference between the two is then reduced successively as the work proceeds. The limiting total vertical deformation at which fracturing of the snow begins is estimated visually with the aid of motion pictures and a ground scale. The permanent displacement corresponding to the total displacement is similarly noted. A correlation between pattern of fracture and permanent displacement is established during excavation.

Figure 3 indicates the manner in which information obtained using 1.0-lb test shots at 1.0-ft increments of depth was extrapolated to larger charges and at the same time the distance between shots straddling critical depth was successively reduced. The 2.5-, 10- and 40-lb shots are routine shots in which the test geometry was held constant in an attempt to correlate instrumentation and breakage effects using the cube root of the charge weight as a scaling factor.

Table VI summarizes values of the strain-energy factor as determined by the method of direct observation and pinpointing and later supplemented by use of motion pictures and the crater cross sections.

Determining the depth ratio at optimum depth

The charge depth at which fracturing proceeds to completion, but no further, is the optimum depth d_0, and the general equation applied to this situation is

$$d_0 = \Delta_0 \; E \sqrt[3]{W}$$

where Δ_0 is the optimum depth ratio and equals $\frac{d_0}{N}$.

Optimum depth d_0 and optimum Δ_0 may be determined in either of two ways. One employs an office technique in which V/W within limits of complete rupture is plotted against the depth ratio Δ to determine the specific value Δ_0, where V/W is maximum. The other combines field and office techniques as in the method of direct observation and pinpointing to determine critical depth. At depth d_0 the energy-utilization number A is unity, and the maximum proportion of the total energy of the explosion is expended in: 1) fractures formed during the rise to peak pressure, and 2) fractures formed during implosion or elastic rebound by release of potential energy stored during loading.

Experience has shown that breakthrough of the gas bubble occurs if the depth ratio is slightly less than Δ_0, and that V/W within limits of complete rupture reaches a maximum just before venting occurs. Experience also has shown that the noise level changes substantially when the gas bubble breaks through, and that breakthrough occurs in materials such as ice and snow immediately after the material is domed to near-hemispherical shape.

The method of direct observation and pinpointing consists of approximating d_0 between a charge that is too deep and does not dome the surface to near-hemispherical shape, and one that is too shallow and domes the surface beyond the hemispherical shape so that plumes begin (Cole, 1948), the

Table VI. Constants for charges of spherical shape.

Charge weight lb W	Materials behavior index B	Strain energy factor E	E^3	BC	E^3 BC	WE^3 BC	Charge weight lb W	Materials behavior index B	Strain energy factor E	E^3	BC	E^3 BC	WE^3 BC
Atlas 60 1958 Surface Δ_0 = 0.58							C-4 1958 Surface Δ_0 = 0.58						
1.0	--	7.3	389	--	--	--	1.0	--	6.2	238.3	--	--	--
2.5	0.61	7.3	389	0.61	237.3	593.2	2.5	0.59	6.2	238.3	0.59	140.1	350.3
5.0	0.51	7.3	389	0.51	197.6	988.1	5.0	0.56	6.2	238.3	0.56	132.5	662.5
10.0	0.42	7.3	389	0.42	164.9	1649.4	10.0	0.52	6.2	238.3	0.52	123.9	1239.3
20.0	--	7.3	389	--	--	--	20.0	--	6.2	238.3	--	--	--
40.0	0.31	7.3	389	0.31	119.8	4792.8	40.0	0.42	6.2	238.3	0.42	101.0	4042.0
Coalite 7S 1958 Surface Δ_0 = 0.57							Atlas 60 Trench Blasts Δ_0 = 0.63						
1.0	0.44	6.0	216	0.44	95.0	95.0	2.5	0.58	6.2	238.3	0.58	138.0	345.0
2.5	0.55	6.0	216	0.55	119.0	297.5	10.0	0.73	6.2	238.3	0.73	174.0	1739.8
5.0	--	6.0	216	--	--	--							
10.0	0.49	6.0	216	0.49	106.0	1060.6	Coalite 7S Trench Blasts Δ_0 = 71						
20.0	--	6.0	216	--	--	--	2.5	0.72	4.8	110.5	0.72	79.6	199.0
40.0	0.43	6.0	216	0.43	92.0	3680.8	10.0	0.86	4.8	110.5	0.86	95.1	951.1

noise level increases abruptly, and fragmentation of the flyrock increases so as to begin to obliterate the primary fracture pattern. Motion pictures record a ground scale, the displacement of the uplifted snow, and venting phenomena. The range of particle sizes is observed, and the shape of the fragments noted.

Figures 1-5 indicate the method of pinpointing and the straddling procedure used in the field to determine Δ_0 in first approximation. Through use of the above method, the 1958 snow-surface data were extrapolated to 160-lb charges as accurately as the charges could be positioned with respect to the pressure gages.

The office procedure (in which field data available at the time of the blast are supplemented by all of the available data to determine d_0 and Δ_0 more accurately) is essentially the same as the office procedure to determine critical depth.

Values of Δ_0 thus determined are summarized in Table VI. In 1958 surface snow and trench snow, both E and Δ_0 were found to be independent of charge weight (in glacier ice, however, they were found to be dependent) (Livingston, 1960b).

Evaluating the materials-behavior index

The materials-behavior index B is a constant for a given type of explosive and weight of charge in a given material. Variation in B is due to: 1) an increase or decrease in lateral confinement depending upon the depth of charge, or 2) an increase or decrease in the failure stress depending both upon the lateral confinement and the loading rate (which in turn depends upon both the material and the explosive).

Evaluation is based upon the equation:

$$B = \frac{V_0}{N^3}$$

where V_0 is the volume within limits of complete rupture at optimum depth, and N is the critical depth.

The materials-behavior index equals a constant of proportionality times a dimensionless ratio of lengths to the third power. The length defined by V_0 is that at which the average energy density within the material is sufficient to complete the failure process. The length defined by N is that at which fracturing begins. Experience has shown that B decreases as energy requirements for deformation without loss of cohesion or for flowage increase. High values of B are indicative of brittle failure, and low values of B are indicative of a more ductile type. A decrease in B is indicative of: 1) an increase in energy density, 2) a change from brittle-acting to more-plastic-acting material, or 3) a decrease in loading rate.

Table VI summarizes the constant quantities B, E^3B, and WE^3B for various weights of each of the test explosives.

The energy-utilization number A

The energy-utilization number is a dimensionless ratio of volumes (one the extent to which the failure occurs at any depth, the other the extent to which failure occurs where the maximum proportion of the energy of the explosion is utilized in loading the material).

It is difficult to measure energy partitioning or to describe it in absolute units. For the present it is most practical to relate energy to charge weight and to relate energy partitioning to a prototype situation in which the maximum proportion of the energy of the explosion is partitioned to loading the material. By use of the theory of relative behavior of materials, it is possible to predict that the proportion of the total energy of the explosion partitioned to loading the material is variable rather than constant, and that the variation depends upon: 1) the loading rate, 2) the relative brittleness or ductility of the material, and 3) the failure stress (which depends upon the average energy density required to complete the primary fracture process).

The method chosen here to describe energy partitioning is one in which geometric similarity is extended to the failure process. The energy-utilization number is assigned a value of unity when primary fractures caused by loading and unloading proceed to completion, but little energy is lost to the atmosphere and little is used to accelerate the flyrock; the volume of snow within limits of complete rupture is maximum; and the depth of the charge equals optimum depth. At charge depths less than optimum depth d_0, energy is left in the gas bubble or is available to and utilized for requirements other than the primary fractures. At charge depths greater than d_0, the quantity of energy available to the fracture process is less than that required (in a given mass of material affected by the disturbance) to extend the fractures to completion. At depths either greater than or less than d_0, $\underline{A}$ is less than 1.0 and V/W within limits of complete rupture is less than the maximum.

The energy-utilization number may be evaluated using the breakage-process equation and the family of curves obtained by plotting V/W within limits of complete rupture against the depth ratio Δ. Transition points, which mark the limits between the various ranges of behavior in cratering, describe maxima, minima, and points of inflection on both the $\underline{A}$ and the V/W vs Δ curves. The use of the transition points as an aid in curve sketching is analogous to use of maxima, minima, and points of inflection determined by differentiating known equations.

The curves of Figures 42-46 were obtained by dividing V/W at any given value of Δ by the constant quantity $E^3 B$ listed in Table VI for the appropriate type of explosive, weight of charge, and type of snow. The points of the figures are based upon the equation:

$$A = \frac{V}{V_0}$$

where V is the volume within limits of complete rupture, and V_0 is the same volume at optimum depth.

Use of the energy-utilization curves is illustrated by the following example problems.

Example problem 1. A 40-lb spherical charge of C-4 is detonated 8.0 ft below the surface of the Greenland Ice Cap. What is the volume of snow within the limits of complete rupture?

Solution: $\Delta = \frac{d_c}{N}$

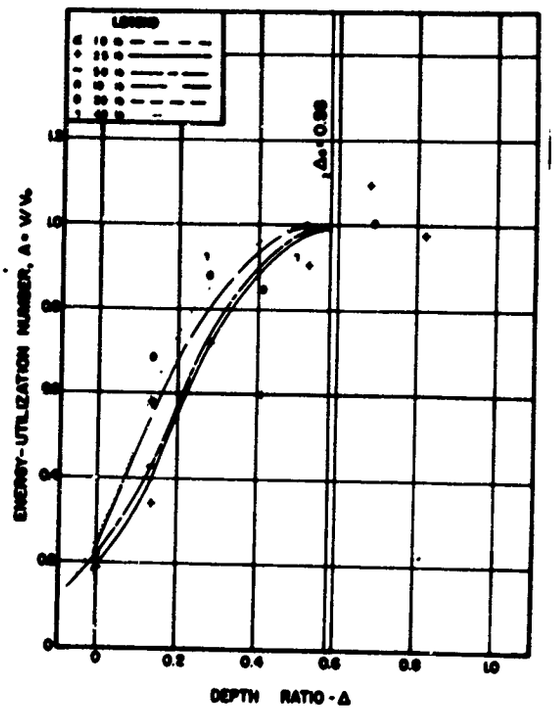

Figure 42. Energy-utilization no., surface snow, Atlas 60.

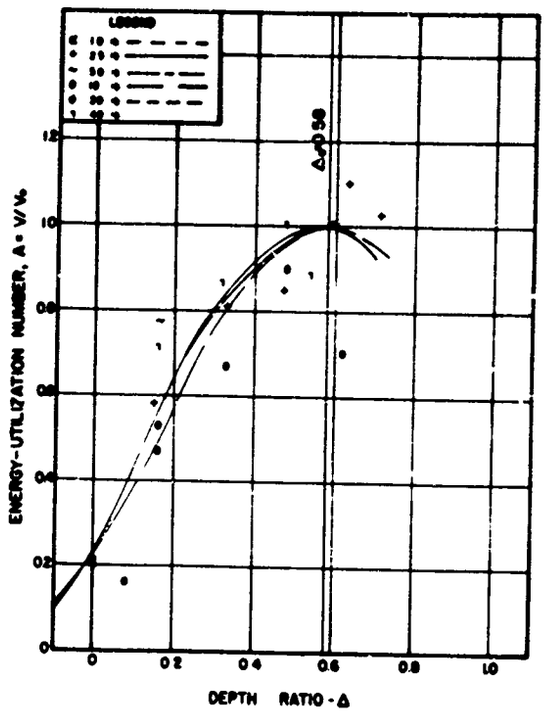

Figure 43. Energy-utilization no., surface snow, C-4.

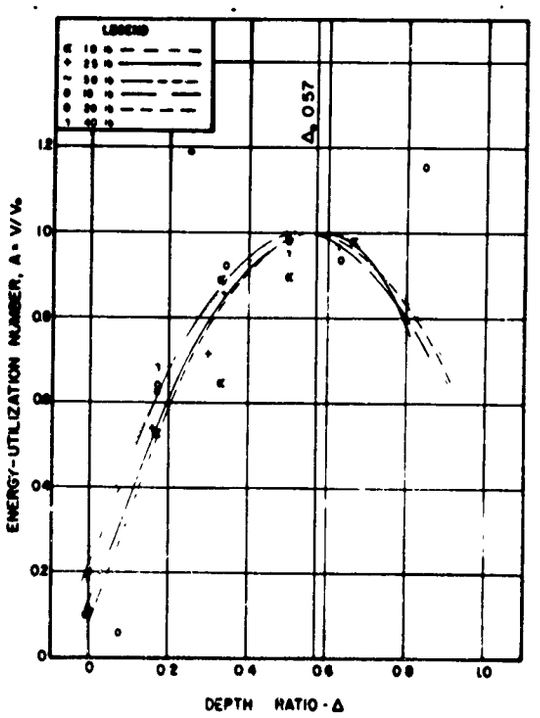

Figure 44. Energy-utilization no., surface snow, Coalite 7S.

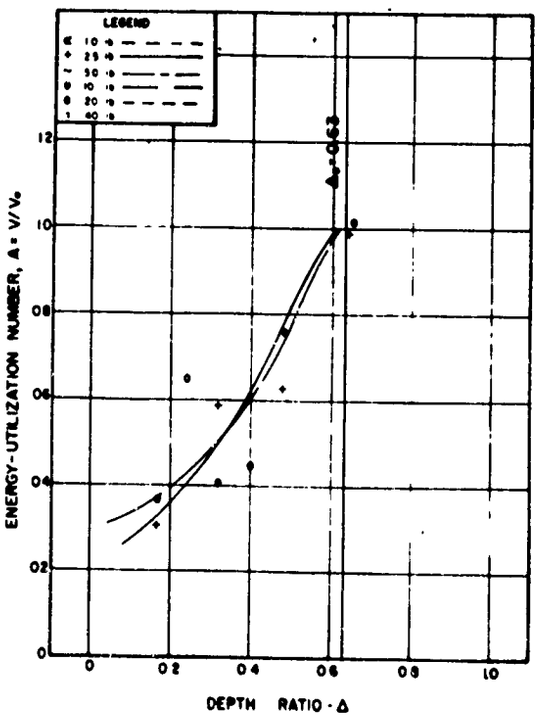

Figure 45. Energy-utilization no., trench snow, Atlas 60.

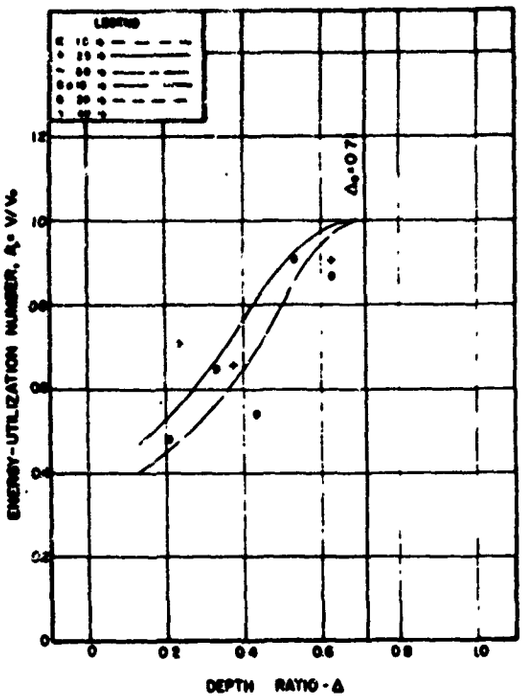

Figure 46. Energy-utilization no., trench snow, Coalite 7S.

and using the strain-energy equation and E from Table VI

$$N = E \sqrt[3]{W} = 6.2 \sqrt[3]{40} = 21.2 \text{ ft}$$

$$\Delta = \frac{8.0}{21.2} = 0.38.$$

The breakage-process equation

$$\frac{V}{W} = ABCE^3$$

can be rewritten as

$$V = (A)(WE^3B)$$

if the charge is of spherical shape (and hence C = 1.0). From Figure 43 at $\Delta = 0.38$, A = 0.92: and from Table VI, $WE^3B = 4042$; so

$$V = (0.92)(4042) = 3719 \text{ ft}^3.$$

Example problem 2. A 10-lb spherical charge of Coalite 7S is set off at a depth of 6.0 ft in 1958 surface snow: another 10-lb spherical charge is set off at the same depth in trench snow: compare the two volumes broken (volumes within limits of complete rupture) per pound of explosive.

Solution for first charge, 1958 surface snow:

From Table VI,

$$E = 6.0$$

$$N = E\sqrt[3]{W} = 6.0\sqrt[3]{10} = 12.92$$

$$\Delta = \frac{d_c}{N} = \frac{6.0}{12.92} = 0.46$$

$$\frac{V}{W} = (E^3 B) \cdot A$$

$$E^3 B = 106.06.$$

From Figure 44 at

$$\Delta = 0.46, \quad A = 0.965$$

$$\frac{V}{W} = 102.3 \text{ ft}^3/\text{lb}.$$

Solution for second charge, trench snow:

From Table VI

$$E = 4.8$$

$$N = E\sqrt[3]{W} = 4.8\sqrt[3]{10} = 10.34$$

$$\Delta = \frac{d_c}{N} = \frac{6.0}{10.34} = 0.58$$

$$\frac{V}{W} = (E^3 B) \cdot A$$

$$E^3 B = 95.11.$$

From Figure 46 at

$$\Delta = 0.58, \quad A = 0.92$$

$$\frac{V}{W} = 87.5 \text{ ft}^3/\text{lb}.$$

Example problem 3. In blasts of glacier ice with 40-lb charges of C-4 at various depths, the maximum volume broken (within limits of complete rupture) is 1600 ft^3, and the corresponding optimum depth is 10.9 ft. If the same charge is used, what volume of Greenland Ice Cap 1958 surface snow would be broken, and at what depth should the charge be placed?

Solution: $V = WE^3ABC$

$C = 1.0$ for spherical charge

$A = 1.0$ at optimum depth.

From Table VI, right column, for a 40-lb charge of C-4,

$$WE^3BC = 4042$$

$$V = (A)(WE^3BC) = (1.0)(4042) = 4042 \text{ ft}^3$$

$$\Delta_0 = 0.58 \text{ and } E = 6.2$$

$$N = E\sqrt[3]{W} = 6.2\sqrt[3]{40} = 21.2 \text{ ft}$$

$$d_0 = \Delta_0 N = 0.58 \times 21.2 = 12.3 \text{ ft.}$$

CRATER EVALUATION

Apparent crater

An apparent crater may be formed by an air burst, a contact burst or an undersnow burst, and the volume of any of these apparent craters will vary with the charge position. A part of the energy of the explosion causes snow to move into the vortex (Fig. 41b); a second part causes scouring of the surface (Fig. 41d); but the relative amount of energy in these parts varies greatly in air bursts, contact bursts, and undersnow bursts. If one relates dimensions of the apparent crater to those of the limits of complete rupture and extreme rupture, the question arises: "After implosion, what proportion of the total energy of the explosion is available to cause an apparent crater to form?" In convention adopted here, the volume of the apparent crater is maximum at the transition from the air-blast range to the secondary-fragmentation range where the maximum volume of apparent crater per pound of explosive occurs and the maximum proportion of the energy of the explosion is available near the snow surface as velocity head.

Figures 47-49 summarize the variation in V/W of the apparent crater with the depth ratio. A depth ratio of zero represents a contact burst, and a negative depth ratio represents an air burst. The volume of the apparent crater varies with the depth ratio, the weight of the charge, and the type of explosive. Inspection of the figures shows that V/W of the apparent crater reaches a maximum in the range $0.15 < \Delta < 0.20$. As the weight of the charge and the scale of the experiment increase, V/W of the apparent crater decreases. The decrease is inconsistent with conventional cube root scaling. The result, however, is predictable from the energy-utilization curves (Fig. 42-44).

In the region where V/W of the apparent crater is maximum, the energy-utilization number ranges from 0.4 to 0.7, depending upon the explosive and the material. The energy-utilization number for a contact burst in 1958 surface snow varies from 0.1 to 0.4 depending upon the explosive, the material, and the weight of the charge. Because the energy-utilization number is a relative measure of the proportion of the energy of the explosive that is partitioned to loading the material, it follows from the relations of Figures 47-49 that the dimensions of the apparent crater in snow (which are determined primarily by events subsequent to loading) are neither predictable with accuracy nor usable as a basis for accurately predicting undersnow damage.

Figures 50-52 summarize the variation in the N-scaled depth of the apparent crater in 1958 surface snow with the depth ratio, and Figures 53-55 summarize the variations in the N-scaled apparent-crater radius with the depth ratio. Both sets of curves are designated preliminary because the evaluation has been empirical. A comprehensive analysis which applies the

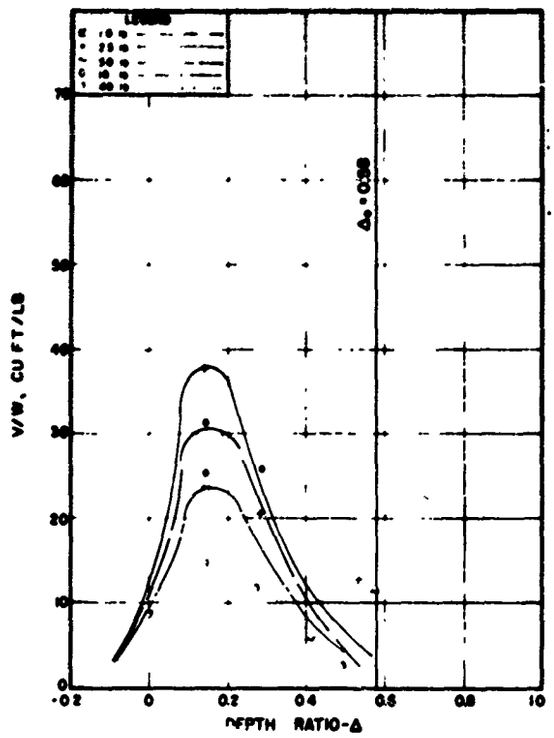

Figure 47. Apparent crater V/W vs Δ, surface snow, Atlas 60.

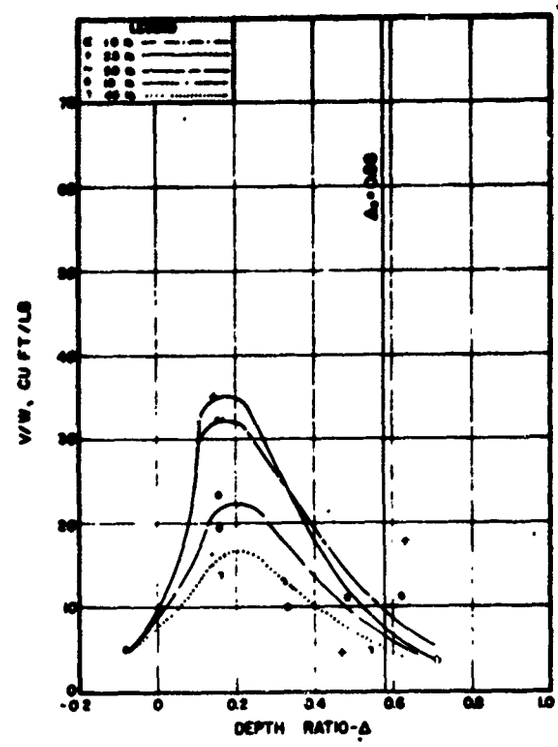

Figure 48. Apparent crater V/W vs Δ, surface snow, C-4.

theory of relative behavior of materials to the apparent crater and which correlates the apparent crater with the limits of complete rupture and with airblast and underground shock effects in snow is beyond the scope of this report.

Evaluating dimensions within limits of complete rupture

To establish geometric similarity, in the system employed here, length and volume measurements are divided by the critical depth, which results in a ratio analogous to the depth ratio.

The interdependence of the N-scaled measurements and the parameters A, B, and C is:

$$\pi K_s (K_r)^2 K_h = K = A \cdot B \cdot C$$

where

K_s is the crater-shape factor

K_r is the N-scaled crater radius

K_h is the N-scaled crater depth

K is the N-scaled crater volume

A is the energy-utilization number

B is the materials-behavior index

C is the stress-distribution number.

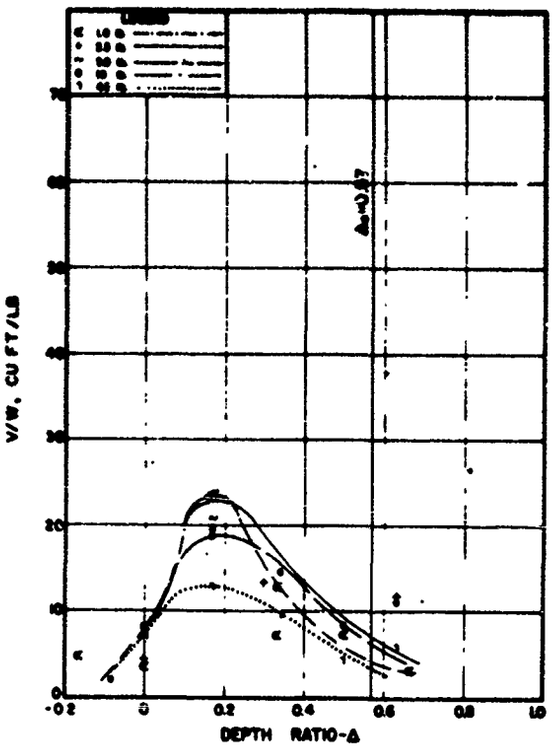

Figure 49. Apparent crater V/W vs Δ, surface snow, Coalite 7S.

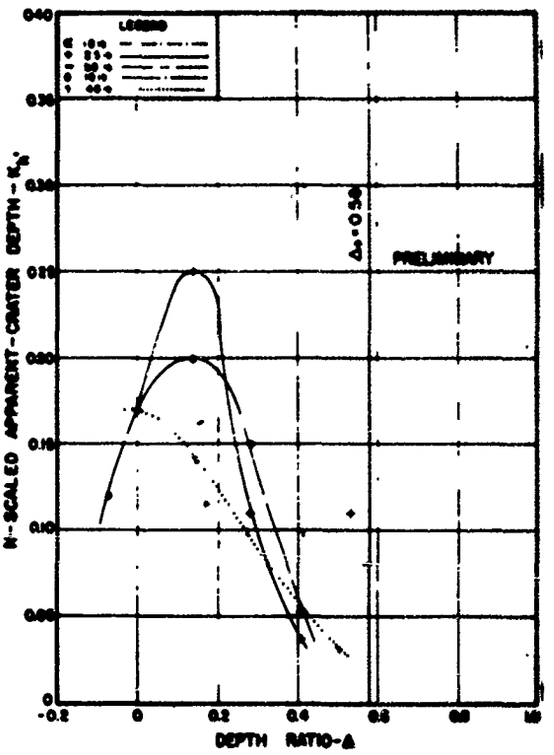

Figure 50. N-scaled apparent-crater depth, surface snow, Atlas 60.

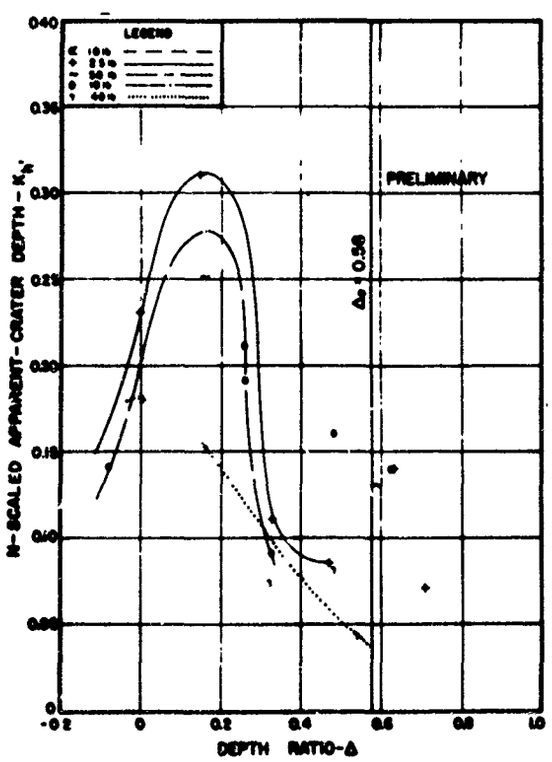

Figure 51. N-scaled apparent-crater depth, surface snow, C-4.

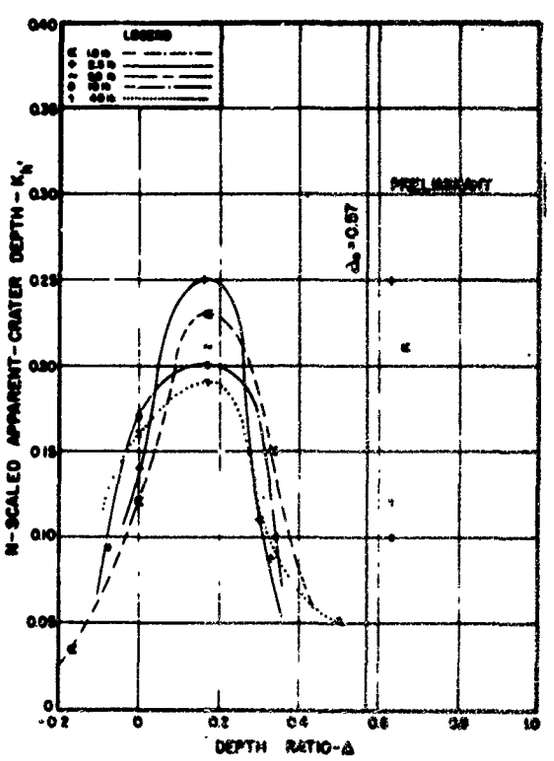

Figure 52. N-scaled apparent-crater depth, surface snow, Coalite 7S.

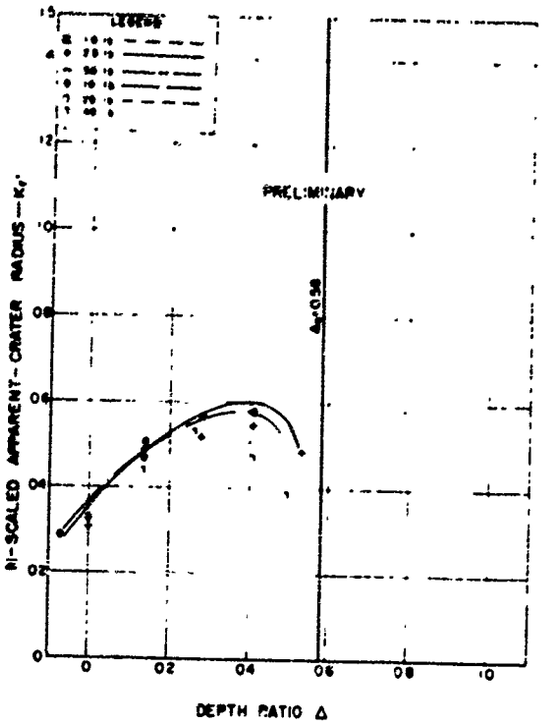

Figure 53. N-scaled apparent-crater radius, surface snow, Atlas 60.

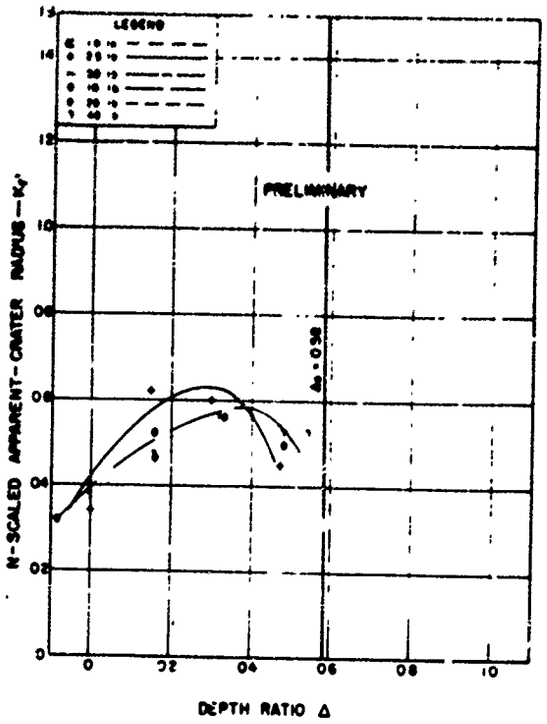

Figure 54. N-scaled apparent-crater radius, surface snow, C-4.

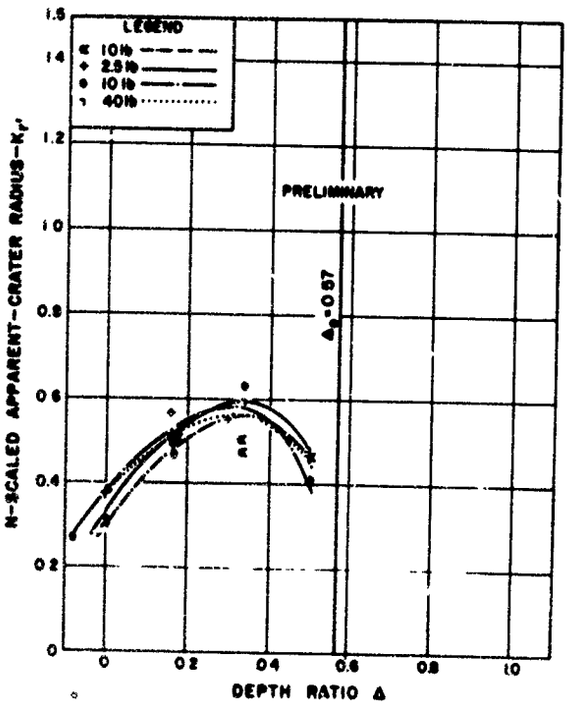

Figure 55. N-scaled apparent-crater radius, surface snow, Coalite 7S.

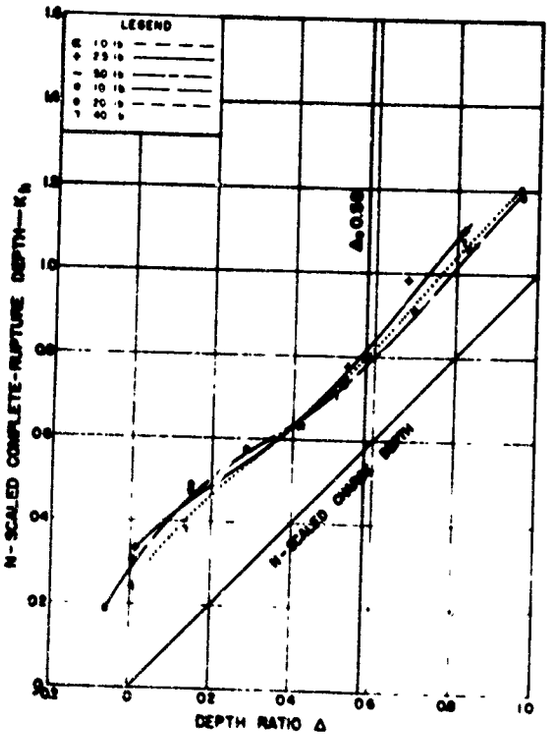

Figure 56. N-scaled complete-rupture depth, surface snow, Atlas 60.

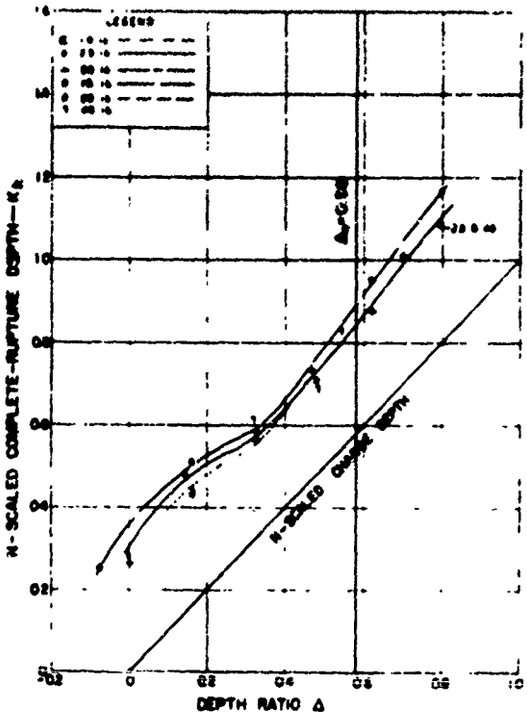

Figure 57. N-scaled complete-rupture depth, surface snow, C-4.

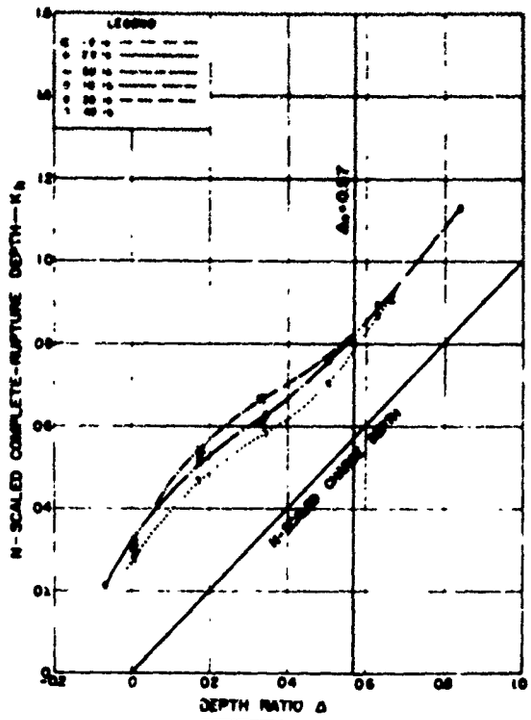

Figure 58. N-scaled complete-rupture depth, surface snow, Coalite 7S.

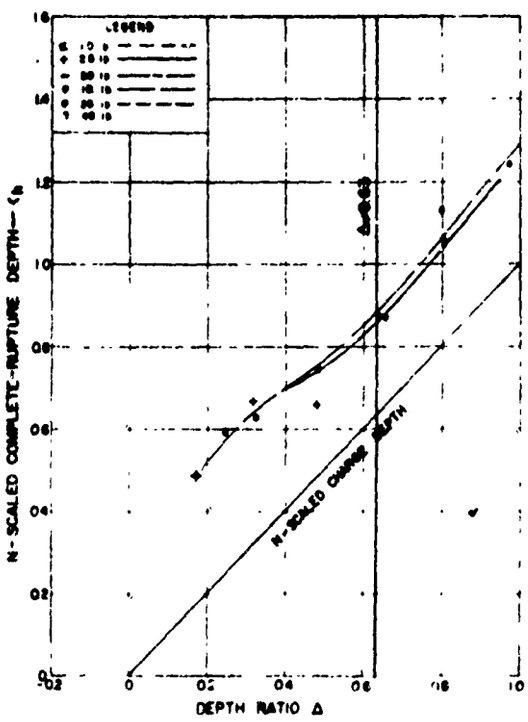

Figure 59. N-scaled complete-rupture depth, trench snow, Atlas 60.

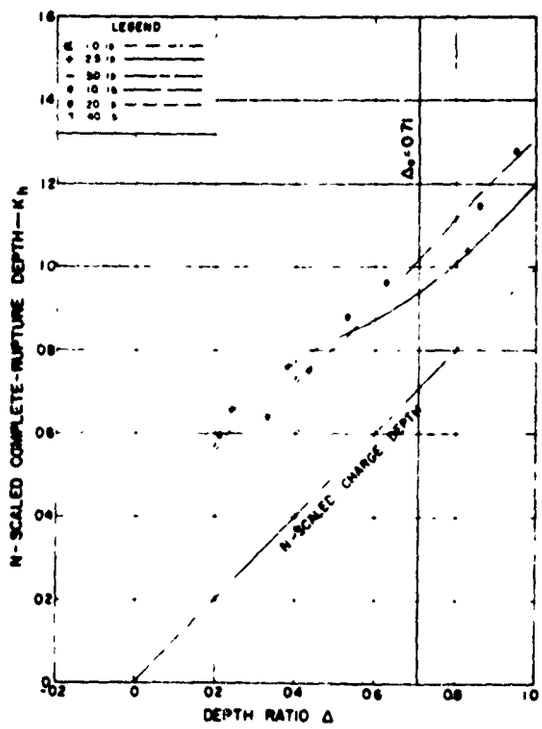

Figure 60. N-scaled complete-rupture depth, trench snow, Coalite 7S.

In blasts with a given weight, type, and shape of explosive under conditions such as employed in the snow tests, the materials-behavior index and stress-distribution number are constants and the N-scaled crater volume, K, is a function of the energy-utilization number. Inasmuch as the shape, the radius, and the depth determine K, each is dependent upon the energy-utilization number, which is a function of the depth ratio.

The N-scaled crater depth K_h

The explosion cavity is destroyed when implosion occurs, so that it is difficult to correlate accurately either the depth of the true crater or the depth of complete rupture with the vertical radius of the explosion cavity (r_v of Fig. 28). The bottom of the explosion cavity before implosion lies somewhere between the bottom of the complete-rupture limit and the bottom of the true-crater limit.

Figures 56-60 summarize the variation of depth of complete rupture with the depth ratio. The shapes of the curves are similar, but the behavior of the material is not independent of charge weight or explosives type. The vertical distance from the center of the charge to the depth of complete rupture is maximum in the region where V/W of the apparent crater is maximum and scouring of the snow is most effective. The distance is minimum in the secondary-fragmentation range at a depth slightly less than the optimum depth where the vortex motion of the snow has its greatest effect upon the limit of complete rupture.

The complete-rupture shape factor K_s

If identical blasts are fired in various materials using a given type of explosive and shape of charge, the shape of the resulting crater varies widely. Various methods of describing the shape of a crater are used, and each has its advantages and disadvantages. Experience has shown that the shape of the crater is an index to the behavior of both the explosive and the material; but the relations are complex because analogous changes may be a result of a change in loading rate, a change from brittle-acting to plastic-acting materials, or a change in energy density.

The crater-shape factor is

$$K_s = \frac{V}{\pi r^2 h}.$$

The crater defined by the limit of complete rupture will be trumpet-shaped for K_s values of less than 1/3, hemispherical for values of 2/3, and bowl- or dish-shaped for values greater than 2/3.

Because the shape is irregular in most materials, and because under field conditions such as occur in the Arctic it is difficult to see all of the cracks, considerable dispersion occurs between values of K_s at a given scaled charge depth computed from the above formula. A slight error when determining the average radius of complete rupture unduly affects the crater-shape factor. A cut-and-try method is used here to minimize the difficulties of field measurement. It is based upon the fact that the volume within limits of complete rupture must satisfy the summary curves of the various parameters of all three of the following equations:

$$V_r = K_s \pi r^2 h$$

$$V_r = WE^{3}ABC$$

$$V_r = KN^{3}.$$

Figures 61-65 summarize the variation in crater shape with the depth ratio. The shape within limits of complete rupture in 1958 surface snow changes from dished to nearly hemispherical as the height of burst decreases, approaching a contact burst. The shape both in 1958 surface snow and trench snow changes moderately as the depth below the surface increases. A local minimum occurs at a depth slightly less than that at which scouring has its greatest effect. The minimum approaches the conical in trench snow which has strength in shear; but the shape is intermediate between hemispherical and conical in lower-density snow. As the depth of charge increases in low-density snow so as to approach that at which the vortex motion is best developed, a local maximum occurs and the shape for small-scale blasts is nearly hemispherical. As the scale of the experiment (or the density and strength of the snow at the charge position) increases, the shape at the local maximum is more nearly conical.

The N-scaled complete-rupture radius K_r

The N-scaled complete-rupture radius is measured horizontally at the surface and is a dimensionless number equal to the horizontal radius of complete rupture divided by the critical depth. Because linear dimensions describing limits of complete rupture are dependent upon volume dimensions, and because they must agree with the parameters of the breakage-process equation, it can be shown that the N-scaled complete-rupture radius equals

$$K_r = \frac{\sqrt{ABC}}{\pi K_s K_h}.$$

Accordingly, if values of A, B, C, K_s, and K_h are fixed, as they are in the evaluation procedure adopted here, the analyst is left little freedom when evaluating K_r.

Figures 66-70 summarize the variation in K_r with the depth ratio separately by explosives type for each of the various weights of explosive charge tested in 1958 surface snow and trench snow. The points indicate the dispersion of individual measurements

$$K_r = \frac{r_r}{N}$$

from the solution obtained using values of K_s, K_h, and A from figures previously presented and values of B as recorded in Table VI.

Inspection of the figures shows that the maximum radius in snow is achieved in the secondary-fragmentation range where K_h is minimum (see Fig. 56-60). Under such conditions, the vortex motion within the snow is well developed and acceleration of the displaced snow is sufficient to destroy the primary fracture pattern. As the material becomes more brittle acting, the maximum value of K_r moves closer to that at optimum depth; and less of the energy of the explosion is required for flowage processes associated with the vortex motion which follows primary fracturing.

A correlation of complete-rupture and extreme-rupture limits

Limits of the true crater and of the apparent crater as defined here for snow bear little direct relation either to energy requirements of the various events that precede venting or to undersnow damage, and thus are eliminated from the following correlation.

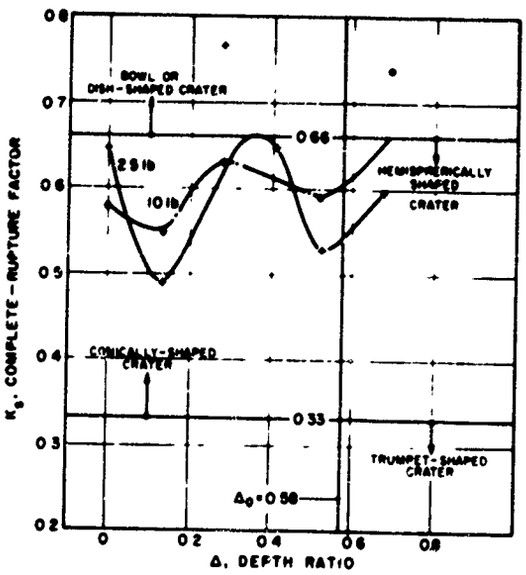

Figure 61. Crater-shape factor, surface snow, Atlas 60.

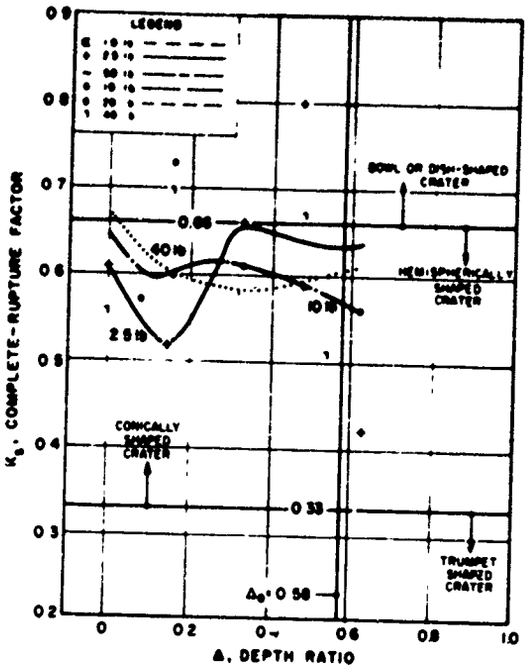

Figure 62. Crater-shape factor, surface snow, C-4.

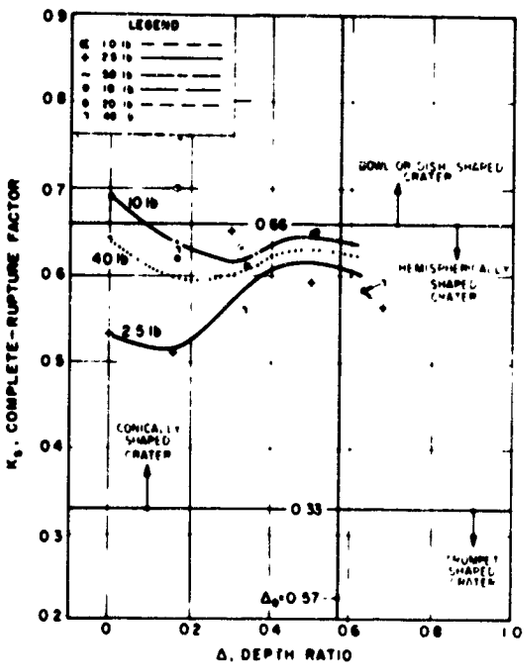

Figure 63. Crater-shape factor, surface snow, Coalite 7S.

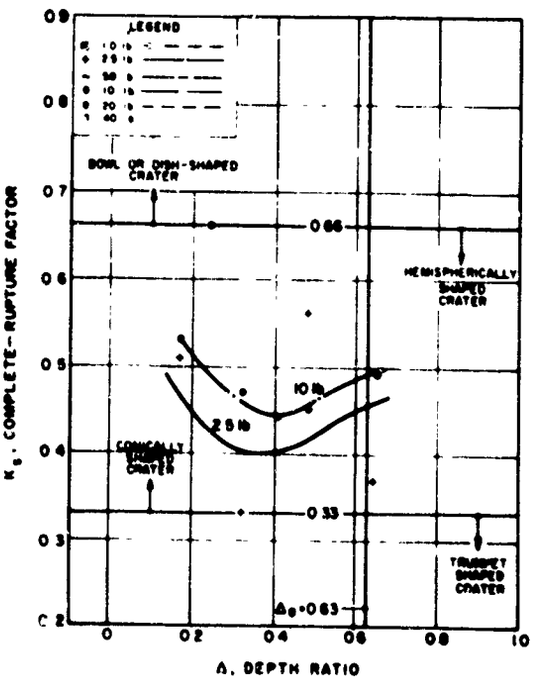

Figure 64. Crater-shape factor, trench snow, Atlas 60.

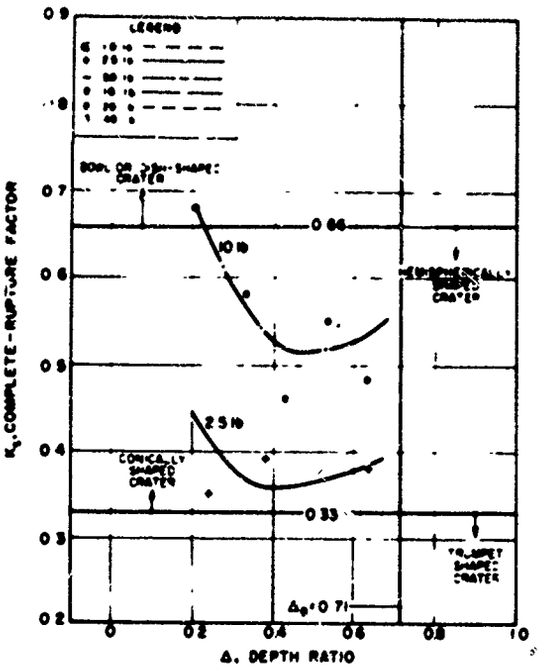

Figure 65. Crater-shape factor, trench snow, Coalite 7S.

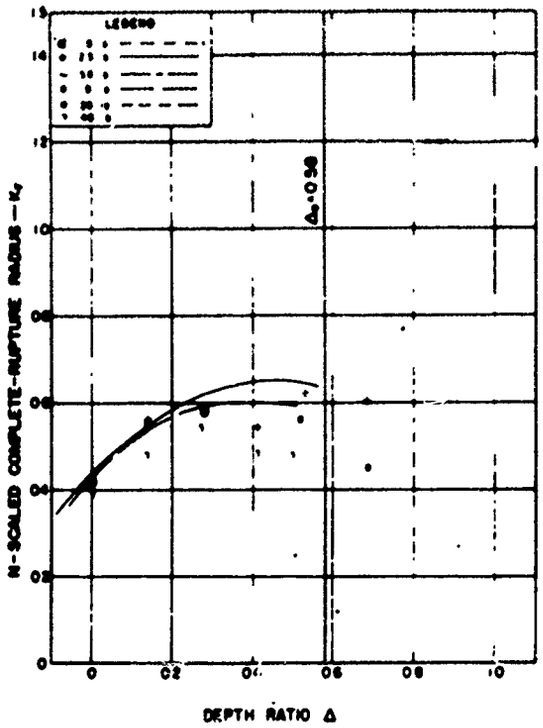

Figure 66. K_r vs Δ, surface snow, Atlas 60.

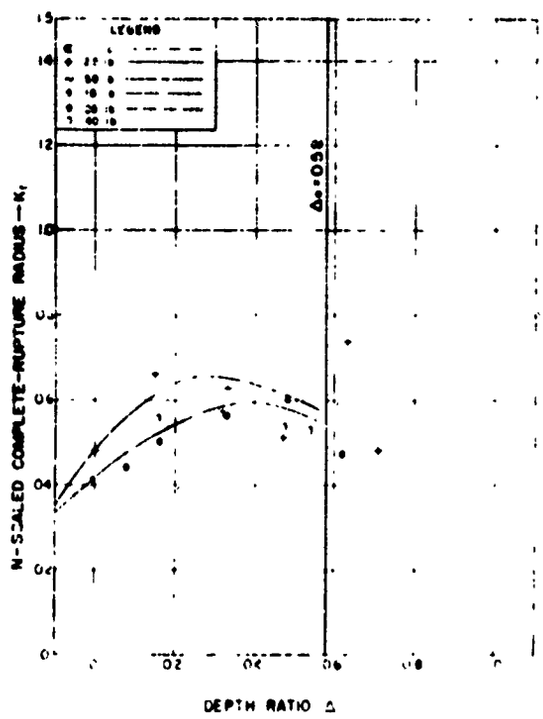

Figure 67. K_r vs Δ, surface snow, C-4.

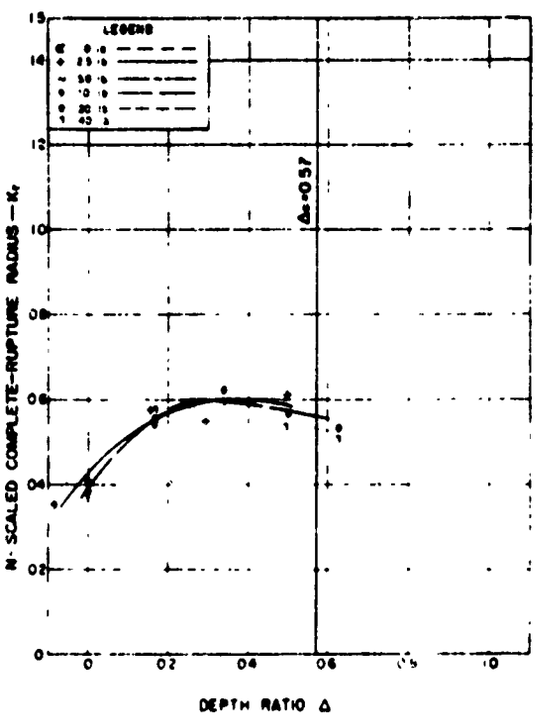

Figure 68. K_r vs Δ, surface snow, Coalite 7S.

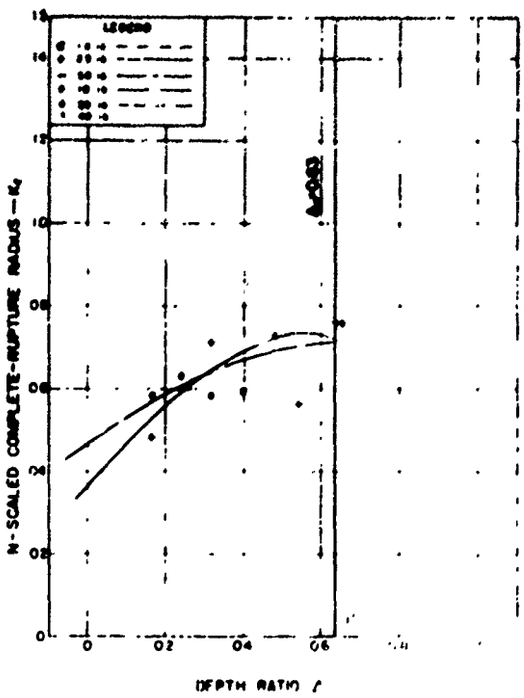

Figure 69. K_r vs Δ, trench snow, Atlas 60.

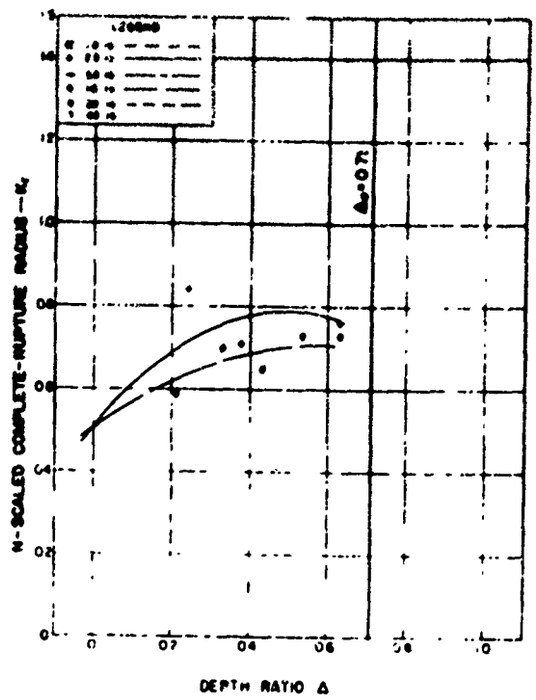

Figure 70. K_r vs Δ, trench snow, Coalite 7S.

According to terminology used here, the extreme-rupture limit relates to a free face at the snow surface and complete rupture ceases to exist if a crater does not exist. Within the range of charge depths greater than critical depth, more of the energy of the explosion is expended for seismic effects and deformation of the snow by compaction than within the primary and secondary fragmentation ranges. Similarly, within the range of charge depth less than that at which maximum scouring occurs, more of the energy of the explosion is expended in the atmosphere and less is available to the snow. Accordingly it seems desirable to confine the present discussion to the fragmentation range.

Figures 71-80 summarize empirically the interrelationships among limits of complete rupture and extreme rupture in snow. Each pair of drawings relates to a given material and includes all of the various weights of charge. As demonstrated in preceding pages, the behavior of the snow is dependent upon the scale of the experiment. For this reason and until a comprehensive analysis of the data is possible, the figures are designated preliminary. The limit of extreme rupture is determined by events that occur within the primary- and the secondary-fragmentation ranges. Extrapolation beyond the fragmentation range is not valid because of considerations of energy partitioning. Similarly, extrapolation of the limits of complete rupture and extreme rupture to charges larger than 40 lb requires the use of the breakage-process equation and is not justified at this stage of the analysis. The figures correlate empirically (using conventional cube-root scaling) the limits of complete rupture and extreme rupture, and illustrate the effect of explosive type. They also illustrate in first approximation the effect of charge depth and type of snow upon the breakage limits.

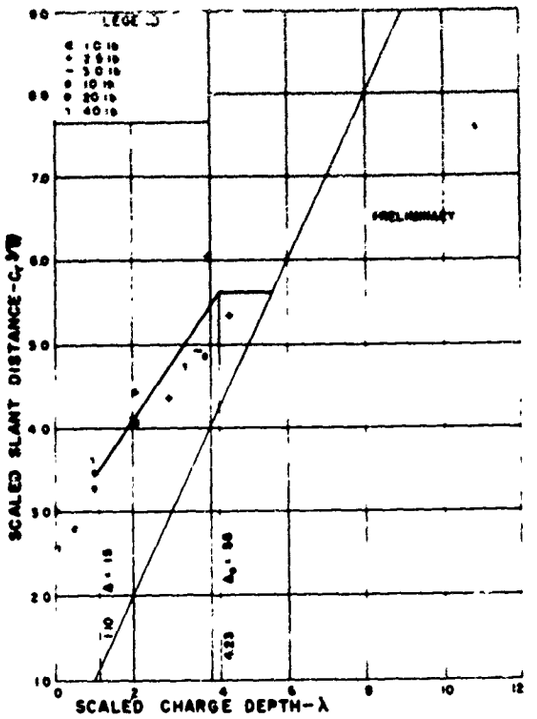

Figure 71. $C_r/\sqrt[3]{W}$ vs λ_c, surface snow, Atlas 60, complete rupture.

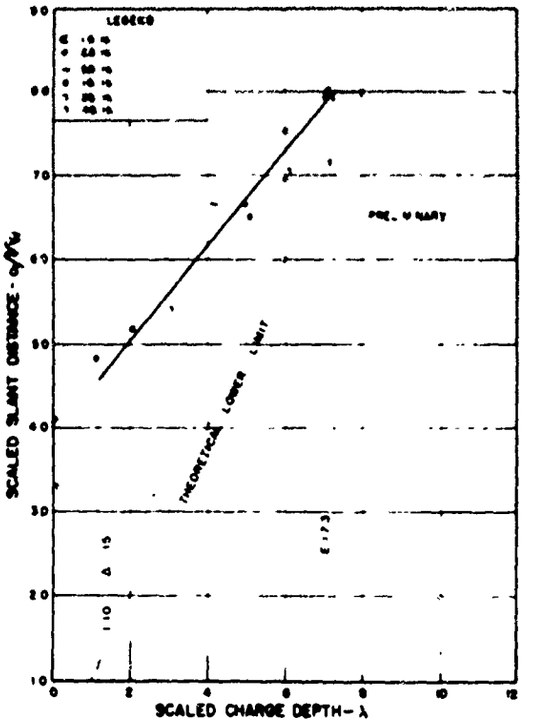

Figure 72. $C_e/\sqrt[3]{W}$ vs λ_c, surface snow, Atlas 60, extreme rupture.

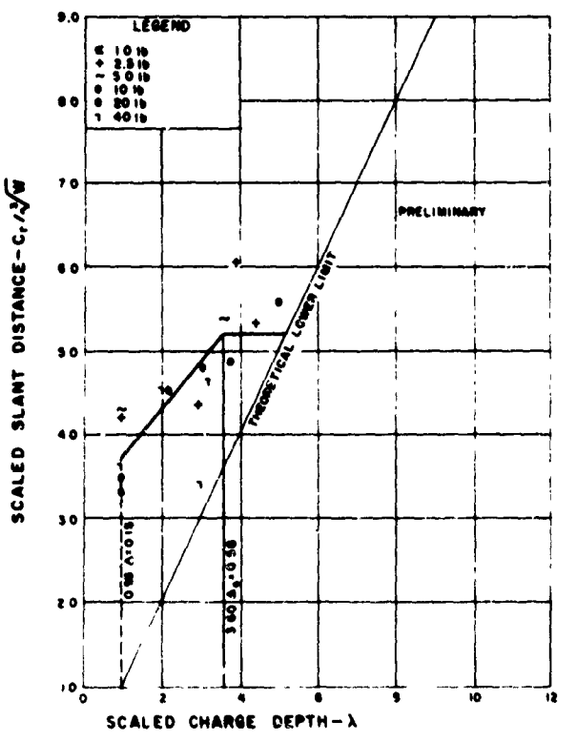

Figure 73. $C_r/\sqrt[3]{W}$ vs λ_c, surface snow, C-4, complete rupture.

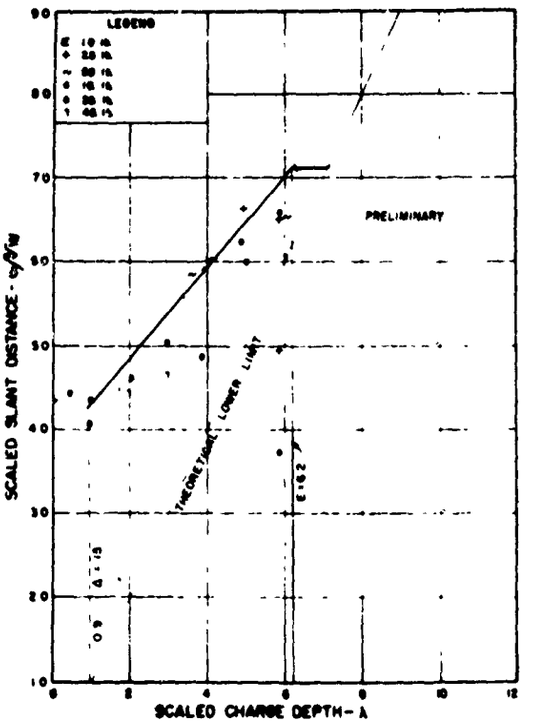

Figure 74. $C_e/\sqrt[3]{W}$ vs λ_c, surface snow, C-4, extreme rupture.

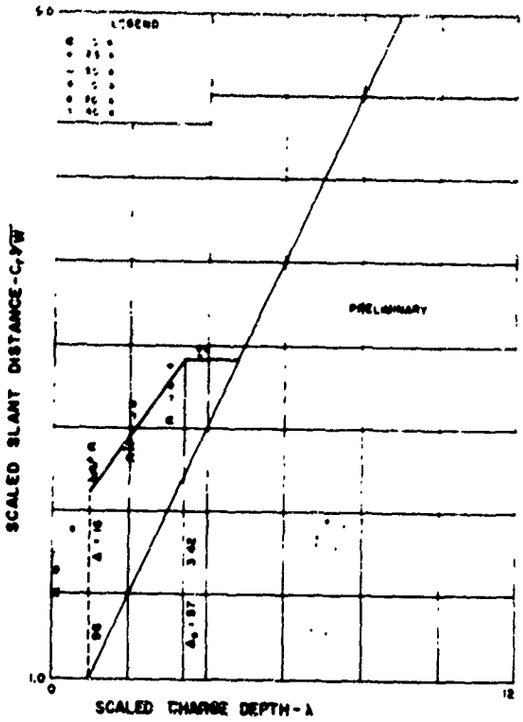

Figure 75. $C_r/\sqrt[3]{W}$ vs λ_c, surface snow, Coalite 7S, complete rupture.

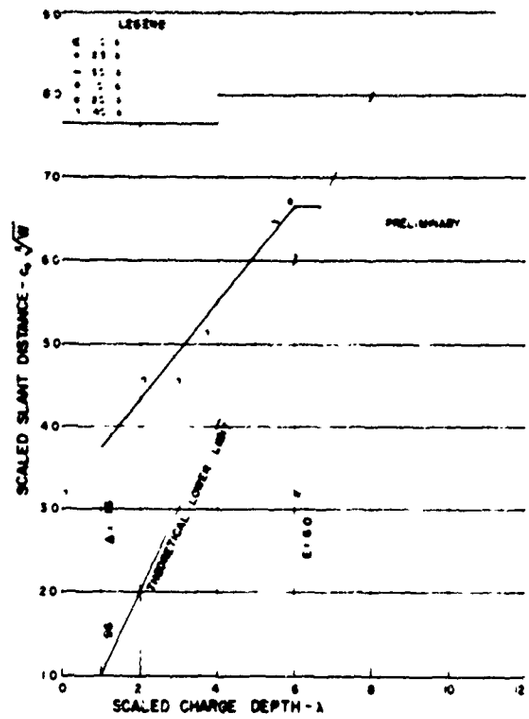

Figure 76. $C_e/\sqrt[3]{W}$ vs λ_c, surface snow, Coalite 7S, extreme rupture.

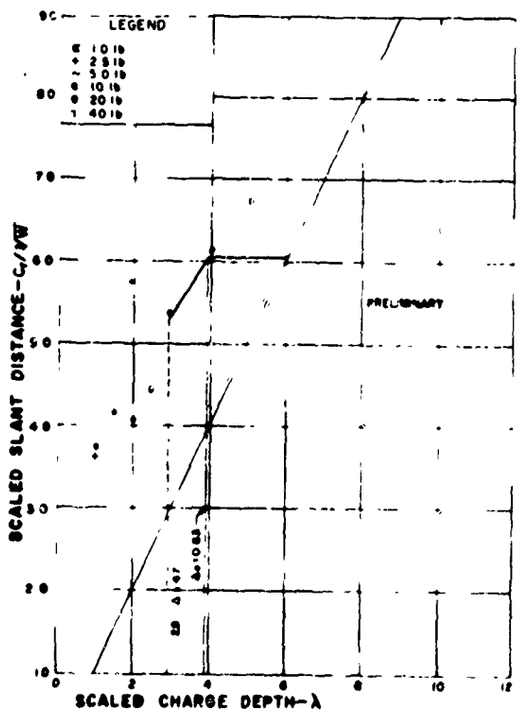

Figure 77. $C_r/\sqrt[3]{W}$ vs λ_c, trench snow, Atlas 60, complete rupture.

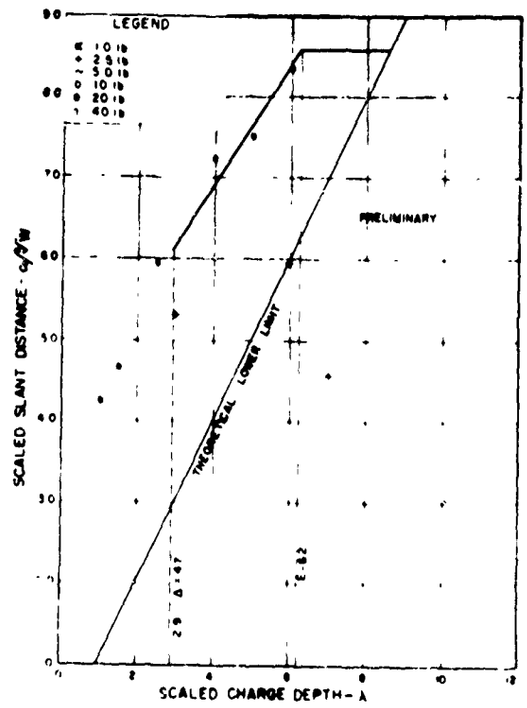

Figure 78. $C_e/\sqrt[3]{W}$ vs λ_c, trench snow, Atlas 60, extreme rupture.

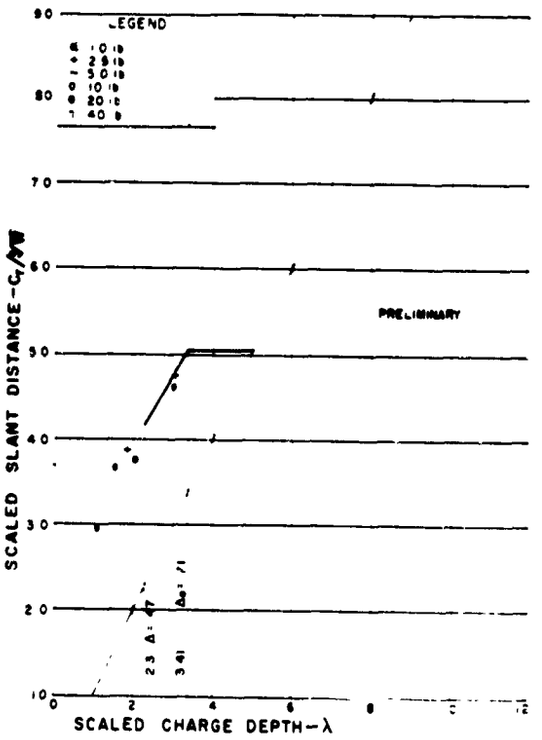

Figure 79. $C_r/\sqrt[3]{W}$ vs λ_c, trench snow, Coalite 7S, complete rupture.

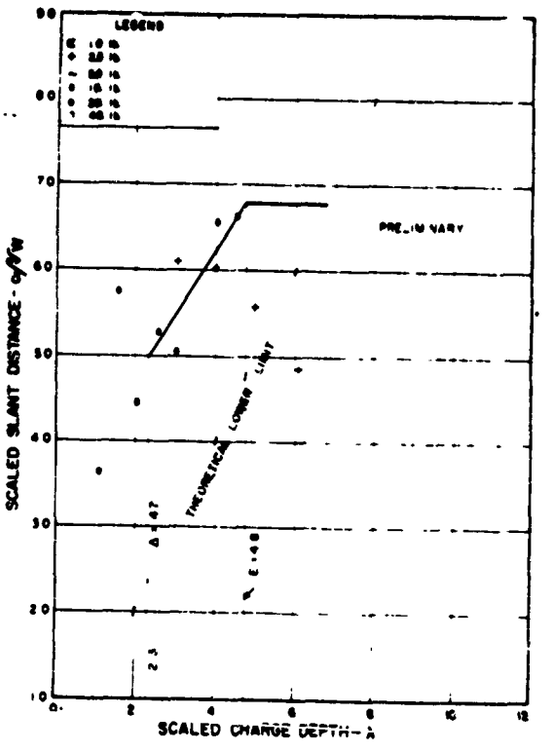

Figure 80. $C_e/\sqrt[3]{W}$ vs λ_c, trench snow, Coalite 7S, extreme rupture.

Dimensions of the cavity

It is logical to consider variation in the dimension of an explosion cavity in snow separately in three different ranges:

a) the secondary cavity where implosion occurs,

b) the primary cavity, Phase II, where doming occurs,

c) the primary cavity, Phase I, at depths greater than that at which doming begins.

The primary cavity is caused by expansion of the gas bubble and compaction of the snow during the rise to peak pressure. The secondary cavity results when the primary cavity fails from the release of potential energy stored during an interval measurable in milliseconds following the beginning of implosion. The secondary cavity is affected by energy stored during dynamic loading, just as an underground excavation subject only to static loading is affected by energy stored during loading as in nature. Depending upon the material, the length of the unsupported span, the shape of the opening, and the time it is unsupported, failure may occur and proceed in a manner familiar to the mining and construction industries.

Whether a camouflet or a crater forms depends upon the depth ratio. The transition limit between crater formation and camouflet formation is referred to here as the lower limit of the doming range. Although the data are insufficient to pinpoint the transition closer than 0.5 $\sqrt[3]{W}$ the transition occurs at Δ's equal to approximately 0.72 in 1958 surface snow and 0.81 in trench snow. At depth ratios lower than the transition limit, failure proceeds into the primary zone of the fragmentation range, where the volume of snow within limits of complete rupture becomes maximum at optimum explosive weight and the secondary cavity no longer exists.

Fracturing and isolation of the snow from its surroundings begin at critical depth, as does implosion. Accordingly, the region $0.72 < \Delta < 1.0$ in 1958 surface snow and the region $0.81 < \Delta < 1.0$ in trench snow are affected by implosion. The effect is one in which the primary cavity is destroyed either wholly or in part. The zone is referred to here as the isolation zone and in it the cavity is a secondary rather than a primary one.

Doming of the snow begins at a depth greater than the critical depth. In the region $1.0 < \Delta < 1.23$ the surface is uplifted and deformation of the roof above the primary cavity proceeds beyond the failure stress. A pattern of fracturing develops due to the uplift, and the strength of the primary cavity is reduced. The region is referred to here as the uplift zone and the cavity as the primary cavity, Phase II.

The test program was directed towards cratering aspects of the problem rather than a study of cavity growth, and available data in each of the ranges are insufficient to permit an analysis. To attempt to correlate camouflet limits in a range where a primary cavity occurs with those in another range where a secondary cavity occurs would not be meaningful.

Ranges of similar behavior in snow

Geometric similarity of cratering phenomena need not be confined to dimensions of the crater, but may be extended to other events or phenomena apparent to the senses. For instance, geometric similarity may be applied to a transition limit or a failure event such as the ones which occur at critical depth and optimum depth. Similarly the beginnings of other specific events may be defined as transition limits and related to the depth ratio. In the terminology of this report, early refers to greater depths and late refers to lesser depths; thus the beginning of a given phenomenon is the deepest point at which it is evident.

Figure 81 illustrates the general case for a given type of explosive, a given weight of charge, and a given material (1958 surface snow). Transition

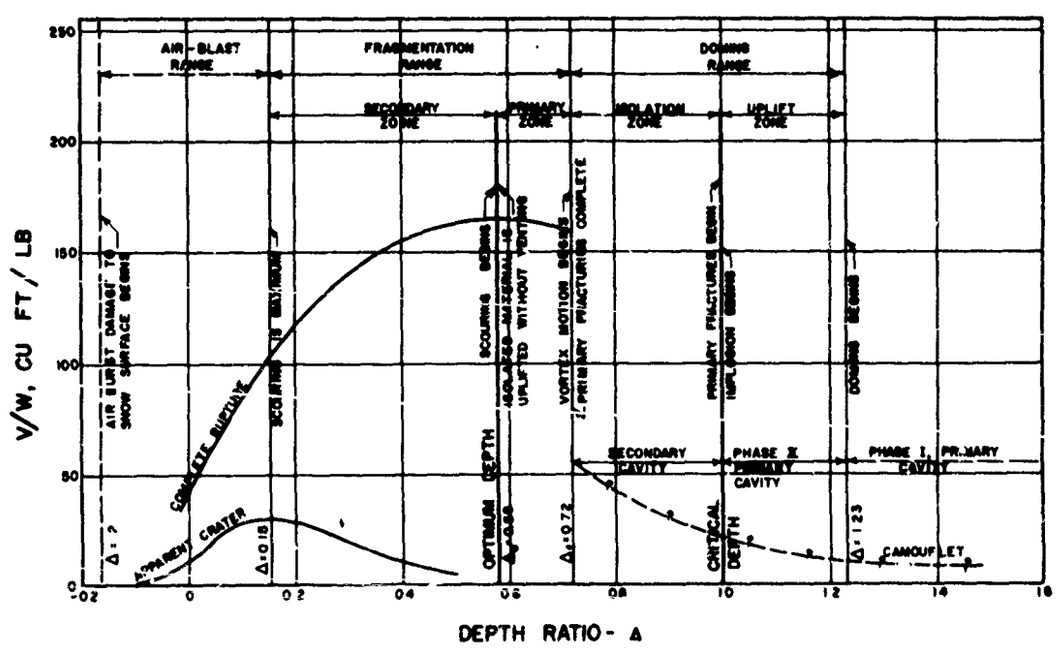

Figure 81. Ranges of similar behavior in 1958 surface snow.

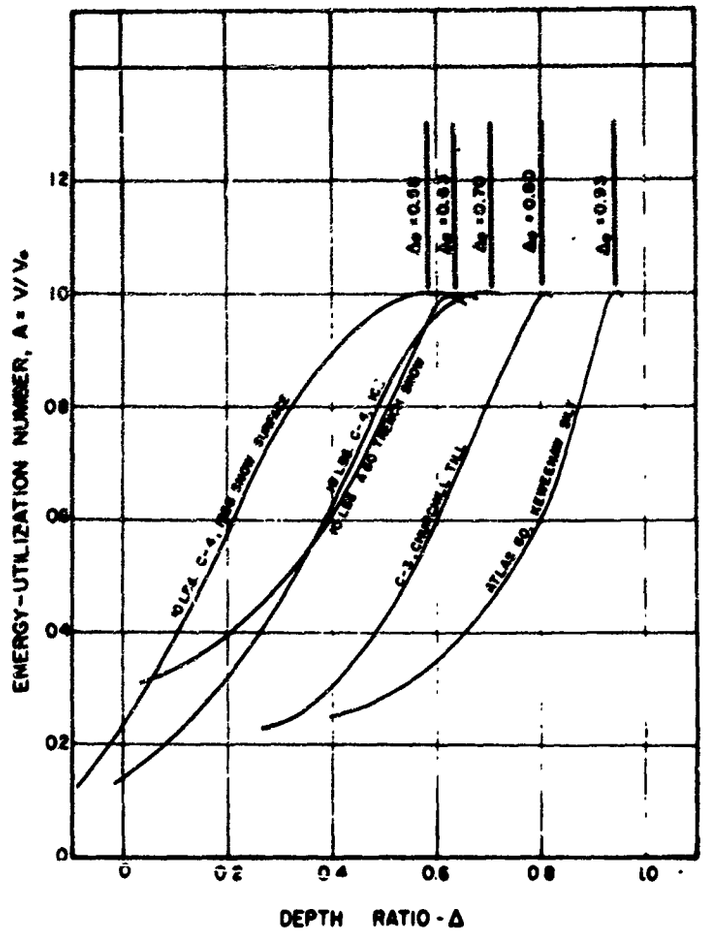

Figure 82. Energy-utilization number A vs Δ in snow, ice, frozen ground.

limits appear as maxima, minima, and points of inflection on the curves which show V/W vs Δ for the limits of complete rupture and for the limits of the apparent crater.

The effect of materials type upon the relation A vs Δ

Figure 82 shows the relation A vs Δ for 1958 surface snow, trench snow, glacier ice, frozen Churchill till, and frozen Keweenaw silt. The curve for trench snow falls in the region of glacier ice. The curve for frozen Churchill till lies in a region of higher depth ratio (lower energy density) than that for trench snow or ice, and the curve for Keweenaw silt lies in a region of still higher depth ratios.

CONCLUSIONS AND RECOMMENDATIONS

We may conclude from these experiments that the failure process in snow differs from that in most other materials. Most probably, the phenomenon of implosion and the vortex and scouring motions, recorded so clearly here, have not been recognized previously in explosions research.

It is recommended that the study be continued so as to supplement the available data, especially in the following areas:

a) the primary cavity, Phase I

b) the primary cavity, Phase II

c) the secondary cavity.

The cratering and cavity data should be extended to HE blasts with one type of explosive in the range not less than 250, 1000 and 4000 lb of explosive. The tests should be fully instrumented and conducted so as to determine each of the transition points of Figure 81.

A preliminary analysis of the available instrumentation data, including seismic measurements and flyrock-travel measurements should be made in advance of the large-scale blasts. The preliminary analysis should be directed toward a correlation of instrumentation and cratering effects and used to plan both of the above phases of the tests.

LITERATURE CITED

Bader, H.; Haefeli, R.; Bucher, E.; Neher, J.; Eckel O.; Thams, Chr.; and Niggli, P. (1939) Der Schnee und seine Metamorphose (Snow and its metamorphism). Beiträge zur Geologie der Schweiz, Geotechnische Serie, Hydrologie, Lieferung 3. U.S. Army Snow, Ice and Permafrost Research Establishment Translation 14, 1954, 313 p.

Bender, J.A. (1957) Air permeability of snow, USA SIPRE Research Report 37, 19 p.

Bentley, Pomeroy, and Dorman (1957) Seismic measurements on the Greenland Ice Cap. Part I: Studies at 76°59' N 56°05'W, Lamont Geological Observatory (Columbia University), New York.

Butkovich, T.R. (1956) Strength studies of high-density snow, USA SIPRE Research Report 18, 19 p.

Cole, R.H. (1948) Underwater explosions. Princeton, N.J.: Princeton University Press, 437 p.

Livingston, C.W. (1956) Excavations in frozen ground, Part I: Explosion tests in Keweenaw silt, USA SIPRE Report 30, 97 p.

_____ (1960a) Application of the Livingston crater theory to blasts in loess and clay, Waterways Experiment Station, Corps of Engineers, U.S. Army, 80 p.

_____ (1960b) Explosions in ice, USA SIPRE Technical Report 75.

Nakaya, Ukichiro (1959) Visco-elastic properties of snow and ice in the Greenland Ice Cap, USA SIPRE Research Report 46, 29 p.

	Data sheets
Apparent-crater dimensions	E1 -E10
True-crater dimensions	F1 -F10
Complete-rupture dimensions	G1 -G10
Extreme-rupture dimensions	H1 -H10
Extreme-rupture dimensions (camouflet and doming range)	H11
Camouflet dimensions	I1 -I10
Crater coefficients, apparent crater	
A60, surface blasts	J1 -J5
A60, trench blasts	J6 -J7
C4, surface blasts	J8 -J12
C7S, surface blasts	J13-J18
C7S, trench blasts	J19-J20
Crater coefficients, true crater and camouflet	
A60, surface blasts	K1 -K5
A60, trench blasts	K6 -K7
C4, surface blasts	K8 -K12
C7S, surface blasts	K13-K18
C7S, trench blasts	K19-K20
Crater coefficients, complete rupture	
A60, surface blasts	L1 -L5
A60, trench blasts	L6 -L7
C4, surface blasts	L8 -L12
C7S, surface blasts	L13-L18
C7S, trench blasts	L19-L20
Crater coefficients, extreme rupture	
A60, surface blasts	M1 -M5
A60, trench blasts	M6 -M7
C4, surface blasts	M8 -M12
C7S, surface blasts	M13-M18
C7S, trench blasts	M19-M20

APPENDIX

Hole Number	APPARENT CRATER												
	Charge Depth, Ft	Charge Height, Lbs Explosive Type	W	Δ	Depth, Ft h	Radius, Ft r_a	Slant Distance Ft c_a	W-Scaled Crater $h'/W^{1/3}$ = K_h'	$r_a/W^{1/3}$ = K_r'	$c_a/W^{1/3}$ = K_c'	Volume, Ft^3 V	V/W	Lip Height Ft
1	1.00	1.0 TS	6.00	0.17	1.40	3.05	3.70	0.23	0.51	0.62	23.64	23.64	0.10
2	2.00	" "	6.00	0.33	0.87	2.80	3.55	0.145	0.47	0.59	12.82	12.82	0.00
2A	2.00	" "	6.00	0.33	0.50	3.00	3.64	0.083	0.50	0.61	7.20	7.20	0.00
3	3.00	" "	6.00	0.50	0.68	2.83	4.10	0.11	0.47	0.68	7.11	7.11	0.00
4	3.95	" "	6.00	0.66	1.27	1.46	4.36	0.21	0.24	0.73	2.97	2.97	0.00
5	4.85	" "	6.00	0.81									
6	6.00	" "	6.00	1.00									
7	0.00	" "	6.00	0.00	0.74	1.74	1.74	0.12	0.29	0.29	3.48	3.48	0.30
8	+1.00	" "	6.00	+0.17	0.20	3.57	3.71	0.033	0.59	0.62	4.61	4.61	0.10
9	1.36	2.5 A60	9.93	0.14	2.50	4.76	4.95	0.25	0.48	0.50	94.60	37.84	0.00
9 1/2	0.00	" "	9.93	0.00	1.73	2.99	2.99	0.17	0.30	0.30	21.69	8.68	0.20
10	2.80	" "	9.93	0.28	1.07	5.06	5.80	0.11	0.51	0.58	51.75	20.70	0.10
11	5.30	" "	9.93	0.53	1.12	4.76	7.08	0.11	0.48	0.71	32.28	12.91	0.10
12	6.76	" "	9.93	0.68									

E-1

Hole Number	APPARENT CRATER												
	Charge Depth, Ft	Charge Height, Lbs Explosive Type	W	Δ	Depth, Ft h	Radius, Ft r_a	Slant Distance Ft c_a	W-Scaled Crater $h'/W^{1/3}$ = K_h'	$r_a/W^{1/3}$ = K_r'	$c_a/W^{1/3}$ = K_c'	Volume, Ft^3 V	V/W	Lip Height Ft
12 1/2	7.17	5.0 A60	12.48	0.57	1.00	5.90	9.38	0.080	0.47	0.75	56.74	11.35	0.20
13	0.11	2.5 "	9.93	0.02	0.48	1.05	8.19	0.048	0.11	0.02	0.68	0.27	0.25
14	9.61	2.5 "	9.93	0.99									
14 1/2	12.34	5.0 "	12.48	0.99									
15	2.20	10.0 "	15.70	0.14									
15R	2.20	10.0 "	15.70	0.14	2.97	7.29	7.60	0.19	0.46	0.48	253.76	25.38	0.10
16	4.30	10.0 "	15.70	0.27									
16R	4.40	10.0 "	15.70	0.28	2.40	8.85	9.80	0.15	0.56	0.62	258.18	25.82	0.00
17	8.10	10.0 "	15.70	0.52									
17 1/2	11.58	20.0 "	19.78	0.59									
18	10.80	10.0 "	15.70	0.69									
18 1/2	12.90	10.0 "	15.70	0.82									
19	15.10	10.0 "	15.70	0.96									
19 1/2	19.48	20.0 "	19.78	0.98									

E-2

APPENDIX

Hole Number	Charge Depth, Ft	Charge Weight, Lbs Explosive Type	W	Δ	Depth, Ft h	Radius, Ft r_o	Slant Distance Ft s_o	R-Scaled Crater h/W = h'	r_o/W = r'	s_o/W = s'	Volume, Ft^3 V	V/W	Lip Height Ft
	APPARENT CRATER												
20 /	22.60	10.0 A60	15.70	1.44									
21	3.32	40.0 "	24.97	0.14	3.46	10.90	11.40	0.14	0.44	0.46	392.67	14.82	0.00
211/2	0.00	40.0 "	24.97	0.00	4.20	8.10	8.10	0.17	0.32	0.32	356.58	8.91	0.90
22	6.80	40.0 "	24.97	0.27	2.48	13.25	14.90	0.099	0.53	0.60	470.81	11.77	0.00
23	12.47	40.0 "	24.97	0.50	0.78	9.50	15.80	0.031	0.39	0.63	106.64	2.67	0.00
231/2	23.00	160.0"	39.64	0.58									
26	20.57	40.0 "	24.97	0.82									
29	24.07	40.0 "	24.97	0.96									
30	1.30	2.5 C4	8.43	0.15	2.60	5.25	5.33	0.31	0.62	0.63	87.76	35.10	0.00
301/2	0.00	2.5 "	8.43	0.00	1.90	2.90	2.90	0.23	0.34	0.34	23.43	9.37	0.50
31	2.70	2.5 "	8.43	0.30	0.94	5.05	5.83	0.11	0.60	0.69	32.39	12.96	0.00
32	4.00	2.5 "	8.43	0.47	0.71	3.76	5.50	0.084	0.45	0.65	11.28	4.51	0.15
33	5.30	2.5 "	8.43	0.63	1.22	5.60	7.78	0.14	0.66	0.92	44.67	17.87	0.10
34	6.63	2.5 "	8.43	0.71	0.60	2.78	6.62	0.071	0.33	0.79	8.67	3.47	0.10

E-3

Hole Number	Charge Depth, Ft	Charge Weight, Lbs Explosive Type	W	Δ	Depth, Ft h	Radius, Ft r_o	Slant Distance Ft s_o	h/W = h'	r_o/W = r'	s_o/W = s'	Volume, Ft^3 V	V/W	Lip Height Ft
	APPARENT CRATER												
341/2	6.22	5.0 C4	10.60	0.59	1.40	4.45	7.77	0.13	0.42	0.73	49.52	9.90	0.10
35	8.00	2.5 C4	8.43	0.95									
351/2	10.14	5.0 C4	10.60	0.96									
36	2.16	10.0 C4	13.33	0.16	2.50	6.30	6.66	0.19	0.47	0.50	193.26	19.33	0.70
37	4.40	10.0 C4	13.33	0.33	1.20	7.45	8.66	0.090	0.56	0.65	97.67	9.77	0.20
38	8.31	10.0 C4	13.33	0.62	1.82	6.22	10.48	0.14	0.47	0.79	112.23	11.22	0.00
381/2	9.48	20.0 C4	16.80	0.56									
39	10.70	10.0 C4	13.33	0.80									
40	12.71	10.0 C4	13.33	0.95									
401/2	16.27	20.0 C4	16.80	0.97									
42	3.37	40.0 C4	21.20	0.16	3.10	10.21	10.72	0.15	0.48	0.51	552.28	13.81	0.20
421/2	0.00	40.0 C4	21.20	0.00	3.90	7.99	7.99	0.18	0.38	0.38	376.57	9.41	0.40
43	6.82	40.0 C4	21.20	0.32	1.53	12.00	13.81	0.072	0.57	0.65	521.71	13.04	0.10
44	11.37	40.0 C4	21.20	0.54	0.92	11.20	15.89	0.043	0.53	0.75	186.51	4.66	0.00

E-4

APPENDIX

Hole Number	Charge Depth, Ft	Charge Height, Lbs Explosive Type	n	Δ	Apparent Crater Depth, Ft a	Apparent Crater Radius, Ft r_a	Apparent Crater Slant Distance Ft s_a	$\frac{a}{r_a} = \frac{a}{r_a}$	$\frac{r_a}{r_a} = \frac{r_a}{r_a}$	$\frac{s_a}{r_a} = \frac{s_a}{r_a}$	Apparent Crater Volume, Ft^3 V	$\frac{V}{r_a^3} = \frac{V}{r_a^3}$	Lip Height Ft
441/2	19.55	C4 160.0	33.67	0.58									
46	20.67	C4 40.0	21.20	0.98									
50	1.33	7S 2.5	8.16	0.16	2.07	4.57	4.79	0.25	0.56	0.59	58.38	23.35	0.10
51	2.48	7S 2.5	8.16	0.30	0.86	4.45	5.06	0.11	0.55	0.62	33.00	13.20	0.00
52	3.13	7S 2.5	8.16	0.63	2.04	3.08	6.07	0.25	0.38	0.74	29.68	11.87	0.40
521/2	3.65	7S 5.0	10.26	0.55									
54	6.33	7S 2.5	8.16	0.78									
54B	7.38	7S 2.5	8.16	0.90									
541/2	9.47	7S 5.0	10.26	0.92									
55	0.00	7S 2.5	8.16	0.00	1.18	2.55	2.55	0.14	0.31	0.31	10.74	4.30	0.20
56	2.20	7S 10.0	12.90	0.17	2.64	6.09	6.48	0.20	0.47	0.50	190.01	12.00	0.30
57	4.45	7S 10.0	12.90	0.34	1.30	8.09	[illegible].21	0.10	0.63	0.71	46.50	14.65	0.00
58	8.14	7S 10.0	12.90	0.63	1.32	7.15	10.88	0.10	0.55	0.84	12.31	11.23	0.00
581/2	9.33	7S 20.0	16.26	0.57									

E-5

Hole Number	Charge Depth, Ft	Charge Height, Lbs Explosive Type	n	Δ	Apparent Crater Depth, Ft a	Apparent Crater Radius, Ft r_a	Apparent Crater Slant Distance Ft s_a	$\frac{a}{r_a} = \frac{a}{r_a}$	$\frac{r_a}{r_a} = \frac{r_a}{r_a}$	$\frac{s_a}{r_a} = \frac{s_a}{r_a}$	Apparent Crater Volume, Ft^3 V	$\frac{V}{r_a^3} = \frac{V}{r_a^3}$	Lip Height Ft
59	12.54	7S 10.0	12.90	0.97									
591/2	21.23	7S 20.0	16.26	1.31									
60	10.84	7S 10.0	12.90	0.84									
63	3.45	7S 40.0	20.52	0.17	3.80	9.84	10.41	0.19	0.48	0.51	510.71	12.77	0.50
631/2	0.00	7S 40.0	20.52	0.00	3.28	7.58	7.58	0.16	0.37	0.37	291.17	7.28	0.30
64	6.95	7S [illegible]	20.52	0.34	1.84	12.23	14.03	0.090	0.60	0.68	377.77	9.44	0.00
65	12.85	40.0	20.52	0.63	2.47	9.80	16.21	0.12	0.48	0.79	230.85	5.77	0.15
651/2	18.90	7S 160.0	20.52	0.92									
67	20.65	7S 40.0	20.52	1.01									
70T	1.36	A60 2.5	8.43	0.17	1.83	4.45	4.63	0.21	0.53	0.55	22.64	9.06	0.00
71T	2.66	A60 2.5	8.43	0.32	2.00	6.25	7.00	0.24	0.74	0.83	81.01	32.40	0.00
72T	5.38	A60 2.5	8.43	0.64	1.88	6.21	8.24	0.22	0.74	0.98	83.89	33.56	0.00
73T	6.86	A60 2.5	8.43	0.81									
74T	8.11	A60 2.5	8.43	0.97									

6

APPENDIX

Hole Number	Charge Depth, Ft	Charge Weight, Lbs Explosive Type	n	Δ	Depth, Ft h	Radius, Ft r_o	Slant Distance Ft σ_o	$\frac{h}{n} = K_h'$	$\frac{r_o}{n} = K_r'$	$\frac{\sigma_o}{n} = K_\sigma'$	Volume, Ft³ V	$\frac{V}{n}$	Lip Height Ft
		APPARENT CRATER											
75T	9.51	A60 2.5	8.43	1.13	—	—	—	—	—	—	—	—	—
76T	2.20	A60 10.0	13.33	0.17	2.10	5.80	6.25	0.15	0.44	0.47	177.43	17.74	0.30
77T	4.30	A60 10.0	13.33	0.32	1.68	6.60	7.85	0.13	0.50	0.59	101.89	10.19	0.10
78T	8.60	A60 10.0	13.33	0.65	—	—	—	—	—	—	—	—	—
79T	10.75	A60 10.0	13.33	0.80	—	—	—	—	—	—	—	—	—
80T	12.95	A60 10.0	13.33	0.97	—	—	—	—	—	—	—	—	—
81T	5.40	A60 10.0	13.33	0.40	1.48	7.10	8.95	0.11	0.53	0.67	111.78	11.18	0.00
82T	3.20	A60 10.0	13.33	0.24	1.38	5.05	6.03	0.10	0.38	0.45	48.67	4.87	0.10
90T	1.58	7S 2.5	6.53	0.24	1.58	5.05	5.35	0.24	0.78	0.83	63.79	25.52	0.00
91T	2.48	7S 2.5	6.53	0.38	2.00	4.36	5.18	0.31	0.66	0.79	51.78	20.71	0.00
92T	5.38	7S 2.5	6.53	0.83	—	—	—	—	—	—	—	—	—
93T	6.78	7S 2.5	6.53	1.04	—	—	—	—	—	—	—	—	—
94T	8.18	7S 2.5	6.53	1.25	—	—	—	—	—	—	—	—	—
96T	2.24	7S 10.0	10.32	0.21	1.45	5.40	5.85	0.14	0.53	0.56	82.99	8.30	0.20

Hole Number	Charge Depth, Ft	Charge Weight, Lbs Explosive Type	n	Δ	Depth, Ft h	Radius, Ft r_o	Slant Distance Ft σ_o	$\frac{h}{n} = K_h'$	$\frac{r_o}{n} = K_r'$	$\frac{\sigma_o}{n} = K_\sigma'$	Volume, Ft³ V	$\frac{V}{n}$	Lip Height Ft
		APPARENT CRATER											
97T	4.34	7S 10.0	10.32	0.43	2.20	5.95	7.40	0.21	0.58	0.71	147.44	14.74	0.15
98T	8.64	7S 10.0	10.32	0.86	—	—	—	—	—	—	—	—	—
99T	9.74	7S 10.0	10.32	0.95	—	—	—	—	—	—	—	—	—
100T	5.44	7S 10.0	10.32	0.53	1.48	5.30	7.55	0.14	0.51	0.74	79.65	7.97	0.10
101T	3.29	7S 10.0	10.32	0.33	1.65	4.50	5.58	0.16	0.44	0.54	46.55	4.66	0.20
200	4.08	A60 2.5	9.93	0.41	0.37	5.35	6.75	0.037	0.54	0.68	13.98	5.59	0.00
201	6.46	A60 10.0	15.70	0.41	0.82	9.00	11.10	0.052	0.57	0.71	109.45	10.95	0.00
202	6.46	7S 10.0	12.90	0.50	1.48	5.30	9.60	0.11	0.41	0.74	83.01	8.30	0.00
210	4.08	C4 2.5	8.43	0.48	—	—	—	—	—	—	—	—	—
211	6.46	C4 10.0	13.33	0.48	2.12	6.65	9.36	0.16	0.50	0.70	111.18	11.12	0.00
212	10.26	C4 40.0	21.20	0.48	1.70	11.15	15.15	0.080	0.53	0.71	453.34	11.34	0.00
220	4.08	7S 2.5	8.16	0.50	—	—	—	—	—	—	—	—	—
220R	4.08	7S 2.5	8.16	0.50	—	—	—	—	—	—	—	—	—
222	10.26	7S 40.0	20.52	0.50	1.06	9.95	14.30	0.052	0.48	0.70	177.47	4.31	0.30

APPENDIX

Hole Number	Charge Depth, Ft	Charge Weight, Lbs Explosive Type	W	Δ	Depth, Ft d_a	Radius, Ft r_a	Slant Distance Ft s_a	$d_a/W^{1/3}$	$r_a/W^{1/3}$	$s_a/W^{1/3}$	Volume, Ft³ V	V/W	Lip Height Ft
	APPARENT CRATER												
230T	4.07	2.5 A60	8.43	0.48	1.30	4.15	6.19	0.15	0.50	0.73	59.14	23.66	0.20
231T	6.46	10.0 A60	13.33	0.48	2.70	7.37	9.86	0.20	0.55	0.74	155.80	15.58	0.00
232	10.26	40.0 A60	24.97	0.41	2.44	11.70	15.58	0.098	0.47	0.62	426.77	10.67	0.30
240T	4.07	2.5 7S	6.53	0.63	0.73	3.56	5.45	0.11	0.55	0.84	98.07	39.23	0.20
241T	6.46	10.0 7S	10.32	0.63	1.42	7.52	9.98	0.14	0.73	0.96	106.78	10.68	0.20
260	+2.15	10.0 C4	13.33	+0.16									
270	+1.08	10.0 C4	13.33	+0.08	1.88	4.31	4.46	0.14	0.32	0.33	49.47	4.95	0.30
270R	+1.08	10.0 C4	13.33	+0.08									
271	+1.08	10.0 A60	15.70	+0.07	1.85	4.44	4.58	0.12	0.28	0.29	36.92	3.69	0.30
272	+1.08	10.0 7S	12.90	+0.08	1.20	3.52	3.71	0.093	0.27	0.29	18.22	1.82	0.20
280	0.00	10.0 C4	13.33	0.00									
281	0.00	10.0 A60	15.70	0.00	2.64	5.00	5.00	0.17	0.32	0.32	106.67	10.67	0.50
282	0.00	10.0 7S	12.90	0.00	2.22	4.87	4.87	0.17	0.38	0.38	80.01	8.00	0.60
290	2.15	10.0 C4	13.33	0.16	2.83	6.94	7.29	0.21	0.52	0.55	233.64	23.36	0.20

Hole Number	Charge Depth, Ft	Charge Weight, Lbs Explosive Type	W	Δ	Depth, Ft d_a	Radius, Ft r_a	Slant Distance Ft s_a	N-Scaled Crater $d_a/W^{1/3}$	N-Scaled Crater $r_a/W^{1/3}$	N-Scaled Crater $s_a/W^{1/3}$	Volume, Ft³ V	V/W	Lip Height Ft
	APPARENT CRATER												
291	2.15	10.0 7S	12.90	0.17	2.52	6.62	6.99	0.20	0.51	0.54	194.11	19.41	0.30
292	2.15	10.0 A60	15.70	0.14	3.10	7.85	8.14	0.20	0.50	0.52	313.75	31.38	0.30
293	1.71	5.0 C4	10.60	0.16	2.60	5.95	6.19	0.25	0.56	0.58	163.08	32.62	0.10
294	1.71	5.0 7S	10.26	0.17	2.12	5.20	5.48	0.21	0.51	0.53	104.47	20.89	0.40
295	1.71	5.0 A60	12.48	0.14	2.36	5.06	5.37	0.19	0.41	0.43	117.74	23.55	0.30
296	3.42	40.0 C4	21.20	0.16									
297	3.42	40.0 7S	20.52	0.17									
298	3.42	40.0 A60	24.97	0.14									

APPENDIX

Blast No	TRUE CRATER										N-Scaled Crater		
	Δ	Charge Height w (lb) Explosive Type	Charge Depth d_c (Ft)	Crater Depth h (Ft)	Crater Radius r (Ft)	Slant Distance to Rig C_t (Ft)	Volume V (Ft^3)	V/W	E	N	$\Delta h = h/N$ N-Scaled Depth	$\Delta r = r/N$ N-Scaled Radius	$\Delta C = C_t/N$ N-Scaled Slant Distance
1	0.17	1.0 TS	1.00	2.12	3.68	3.92	32.99	32.99	6.00	6.00	0.35	0.61	0.65
2	0.33	1.0 "	2.00	2.90	2.80	3.43	47.11	47.11	6.00	6.00	0.48	0.47	0.57
2A	0.33	1.0 "	2.00	2.90	3.00	3.64	44.31	44.31	6.00	6.00	0.48	0.50	0.61
3	0.50	1.0 "	3.00	4.00	2.80	4.92	62.58	62.58	6.00	6.00	0.67	0.47	0.82
4	0.66	1.0 "	3.95	5.40	2.10	5.85	73.32	73.32	6.00	6.00	0.90	0.35	0.98
5	0.81	1.0 "	4.85						6.00	6.00			
6	1.00	1.0 "	6.00						6.00	6.00			
7	0.00	1.0 "	0.00	1.00	1.95	2.19	6.04	6.04	6.00	6.00	0.17	0.32	0.36
8	<0.17	1.0 "	+1.00	0.24	3.70	3.72	4.61	4.61	6.00	6.00	0.04	0.62	0.62
9	0.14	2.5 A60	1.36	8.36	4.00	5.81	123.45	49.38	7.30	9.93	0.84	0.40	0.59
91/2	0.00	2.5 "	0.00	2.02	3.35	3.92	36.10	14.44	7.30	9.93	0.20	0.34	0.40
10	0.28	2.5 "	2.80	4.40	5.10	6.75	226.16	90.46	7.30	9.93	0.44	0.51	0.68
11	0.53	2.5 "	5.30	6.70	4.80	8.19	240.44	96.18	7.30	9.93	0.67	0.48	0.82
12	0.68	2.5 "	6.76	8.36	5.72	10.64	736.28	294.51	7.30	9.93	0.84	0.58	1.07

F-1

Blast No	TRUE CRATER										N-Scaled Crater		
	Δ	Charge Height w (lb) Explosive Type	Charge Depth d_c (Ft)	Crater Depth h (Ft)	Crater Radius r (Ft)	Slant Distance to Rig C_t (Ft)	Volume V (Ft^3)	V/W	E	N	$\Delta h = h/N$ N-Scaled Depth	$\Delta r = r/N$ N-Scaled Radius	$\Delta C = C_t/N$ N-Scaled Slant Distance
121/2	0.57	5.0 A40	7.17	9.66	6.06	11.39	611.63	122.33	7.30	12.48	0.77	0.49	0.91
13	0.82	2.5 "	8.11						7.30	9.93			
14	0.99	2.5 "	9.61						7.30	9.93			
141/2	0.99	5.0 "	12.34						7.30	12.48			
15	0.14	10.0 "	2.20						7.30	15.70			
15R	0.14	10.0 "	2.20	6.33	7.74	10.03	556.55	55.66	7.30	15.70	0.40	0.49	0.64
16	0.27	10.0 "	4.30						7.30	15.70			
16R	0.28	10.0 "	4.40	6.88	8.84	11.19	890.02	89.00	7.30	15.70	0.44	0.56	0.71
17	0.52	10.0 "	8.10	10.47	8.26	13.32	992.40	99.24	7.30	15.70	0.67	0.53	0.85
171/2	0.59	20.0 "	11.58						7.30	19.78			
18	0.69	10.0 "	10.80						7.30	15.70			
181/2	0.82	10.0 "	12.90						7.30	15.70			
19	0.96	10.0 "	15.10						7.30	15.70			
191/2	0.98	20.0 "	19.48						7.30	19.78			

F-2

Blast No	TRUE CRATER										N-Scaled Crater		
	Δ	Charge Weight W (lb) Explosive Type	Charge Depth d_c (Ft)	Crater Depth h (Ft)	Crater Radius r (Ft)	Slant Distance to Rig C_t (Ft)	Volume V (Ft^3)	V/W	E	N	K_h = h/N N-Scaled Depth	K_r = r/N N-Scaled Radius	K_c = C_t/N N-Scaled Slant Distance
20	1.44	10.0 A60	22.60						7.30	15.70			
21	0.14	40.0 "	3.32	7.42	11.30	13.53	1516.01	37.90	7.30	24.97	0.30	0.45	0.54
211/2	0.00	40.0 "	0.00	4.82	8.60	9.87	474.49	11.86	7.30	24.97	0.19	0.34	0.40
22	0.27	40.0 "	6.80	10.18	13.22	16.67	2165.50	54.14	7.30	24.97	0.41	0.53	0.81
23	0.50	40.0 "	12.47	16.56	10.30	19.53	2843.50	71.09	7.30	24.97	0.66	0.41	0.78
231/2	0.58	160.0"	23.00						7.30	39.64			
26	0.82	40.0 "	20.57						7.30	24.97			
29	0.96	40.0 "	24.07						7.30	24.97			
30	0.15	2.5 C4	1.30	4.10	5.20	6.51	133.90	53.56	6.20	8.43	0.49	0.62	0.77
301/2	0.00	2.5 "	0.00	1.90	2.98	3.54	23.43	9.37	6.20	8.43	0.23	0.35	0.42
31	0.33	2.5 "	2.70	3.90	5.10	7.55	162.73	65.09	6.20	8.43	0.46	0.60	0.90
32	0.47	2.5 "	4.00	5.28	8.20	6.77	215.44	86.18	6.20	8.43	0.63	0.50	0.80
33	0.63	2.5 "	5.30	6.15	5.09	7.99	174.60	69.84	6.20	8.43	0.73	0.60	0.95
34	0.71	2.5 "	6.00	7.75	2.95	8.45	177.51	71.00	6.20	8.43	0.92	0.35	1.00

F-3

Blast No	TRUE CRATER										N-Scaled Crater		
	Δ	Charge Weight W (lb) Explosive Type	Charge Depth d_c (Ft)	Crater Depth h (Ft)	Crater Radius r (Ft)	Slant Distance to Rig C_t (Ft)	Volume V (Ft^3)	V/W	E	N	K_h = h/N N-Scaled Depth	K_r = r/N N-Scaled Radius	K_c = C_t/N N-Scaled Slant Distance
341/2	0.59	5.0 C4	6.22	8.00	4.61	9.20	244.67	48.93	6.20	10.60	0.75	0.43	0.87
35	0.95	2.5 "	8.00						6.20	8.43			
351/2	0.96	5.0 "	10.14						6.20	10.60			
36	0.14	10.0"	2.16	4.80	6.49	8.07	317.22	31.72	6.20	13.33	0.36	0.49	0.61
37	0.33	10.0"	4.40	6.40	7.47	9.85	406.86	40.69	6.20	13.33	0.48	0.56	0.74
38	0.62	10.0"	8.31	11.46	6.21	13.00	753.79	75.38	6.20	13.33	0.86	0.47	0.98
381/2	0.56	20.0"	9.40						6.20	16.80			
39	0.80	10.0"	10.70						6.20	13.33			
40	0.95	10.0"	12.71						6.20	13.33			
401/2	0.97	20.0"	16.27						6.20	16.80			
42	0.28	40.0"	3.37	7.22	10.42	12.66	1220.32	30.51	6.20	21.20	0.34	0.49	0.60
421/2	0.00	40.0"	0.00	5.80	8.24	10.57	569.64	14.24	6.20	21.20	0.27	0.39	0.50
43	0.32	40.0"	6.82	9.60	12.09	15.43	1744.22	43.61	6.20	21.20	0.45	0.57	0.73
44	0.54	40.0"	11.37	14.03	13.20	21.00	1736.02	43.42	6.20	21.20	0.66	0.62	0.99

F-4

Blast No	TRUE CRATER										N-Scaled Crater		
	Δ	Charge Weight W (lb) Explosive Type	Charge Depth d_c (Ft)	Crater Depth h (Ft)	Crater Radius r (Ft)	Slant Distance to Rig C_t (Ft)	Volume V (Ft^3)	V/W	E	N	h_n = h/N N-Scaled Depth	r_n = r/N N-Scaled Radius	C_{tn} = C_t/N N-Scaled Slant Distance
441/2	0.58	160.0 C4	19.55						6.20	33.67			
46	0.98	40.0 "	20.67						6.20	21.20			
50	0.36	2.5 TS	1.22	3.14	4.50	5.57	90.28	36.11	6.00	20.36	0.30	0.50	0.00
51	0.30	2.5 "	2.40	4.10	4.47	6.12	123.61	49.44	6.00	8.16	0.51	0.55	0.75
52	0.43	2.5 "	5.13	6.76	3.12	7.45	164.64	66.66	6.00	8.16	0.83	0.38	0.91
521/2	0.55	5.0 "	5.65						6.00	10.26			
54	0.70	2.5 "	6.33	0.90	2.09	2.31	2.53	1.01	6.00	8.16	0.12	0.26	0.28
540	0.90	2.5 "	7.38						6.00	8.16			
541/2	0.92	5.0 "	9.47						6.00	10.26			
55	0.00	2.5 "	0.00	1.56	3.22	3.58	20.04	8.02	6.00	8.16	0.19	0.39	0.44
56	0.17	10.0"	2.20	4.52	6.95	8.30	457.27	45.73	6.00	12.90	0.35	0.54	0.64
57	0.34	10.0"	4.45	5.82	8.09	9.96	501.44	50.14	6.00	12.90	0.45	0.63	0.77
58	0.63	10.0"	8.14	10.40	6.19	12.10	505.20	50.52	6.00	12.90	0.81	0.48	0.94
581/2	0.57	20.0"	9.33						6.00	16.26			

F-5

Blast No	TRUE CRATER										N-Scaled Crater		
	Δ	Charge Weight W (lb) Explosive Type	Charge Depth d_c (Ft)	Crater Depth h (Ft)	Crater Radius r (Ft)	Slant Distance to Rig C_t (Ft)	Volume V (Ft^3)	V/W	E	N	h_n = h/N N-Scaled Depth	r_n = r/N N-Scaled Radius	C_{tn} = C_t/N N-Scaled Slant Distance
59	0.97	10.0 TS	12.54						6.00	12.90			
59 1/2	1.31	20.0 TS	21.23						6.00	16.26			
60	0.84	10.0 TS	10.84						6.00	12.90			
62	0.17	40.0 TS	3.45	7.88	9.00	12.59	1181.38	29.53	6.00	20.52	0.38	0.48	0.61
63 1/2	0.00	40.0 TS	0.00	4.80	7.69	9.07	422.69	10.57	6.00	20.52	0.23	0.37	0.44
64	0.34	40.0 TS	6.95	9.00	12.24	15.21	2188.37	54.71	6.00	20.52	0.44	0.70	0.74
65	0.63	40.0 TS	12.85	16.42	14.44	21.98	3018.01	75.45	6.00	20.52	0.80	0.70	1.07
65 1/2	0.92	160.0 TS	18.90						6.00	20.52			
67	1.01	40.0 TS	20.65						6.00	20.52			
70 T	0.17	2.5 A60	1.36	1.68	4.34	4.67	48.86	19.54	6.20	8.43	0.20	0.52	0.55
71 T	0.32	2.5 A60	2.66	3.80	5.95	7.06	112.80	45.12	6.20	8.43	0.45	0.71	0.84
72 T	0.64	2.5 A60	5.38	6.88	5.77	8.94	246.47	98.59	6.20	8.43	0.82	0.68	1.06
73 T	0.81	2.5 A60	6.86						6.20	8.43			
74 T	0.97	2.5 A60	8.11						6.20	8.43			

6

APPENDIX

Blast No	TRUE CRATER										N-Scaled Crater		
	Δ	Charge Weight W (lb) Explosive Type	Charge Depth d_c (Ft)	Crater Depth h (Ft)	Crater Radius r (Ft)	Slant Distance to Rig C_t (Ft)	Volume V (Ft^3)	V/W	E	N	Δ_h = h/N N-Scaled Depth	Δ_r = r/N N-Scaled Radius	Δ_c = C_t/N N-Scaled Slant Distance
75 T	1.13	2.5^{A60}	9.51						6.20	8.43			
76 T	0.17	10.0^{A60}	2.20	2.90	5.82	6.50	220.40	22.05	6.20	13.33	0.22	0.44	0.48
77 T	0.32	10.0^{A60}	4.30	6.10	7.62	9.75	393.71	39.37	6.20	13.33	0.46	0.58	0.73
78 T	0.65	10.0^{A60}	8.60	10.91	5.82	12.37	1069.19	106.92	6.20	13.33	0.82	0.44	0.93
79 T	0.80	10.0^{A60}	10.75						7.20	13.33			
80 T	0.97	10.0^{A60}	12.95						7.20	13.33			
81 T	0.40	10.0^{A60}	5.40	7.47	7.09	10.44	476.22	47.62	7.20	13.33	0.56	0.53	0.78
82 T	0.24	10.0^{A60}	3.20	5.67	6.74	8.32	466.57	46.66	6.20	13.33	0.43	0.51	0.66
90 T	0.24	2.5^{B60}	1.50	2.64	5.47	6.00	106.37	42.15	4.00	6.53	0.40	0.84	0.94
91 T	0.39	2.5^{T5}	2.40	3.06	4.41	5.56	109.25	41.30	4.00	6.53	0.47	0.68	0.85
92 T	0.83	2.5^{B5}	5.38						4.00	6.53			
93 T	1.04	2.5^{T5}	6.70						4.00	6.53			
94 T	1.25	2.5^{T5}	8.10						4.00	6.53			
96 T	0.21	10.0^{T5}	2.24	3.64	5.95	6.99	185.43	18.54	4.00	10.32	0.35	[illegible]	0.68

F-7

Blast No	TRUE CRATER										N-Scaled Crater		
	Δ	Charge Weight W (lb) Explosive Type	Charge Depth d_c (Ft)	Crater Depth h (Ft)	Crater Radius r (Ft)	Slant Distance to Rig C_t (Ft)	Volume V (Ft^3)	V/W	E	N	Δ_h = h/N N-Scaled Depth	Δ_r = r/N N-Scaled Radius	Δ_c = C_t/N N-Scaled Slant Distance
97 T	0.43	10.0^{T5}	4.34	6.02	6.73	9.04	407.94	40.79	4.00	10.32	0.59	0.65	0.88
98 T	0.86	10.0^{T5}	8.64						4.00	10.32			
99 T	0.95	10.0^{T5}	9.74						6.00	10.32			
100T	0.53	10.0^{T5}	5.44	7.66	6.12	9.81	411.96	41.20	6.00	10.32	0.74	0.59	0.95
101T	0.33	10.0^{T5}	3.29	4.80	6.36	7.97	347.48	34.77	6.00	10.32	0.46	0.61	0.78
200	0.41	2.5^{A60}	4.08	5.44	4.87	7.30	186.96	74.78	7.30	9.93	0.55	0.49	0.74
201	0.41	10.0^{A60}	8.46	9.06	7.51	11.77	839.64	83.96	7.30	15.70	0.58	0.48	0.75
202	0.50	10.0^{T5}	6.46	8.48	7.14	11.09	828.98	82.70	6.00	12.90	0.66	0.55	0.86
210	0.48	2.5^{C4}	4.08						6.20	8.43			
211	0.48	10.0^{C4}	6.48	8.80	7.54	11.28	983.85	98.38	6.20	13.33	0.63	0.57	0.85
212	0.48	40.0^{C4}	10.26	13.18	11.17	17.30	1773.87	44.35	6.20	21.20	0.62	0.53	0.82
220	0.50	2.5^{T5}	4.00	5.76	5.01	7.44	196.46	78.56	6.00	8.16	0.71	0.61	0.94
220B	0.50	2.5^{T5}	4.00						6.00	8.16			
222	0.50	40.0^{T5}	10.26	14.84	13.60	20.14	2462.73	61.57	6.00	20.52	0.72	0.66	0.98

F-8

APPENDIX

Blast No	TRUE CRATER										N-Scaled Crater		
	Δ	Charge Height = (lb) Explosive Type	Charge Depth d_c (Ft)	Crater Depth h (Ft)	Crater Radius r (Ft)	Slant Distance to Rim C_t (Ft)	Volume v (Ft^3)	V/W	E	N	Δ_h = h/N N-Scaled Depth	Δ_r = r/N N-Scaled Radius	Δ_c = C_t/N N-Scaled Slant Distance
2307	0.08	2.5^{A60}	4.07	4.81	4.67	8.21	154.76	61.90	6.20	8.43	0.57	0.55	0.74
2317	0.08	10.0^{A60}	6.46	8.66	5.64	11.54	741.84	74.18	6.20	13.33	0.65	0.50	0.87
232	0.41	40.0^{A60}	10.26	13.50	11.74	17.91	2847.25	71.18	7.30	24.97	0.54	0.47	0.72
2407	0.63	2.5^{TS}	4.07	5.22	4.80	7.09	145.67	58.27	4.80	6.53	0.80	0.74	1.09
2417	0.63	10.0^{TS}	6.46	8.74	7.53	11.59	767.64	76.76	4.80	10.32	0.85	0.73	1.13
260	+0.16	10.0^{C4}	+2.15						6.20	13.33			
270	+0.08	10.0^{C4}	+1.08	1.86	4.33	4.73	69.47	4.95	6.20	13.33	0.14	0.32	0.35
270R	+0.08	10.0^{C4}	+1.08						6.20	13.33			
271	+0.08	10.0^{A60}	+1.08	0.93	4.50.	4.59	36.92	3.69	7.30	15.70	0.059	0.29	0.29
272	+0.08	10.0^{TS}	+1.08	1.30	3.85	3.32	40.22	1.82	6.00	12.90	0.10	0.24	0.26
280	0.00	10.0^{C4}	0.00						6.20	13.33			
281	0.09	10.0^{A60}	0.09	3.80	5.80	6.98	160.30	16.03	7.30	15.70	0.24	0.37	0.44
282	0.09	10.0^{TS}	0.06	3.54	4.42	5.54	82.62	8.26	6.00	12.90	0.20	0.34	0.43
290	0.16	10.0^{C4}	2.15	5.28	7.07	8.83	460.42	46.04	6.20	13.33	0.39	0.53	0.66

F-9

Blast No	TRUE CRATER										N-Scaled Crater		
	Δ	Charge Height = (lb) Explosive Type	Charge Depth d_c (Ft)	Crater Depth h (Ft)	Crater Radius r (Ft)	Slant Distance to Rim C_t (Ft)	Volume v (Ft^3)	V/W	E	N	Δ_h = h/N N-Scaled Depth	Δ_r = r/N N-Scaled Radius	Δ_c = C_t/N N-Scaled Slant Distance
291	0.17	10Ts	2.15	4.46	6.72	8.09	383.67	38.37	6.00	12.90	0.35	0.52	0.63
292	0.14	10A60	2.15	4.63	6.32	9.51	527.17	52.72	7.30	15.70	0.29	0.53	0.61
293	0.16	5.C4	1.71	4.34	5.96	7.36	258.99	51.80	6.30	10.60	0.41	0.56	0.69
294	0.17	5 Ts	1.71	4.39	5.30	6.87	204.31	40.86	6.00	10.26	0.43	0.52	0.67
295	0.14	5A60	1.71	4.96	5.43	7.37	255.32	51.06	7.30	12.48	0.40	0.44	0.59
296	0.16	40C4	3.42						6.20	21.20			
297	0.17	40 Ts	3.42						6.00	20.52			
298	0.14	40A60	3.42						7.30	24.97			

F-10

Blast No	COMPLETE RUPTURE								N-Scaled Complete Rupture			
	Charge Depth ft d_c	Δ	Depth of Complete Rupture, ft h_r	Complete Rupture Radius, ft r_r	Slant Distance to Limit, ft	Volume ft^3 V_r	V_r/W	Critical Depth, W ft	$W^{\frac{1}{3}}$	$h_r/W^{\frac{1}{3}}$ Depth	$r_r/W^{\frac{1}{3}}$ Radius	$V_r/W^{\frac{1}{3}}$ Volume
1	1.00	0.17	3.24	3.67	3.80	50.72	50.72	6.00	216.00	0.54	0.61	0.23
2	2.00	0.33	4.00	3.00	3.60	62.00	62.00	6.00	216.00	0.67	0.50	0.29
2A	2.00	0.33	3.66	3.17	3.75	84.45	84.45	6.00	216.00	0.61	0.53	0.39
3	3.00	0.50	4.18	2.80	4.10	85.63	85.63	6.00	216.00	0.70	0.47	0.40
4	3.95	0.99	[illegible]	[illegible]	5.00	92.69	92.69	6.00	216.00	0.91	0.51	0.43
5	4.85	0.81						6.00	216.00			
6	6.00	1.00						6.00	216.00			
7	0.00	0.00	1.70	1.95	1.95	9.10	9.10	6.00	216.00	0.30	0.33	0.04
8	-1.00	-0.17						6.00	216.00			
9	1.36	0.14	4.33	5.52	5.69	103.54	81.42	9.93	979.15	0.44	0.56	0.21
9 1/2	0.00	0.00	3.25	4.13	4.13	12.38	44.95	9.93	979.15	0.33	0.42	0.11
10	2.80	0.28	5.38	5.75	6.40	127.47	170.99	9.93	979.15	0.54	0.58	0.44
11	5.20	0.52	8.60	6.11	8.09	237.29	214.92	9.93	979.15	0.87	0.62	0.55
12	6.76	0.68	9.72	5.99	9.03	253.21	261.28	9.93	979.15	0.98	0.60	0.67

C-1

Blast No	COMPLETE RUPTURE								N-Scaled Complete Rupture			
	Charge Depth ft d_c	Δ	Depth of Complete Rupture, ft h_r	Complete Rupture Radius, ft r_r	Slant Distance to Limit, ft	Volume ft^3 V_r	V_r/W	Critical Depth, W ft	$W^{\frac{1}{3}}$	$h_r/W^{\frac{1}{3}}$ Depth	$r_r/W^{\frac{1}{3}}$ Radius	$V_r/W^{\frac{1}{3}}$ Volume
12 1/2	7.17	0.87	10.75	7.53	10.40	1121.75	224.35	12.40	1943.76	0.86	0.60	0.58
13	8.11	0.82	10.94	4.85	9.45	579.97	231.99	9.93	979.15	1.10	0.49	0.59
14	9.61	0.99						9.93	979.15			
14 1/2	12.34	0.99						12.40	1943.76			
15	2.20	0.14						15.70	3869.09			
15 B	2.20	0.14	7.52	8.50	8.96	960.47	96.05	15.70	3869.09	0.48	0.55	0.25
16	4.30	0.27						15.70	3869.09			
16 B	4.40	0.28	9.00	9.06	10.06	1655.07	165.59	15.70	3869.09	0.57	0.58	0.38
17	8.10	0.52	11.37	8.84	11.99	1645.24	164.52	15.70	3869.09	0.72	0.56	0.43
17 1/2	11.88	0.89						19.78	7738.09			
18	10.99	0.69	14.36	7.07	18.93	1665.13	166.51	15.70	3869.09	0.91	0.45	0.43
18 1/2	12.99	0.82						15.70	3869.09			
19	15.10	0.96						15.70	3869.09			
19 1/2	19.48	0.98						19.78	7738.09			

C-2

Blast No	COMPLETE RUPTURE								N-Scaled Complete Rupture			
	Charge Depth d_c ft	Δ	Depth of Complete Rupture, h_r ft	Complete Rupture Radius, r_r ft	Slant Distance to Limit, ft	Volume ft³ V_r	V_r/W	Critical Depth, W ft	$\sqrt[3]{W}$	$\frac{d_c}{\sqrt[3]{W}}$ Depth	$\frac{r_r}{\sqrt[3]{W}}$ Radius	$\frac{V_r}{\sqrt[3]{W}}$ Volume
20	22.60	1.44						15.70	3869.09			
21	3.32	0.14	9.58	11.95	12.40	2797.20	69.93	24.97	5568.02	0.30	0.48	0.18
21 1/2	0.00	0.00	6.04	9.63	9.63	933.40	23.34	24.97	5568.02	0.24	0.39	0.06
22	6.00	0.27	13.12	13.54	15.15	4456.94	111.42	24.97	5568.02	0.53	0.54	0.29
23	12.47	0.06	17.82	12.00	17.36	4480.41	112.02	24.97	5568.02	0.71	0.48	0.29
23 1/2	23.00	0.58						39.66	2287.51			
26	20.37	0.82						24.97	5568.02			
29	24.07	0.96						24.97	5568.02			
30	1.20	0.15	5.56	5.70	5.70	203.45	81.39	8.43	599.06	0.40	0.66	0.34
30 1/2	0.00	0.00	2.23	4.07	4.07	70.92	28.37	8.43	599.06	0.26	0.48	0.12
31	2.70	0.33	4.03	5.35	5.99	285.37	114.15	8.43	599.06	0.37	0.63	0.48
32	4.00	0.47	4.20	4.34	5.99	297.22	118.90	8.43	599.06	0.74	0.51	0.50
33	5.30	0.63	7.46	6.28	8.22	384.76	153.90	8.43	599.06	0.88	0.74	0.64
34	6.00	0.71	8.56	4.08	7.26	362.66	145.07	8.43	599.06	1.02	0.48	0.61

C-3

Blast No	COMPLETE RUPTURE								N-Scaled Complete Rupture			
	Charge Depth d_c ft	Δ	Depth of Complete Rupture, h_r ft	Complete Rupture Radius, r_r ft	Slant Distance to Limit, ft	Volume ft³ V_r	V_r/W	Critical Depth, W ft	$\sqrt[3]{W}$	$\frac{d_c}{\sqrt[3]{W}}$ Depth	$\frac{r_r}{\sqrt[3]{W}}$ Radius	$\frac{V_r}{\sqrt[3]{W}}$ Volume
34 1/2	6.22	0.59	9.20	5.61	8.37	667.55	133.51	10.60	1191.02	0.87	0.53	0.56
35	8.00	0.95						8.43	599.06			
35 1/2	10.14	0.96						10.60	1191.02			
36	2.16	0.16	5.71	6.68	7.02	581.23	58.12	13.33	2368.59	0.43	0.50	0.25
37	4.40	0.33	7.76	7.52	8.71	835.16	83.52	13.33	2368.59	0.58	0.56	0.35
38	8.31	0.62	12.64	6.25	10.39	864.67	86.47	13.33	2368.59	0.95	0.47	0.37
38 1/2	9.48	0.56						16.00	4741.63			
39	10.70	0.80						13.33	2368.59			
40	12.71	0.95						13.33	2368.59			
40 1/2	16.27	0.97						16.00	4741.63			
42	3.37	0.16	9.43	11.83	12.19	2921.42	73.04	21.20	9528.13	0.44	0.56	0.31
42 1/2	0.00	0.00	4.24	8.75	8.75	845.12	21.13	21.20	9528.13	0.29	0.41	0.09
43	6.82	0.32	13.09	12.10	13.89	3515.88	87.90	21.20	9528.13	0.62	0.57	0.37
44	11.37	0.54	17.53	11.32	16.04	3611.73	90.29	21.20	9528.13	0.83	0.53	0.38

C-4

Blast No	COMPLETE RUPTURE								N-Scaled Complete Rupture			
	Charge Depth d_c ft	Δ	Depth of Complete Rupture, h_r ft	Complete Rupture Radius, r_r ft	Slant Distance to Limit, ft	Volume V_r ft^3	V_r/N	Critical Depth, N ft	N^3	Depth $\frac{h_r}{N}$	Radius $\frac{r_r}{N}$	Volume $\frac{V_r}{N^3}$
44 1/2	19.55	0.50						33.67	38170.65			
46	20.67	0.98						21.20	9520.12			
50	1.33	0.16	4.60	4.69	4.88	161.70	64.68	8.16	543.34	0.56	0.57	0.30
51	2.40	0.30	5.27	4.46	5.10	213.65	85.46	8.16	543.34	0.65	0.55	0.39
52	5.13	0.63						8.16	543.34			
52 1/2	5.65	0.55						10.26	1080.05			
54	6.33	0.78						8.16	543.34			
54 B	7.38	0.90						8.16	543.34			
54 1/2	9.47	0.92						10.26	1080.06			
55	0.00	0.00	1.00	3.36	3.36	33.62	13.45	8.16	543.34	0.12	0.41	0.60
56	2.30	0.17	4.60	6.99	7.33	683.70	68.37	12.90	2146.69	0.36	0.54	0.32
57	4.45	0.34	8.00	8.06	9.21	991.01	99.10	12.90	2146.69	0.62	0.62	0.46
58	8.14	0.63	11.54	6.08	10.66	1000.47	100.05	12.90	2146.69	0.89	0.53	0.47
58 1/2	9.33	0.57						16.26	4290.94			

G-5

Blast No	COMPLETE RUPTURE								N-Scaled Complete Rupture			
	Charge Depth d_c ft	Δ	Depth of Complete Rupture, h_r ft	Complete Rupture Radius, r_r ft	Slant Distance to Limit, ft	Volume V_r ft^3	V_r/N	Critical Depth, N ft	N^3	Depth $\frac{h_r}{N}$	Radius $\frac{r_r}{N}$	Volume $\frac{V_r}{N^3}$
59	12.54	0.97						12.90	2146.69			
59 1/2	21.23	1.31						16.26	4290.94			
60	10.04	0.84	14.55	5.67	12.23	1235.60	123.56	12.90	2146.69	1.13	0.44	0.58
63	3.45	0.17	9.56	11.62	12.12	2550.40	63.76	20.52	8640.36	0.47	0.57	0.30
63 1/2	0.00	0.00	5.00	7.76	7.76	698.75	17.47	20.52	8640.36	0.30	0.38	0.08
64	6.95	0.34	11.00	12.24	14.00	3155.62	78.89	20.52	8640.36	0.58	0.60	0.37
65	12.85	0.63	17.07	10.51	16.60	3605.85	90.15	20.52	8640.36	0.87	0.51	0.42
65 1/2	18.90	0.92						20.52	8640.36			
67	26.65	1.01						20.52	8640.36			
70 T	1.34	0.17	4.34	4.10	4.32	109.02	43.59	8.43	599.06	0.48	0.48	0.18
71 T	2.66	0.32	5.67	5.92	6.59	290.09	81.16	8.43	599.06	0.67	0.71	0.34
72 T	5.38	0.64	7.36	6.32	8.20	342.18	136.86	8.43	599.06	0.87	0.74	0.57
73 T	6.86	0.81						8.43	599.06			
74 T	8.11	0.97						8.43	599.06			

G-6

Blast No	COMPLETE RUPTURE											
									N-Scaled Complete Rupture			
	Charge Depth d_c ft	Δ	Depth of Complete Rupture, d_r ft	Complete Rupture Radius, r_r ft	Slant Distance to Limit, ft	Volume ft^3 V_r	V_r/W	Critical Depth, W ft	W$^{\frac{1}{3}}$	Depth $d_r/W^{\frac{1}{3}}$	Radius $r_r/W^{\frac{1}{3}}$	Volume $V_r/W^{\frac{1}{3}}$
75 T	9.51	1.13						8.43	599.00			
76 T	2.20	0.17	6.42	7.75	8.06	642.39	64.24	13.33	2360.59	0.48	0.58	0.28
77 T	4.30	0.23	6.26	7.62	8.75	712.16	71.22	13.33	2360.59	0.43	0.56	0.29
78 T	8.60	0.65	11.67	9.99	13.18	1781.16	178.12	13.33	2360.59	0.87	0.76	0.75
79 T	10.75	0.30						13.33	2360.59			
80 T-	12.95	0.97						13.33	2360.59			
81 T	5.40	0.40	9.22	7.85	9.53	791.71	79.17	13.33	2360.59	0.70	0.59	0.33
82 T	3.20	0.24	7.79	8.37	8.96	1124.69	112.47	13.33	2360.59	0.59	0.63	0.47
90 T	1.58	0.24	6.32	5.49	5.71	142.83	57.13	6.53	278.45	0.66	0.84	0.51
91 T	2.48	0.38	5.09	4.67	5.29	133.11	53.24	6.53	278.45	0.76	0.71	0.47
92 T	5.38	0.83						6.53	278.45			
93 T	6.78	1.04						6.53	278.45			
94 T	8.18	1.25						6.53	278.45			
96T	2.24	0.21	6.05	5.93	6.34	458.77	45.88	10.32	1099.10	0.59	0.58	0.41

C-7

Blast No	COMPLETE RUPTURE											
									N-Scaled Complete Rupture			
	Charge Depth d_c ft	Δ	Depth of Complete Rupture, d_r ft	Complete Rupture Radius, r_r ft	Slant Distance to Limit, ft	Volume ft^3 V_r	V_r/W	Critical Depth, W ft	W$^{\frac{1}{3}}$	Depth $d_r/W^{\frac{1}{3}}$	Radius $r_r/W^{\frac{1}{3}}$	Volume $V_r/W^{\frac{1}{3}}$
97 T	4.24	0.43	7.72	6.77	8.04	515.73	51.57	10.32	1099.10	0.75	0.65	0.47
98 T	8.64	0.86						10.32	1099.10			
99 T	9.74	0.95						10.32	1099.10			
100T	5.44	0.53	9.00	7.50	9.26	869.69	86.97	10.32	1099.10	0.88	0.73	0.80
101T	3.29	0.33	6.59	7.17	7.89	621.35	62.14	10.32	1099.10	0.64	0.60	0.57
200	4.08	0.41	6.13	5.38	6.75	354.11	141.64	9.93	979.15	0.62	0.54	0.36
201	6.46	0.41	9.93	8.96	10.95	1406.93	140.69	15.70	3869.89	0.63	0.57	0.36
202	6.46	0.50	9.68	7.28	9.73	1045.78	104.58	12.90	2146.69	0.75	0.56	0.49
210	4.08	0.48						8.43	599.00			
211	6.46	0.48	9.32	8.02	10.30	116.11	111.61	13.33	2360.59	0.70	0.60	0.47
212	10.26	0.48	14.53	11.54	11.77	4967.00	101.46	21229	9528.12	0.69	0.54	0.43
220	4.08	0.50	6.40	5.01	6.46	295.56	118.22	8.16	543.24	0.78	0.61	0.54
220B	4.08	0.50						8.16	543.24			
222	10.26	0.50	14.27	11.03	15.06	3545.55	88.64	20.52	8640.24	0.70	0.54	0.41

C-8

Blast No	COMPLETE RUPTURE											
									N-Scaled Complete Rupture			
	Charge Depth ft d_c	Δ	Depth of Complete Rupture, ft h_r	Complete Rupture Radius, ft r_r	Slant Distance to Limit, ft	Volume ft³ V_r	V/W	Critical Depth, W ft	$W^{1/3}$	$h_r/W^{1/3}$ Depth	$r_r/W^{1/3}$ Radius	$V/W^{1/3}$ Volume
230T	4.07	0.48	5.56	4.72	6.23	217.27	86.91	8.43	599.08	0.66	0.57	0.36
231T	6.46	0.48	9.95	9.69	11.65	1324.83	132.48	13.33	2368.59	0.74	0.73	0.55
232	10.26	0.48	15.85	11.95	15.75	3883.70	97.09	24.97	15868.82	0.63	0.48	0.25
240T	4.07	0.63	6.08	4.99	6.44	181.63	72.63	6.53	278.45	0.94	0.76	0.64
241T	6.46	0.63	9.87	7.51	9.96	830.59	83.06	10.32	1099.18	0.96	0.73	0.76
269	+2.15	+0.16						13.33	2368.59			
270	+1.08	+0.08	3.38	5.86	5.96	201.88	20.19	13.33	2368.59	0.25	0.44	0.09
270B	+1.08	+0.08						13.33	2368.59			
271	+1.08	+0.07						15.70	3869.89			
272	+1.08	+0.08	2.55	4.57	4.78	66.41	6.64	12.90	2146.69	0.20	0.35	0.03
280	0.00	0.00						13.33	2368.59			
281	0.00	0.00	4.78	6.59	6.59	379.72	37.87	15.70	3869.89	0.30	0.42	0.10
282	0.00	0.00	4.01	4.96	4.96	212.53	21.25	12.90	2146.69	0.31	0.38	0.10
290	2.15	0.16	6.77	7.18	7.50	657.13	65.71	13.33	2368.59	0.51	0.54	0.28

Blast No	COMPLETE RUPTURE											
									N-Scaled Complete Rupture			
	Charge Depth ft d_c	Δ	Depth of Complete Rupture, ft h_r	Complete Rupture Radius, ft r_r	Slant Distance to Limit, ft	Volume ft³ V_r	V/W	Critical Depth, W ft	$W^{1/3}$	$h_r/W^{1/3}$ Depth	$r_r/W^{1/3}$ Radius	$V/W^{1/3}$ Volume
291	2.15	0.17	6.74	7.13	7.45	665.82	66.58	12.90	2146.67	0.52	0.55	0.31
292	2.15	0.14	7.17	9.59	9.83	1136.42	113.64	15.70	3869.89	0.46	0.61	0.29
293	1.71	0.16	5.40	7.18	7.37	511.42	102.28	10.60	1191.02	0.51	0.68	0.43
294	1.71	0.17	5.23	5.51	5.77	325.18	65.04	10.26	1080.05	0.51	0.54	0.30
295	1.71	0.14	5.38	6.29	6.52	424.39	84.88	12.48	1943.76	0.43	0.50	0.22
296	3.42	0.16						21.20	9528.13			
297	3.42	0.17						20.52	8640.36			
298	3.42	0.14						24.97	15868.82			

APPENDIX

Blast No	Extreme Rupture: Charge Depth ft d_c	Δ	Depth of Extreme Rupture h_e ft	Extreme Rupture Radius, ft r_e	Slant Distance to Limit, ft	Volume ft^3 V_e	V_e/W	Critical Depth, N ft	N-Scaled Extreme Rupture: $W^{1/3}$	Depth $h_e/W^{1/3}$	Radius $r_e/W^{1/3}$	Volume $V_e/W^{1/3}$	
1	1.00	0.17						6.00	216.00				
2	2.00	0.33						6.00	216.00				
2A	2.00	0.33						6.00	216.00				
3	3.00	0.50						6.00	216.00				
4	3.95	0.66						6.00	216.00				
5	4.85	0.81						6.00	216.00				
6	6.00	1.00						6.00	216.00				
7	0.00	0.00						6.00	216.00				
8	+1.00	+0.17						6.00	216.00				
9	1.36	0.14						9.93	979.15				
9 1/2	0.00	0.00						9.93	979.15				
10	2.80	0.28						9.93	979.15				
11	5.30	0.53						9.93	979.15				
12	6.76	0.68						9.93	979.15				

B - 1

Blast No	Extreme Rupture: Charge Depth ft d_c	Δ	Depth of Extreme Rupture h_e ft	Extreme Rupture Radius, ft r_e	Slant Distance to Limit, ft	Volume ft^3 V_e	V_e/W	Critical Depth, N ft	N-Scaled Extreme Rupture: $W^{1/3}$	Depth $h_e/W^{1/3}$	Radius $r_e/W^{1/3}$	Volume $V_e/W^{1/3}$	
12 1/2	7.17	0.57	11.10	8.23	10.92	1559.01	311.80	12.48	1943.76	0.89	0.66	0.80	
13	8.11	0.82	10.94	4.86	9.46	579.97	231.99	9.93	979.15	1.10	0.49	0.59	
14	9.61	0.99	12.33	5.32	10.98	897.15	358.86	9.93	979.15	1.24	0.54	0.92	
14 1/2	12.34	0.99						12.48	1943.76				
15	2.20	0.14						15.70	3869.89				
15B	2.20	0.14	9.01	8.50	8.78	1509.03	150.90	15.70	3869.89	0.57	0.54	0.39	
16	4.30	0.27						15.70	3869.89				
16B	4.40	0.28	9.00	9.98	10.91	2167.78	216.78	15.70	3869.89	0.57	0.64	0.56	
17	8.10	0.52						15.70	3869.89				
17 1/2	11.58	0.59						19.78	7738.89				
18	10.80	0.69	15.81	8.79	13.93	2698.50	269.85	15.70	3869.89	1.01	0.56	0.70	
18 1/2	12.90	0.82	16.66	9.75	16.17	3785.95	378.60	15.70	3869.89	1.06	0.62	0.98	
19	15.10	0.96						15.70	3869.89				
19 1/2	19.48	0.98						19.78	7738.89				

B - 2

Blast No	EXTREME RUPTURE								N-Scaled Extreme Rupture				
	Charge Depth ft d_c	Δ	Depth of Extreme Rupture, ft d_e	Extreme Radius, ft r_e	Slant Distance to Limit, ft	Volume ft^3 V_e	V_e/W	Critical Depth, N ft	$W^{1/3}$	$d_e/W^{1/3}$ Depth	$r_e/W^{1/3}$ Radius	$V_e/W^{1/3}$ Volume	
20	22.60	1.44						15.70	3869.09				
21	3.32	0.14						24.97	15568.82				
211/2	0.00	0.00	6.23	10.72	10.72	1765.52	44.16	24.97	15568.82	0.25	0.48	0.11	
22	6.80	0.27						24.97	15568.82				
23	12.47	0.50						24.97	15568.82				
231/2	23.00	0.58						39.64	62287.51				
26	20.57	0.82						24.97	15568.82				
29	24.07	0.96						24.97	15568.82				
30	1.30	0.15						8.43	599.06				
301/2	0.00	0.00	3.10	5.99	5.99	201.67	89.67	8.43	599.06	0.37	0.71	0.34	
31	2.70	0.33						8.43	599.06				
32	4.00	0.47						8.43	599.06				
33	5.30	0.63						8.43	599.06				
34	6.00	0.71						8.43	599.06				

B - 3

Blast No	EXTREME RUPTURE								N-Scaled Extreme Rupture				
	Charge Depth ft d_c	Δ	Depth of Extreme Rupture, ft d_e	Extreme Radius, ft r_e	Slant Distance to Limit, ft	Volume ft^3 V_e	V_e/W	Critical Depth, N ft	$W^{1/3}$	$d_e/W^{1/3}$ Depth	$r_e/W^{1/3}$ Radius	$V_e/W^{1/3}$ Volume	
341/2	6.22	0.59	10.12	7.62	9.84	1057.02	211.41	10.60	1191.02	0.95	0.72	0.89	
35	0.00	0.95	10.37	4.01	8.95	412.73	165.07	8.43	599.06	1.23	0.48	0.69	
351/2	10.14	0.96						10.60	1191.02				
36	2.16	0.16	6.26	8.66	8.93	1101.18	110.12	13.33	2368.59	0.47	0.65	0.46	
37	4.40	0.33	7.75	8.77	9.81	1243.51	124.35	13.33	2368.59	0.58	0.66	0.53	
38	8.21	0.62	12.68	6.58	10.60	1270.05	127.01	13.33	2368.59	0.93	0.49	0.54	
381/2	9.48	0.56						16.80	4741.63				
39	10.70	0.80	15.65	8.94	13.38	2937.44	293.74	13.33	2368.59	1.17	0.69	1.24	
40	12.71	0.95	16.34	6.65	14.34	1826.47	182.65	13.33	2368.59	1.23	0.50	0.77	
401/2	16.27	0.97	19.57	8.75	18.47	4187.27	209.36	16.80	4741.63	1.16	0.52	0.88	
42	3.37	0.16						21.20	9528.13				
421/2	0.00	0.00	7.27	10.35	10.35	1288.31	32.21	21.20	9528.13	0.34	0.49	0.14	
43	6.82	0.32	14.17	13.31	14.96	6136.75	153.42	21.20	9528.13	0.67	0.63	0.64	
44	11.37	0.54						21.20	9528.13				

B - 4

Shot No	Charge Depth ft d_c	Δ	Depth of Extreme Rupture ft D_e	Extreme Rupture Radius, ft r_e	Slant Distance to Limit, ft	Volume ft³ V_e	V_e/W	Critical Depth, W ft	W-Scaled Extreme Rupture: $W^{1/3}$	Depth $D_e/W^{1/3}$	Radius $r_e/W^{1/3}$	Volume $V_e/W^{1/3}$	
	EXTREME RUPTURE												
44 1/2	19.55	0.58						33.67	38170.63				
46	20.67	0.98	25.96	13.43	24.65	11118.25	277.96	21.20	9528.13	1.22	0.63	1.17	
50	1.33	0.16						8.16	543.34				
51	2.40	0.30						8.16	543.34				
52	5.13	0.63						8.16	543.34				
52 1/2	5.68	0.55						10.26	1080.05				
54	6.33	0.78						8.16	543.34				
54 B	7.38	0.90						8.16	543.34				
54 1/2	9.47	0.92	12.80	5.87	11.14	5288.16	277.96	10.26	1080.05	1.25	0.57	1.29	
55	0.00	0.00						8.16	543.34				
56	2.20	0.17						12.90	2146.69				
57	4.45	0.34						12.90	2146.69				
58	8.14	0.63						12.90	2146.69				
58 1/2	9.33	0.57						16.26	4298.94				

H - 5

Shot, N	Charge Depth ft d_c	Δ	Depth of Extreme Rupture ft D_e	Extreme Rupture Radius, ft r_e	Slant Distance to Limit, ft	Volume ft³ V_e	V_e/W	Critical Depth, W ft	W-Scaled Extreme Rupture: $W^{1/3}$	Depth $D_e/W^{1/3}$	Radius $r_e/W^{1/3}$	Volume $V_e/W^{1/3}$	
	EXTREME RUPTURE												
59	12.54	0.97	15.86	7.47	14.59	2197.90	219.79	12.90	2146.69	1.23	0.58	1.02	
591/2	21.23	1.31				2124.09	106.20	16.26	4298.94			0.49	
60	10.84	0.84						12.90	2146.69				
63	3.45	0.17						20.52	8640.36				
631/2	0.00	0.00	6.00	10.53	10.53	1487.41	37.19	20.52	8640.36	0.29	0.51	0.17	
64	6.95	0.34	13.68	14.08	15.70	5854.74	146.37	20.52	8640.36	0.67	0.69	0.68	
65	12.85	0.63	18.07	13.19	18.41	6142.86	153.57	20.52	8640.36	0.88	0.64	0.71	
651/2	18.90	0.92						20.52	8640.36				
67	20.65	1.01	25.56	9.54	22.75	9134.25	228.36	20.52	8640.36	1.25	0.46	1.06	
70T	1.36	0.17						8.43	599.08				
71T	2.66	0.32						8.43	599.08				
72T	5.38	0.64						8.43	599.08				
73T	6.86	0.81						8.43	599.08				
74T	8.11	0.97	11.19	5.60	9.86	855.72	342.29	8.43	599.08	1.33	0.66	1.42	

H-6

Shot N	Charge Depth ft	Δ	Depth of Cavity Centerline ft	Horizontal Radius ft	Slant Distance to Limit, ft	Volume ft³	V_e/W	Critical Depth, N ft	N-scaled Cavity Size N^3	Depth	Radius	Volume
75 T	9.51	1.13				839.30	135.75	8.43	599.08			0.57
76 T	2.20	0.17	6.90	8.68	8.95	1075.21	107.52	13.33	2368.59	0.52	0.65	0.46
77 T	4.30	0.32						13.33	2368.59			
78 T	8.60	0.65	11.70	12.56	15.22	3381.68	338.17	13.33	2368.59	0.89	0.94	1.42
79 T	10.75	0.80	15.15	11.93	16.06	4196.98	419.70	13.33	2368.59	1.13	0.90	1.76
80 T	12.95	0.97	16.55	11.64	17.41	5055.69	505.57	13.33	2368.59	1.24	0.87	2.14
81 T	5.40	0.40	9.44	11.18	12.42	2507.84	280.78	13.33	2368.59	0.71	0.84	1.06
82 T	3.20	0.24	8.10	10.87	11.33	2517.19	251.72	13.33	2368.59	0.61	0.81	1.06
90 T	1.58	0.24						6.53	278.45			
91 T	2.48	0.38						6.53	278.45			
92 T	5.38	0.83	7.98	5.72	7.85	501.44	200.58	6.53	278.45	1.21	0.88	1.79
93 T	6.78	1.04	9.01	5.56	8.77	699.52	279.81	6.53	278.45	1.38	0.85	2.52
94 T	8.18	1.25				285.82	114.73	6.53	278.45			1.03
96 T	2.24	0.21	6.58	7.23	7.57	867.95	86.80	10.32	1099.10	0.64	0.70	0.78

H - 7

Shot N	Charge Depth ft	Δ	Depth of Cavity Centerline ft	Horizontal Radius ft	Slant Distance to Limit, ft	Volume ft³	V_e/W	Critical Depth, N ft	N-scaled Cavity Size N^3	Depth	Radius	Volume
97 T	4.34	0.43	8.25	8.98	9.97	1145.55	114.56	10.32	1099.10	0.80	0.88	1.08
98 T	8.64	0.86	12.00	10.81	13.84	2120.90	212.09	10.32	1099.10	1.16	1.05	1.93
99 T	9.74	0.95	13.30	9.25	13.43	3610.00	361.00	10.32	1099.10	1.29	0.90	3.28
100T	5.44	0.53	9.18	9.68	11.10	2705.92	270.59	10.32	1099.10	0.89	0.94	2.46
101T	3.29	0.33	8.22	11.14	11.62	2499.46	249.95	10.32	1099.10	0.80	1.08	2.26
200	4.08	0.41						9.93	979.15			
201	6.46	0.41						15.70	3869.89			
202	6.46	0.50						12.90	2146.69			
210	4.08	0.48						8.43	599.08			
211	6.48	0.48	9.86	8.57	10.73	1566.85	156.68	13.33	2368.59	0.74	0.64	0.66
212	10.26	0.48	8.11	14.00	17.36	7504.43	187.61	21.20	9528.13	0.38	0.66	0.79
220	4.08	0.50						8.16	543.34			
220R	4.08	0.50						8.16	543.34			
222	10.26	0.50	14.43	14.03	17.38	5674.19	141.85	20.52	8640.34	0.70	0.68	0.66

H - 8

Blast No.	Charge Depth d_c ft	Δ	Depth of Extreme Rupture h_e ft	Extreme Rupture Radius r_e ft	Slant Distance to Limit, ft	Volume V_e ft³	V_e/W	Critical Depth, W ft	W-Scaled Extreme Rupture: W^3	Depth h_e/W	Radius r_e/W	Volume V_e/W^3
230 T	4.07	0.48	5.56	5.68	6.99	393.09	157.24	8.43	599.09	0.66	0.67	0.65
231 T	6.46	0.49	10.26	10.94	12.50	2561.31	256.13	13.33	2368.59	0.77	0.83	1.08
232	10.26	0.41	17.52	14.60	17.84	6912.50	172.81	24.97	[illegible]	0.70	0.58	0.44
240 T	4.07	0.63	6.26	7.67	8.68	750.16	300.06	6.53	278.49	0.96	1.18	2.69
241 T	6.46	0.53	10.27	8.75	10.88	1800.04	180.00	10.[illegible]	1099.10	1.00	0.85	1.64
260	+2.15	+0.16						13.33	2368.59			
270	+1.08	+0.08	3.73	9.29	9.35	529.06	52.91	13.33	2368.59	0.28	0.70	0.22
270 R	+1.08	+0.08	4.50	6.62	6.71	227.92	22.79	18.[illegible]	2368.59			
271	+1.08	+0.07	4.50	6.62	6.71	277.92	22.79	15.70	3869.89	0.29	0.42	0.06
272	+1.08	+0.08	2.92	6.37	6.46	224.22	22.42	12.90	2146.68	0.23	0.49	0.10
280	0.00	0.00						13.33	2368.59			
281	0.00	0.00	5.90	8.64	8.64	707.16	70.72	15.70	3869.89	0.35	0.55	0.18
282	0.00	0.00						18.90	2164.69			
290	2.15	0.16	7.38	8.47	8.74	18		13.33	2368.59	0.55	0.64	0.50

Blast No.	Charge Depth d_c ft	Δ	Depth of Extreme Rupture h_e ft	Extreme Rupture Radius r_e ft	Slant Distance to Limit, ft	Volume V_e ft³	V_e/W	Critical Depth, W ft	W-Scaled Extreme Rupture: W^3	Depth h_e/W	Radius r_e/W	Volume V_e/W^3
291	2.15	0.17						12.90	2146.69			
292	2.15	0.14						15.70	3869.89			
293	1.71	0.16						10.60	1191.02			
294	1.71	0.17						10.26	1080.05			
295	1.71	0.14						12.48	1943.76			
296	3.42	0.16						21.20	9528.13			
297	3.42	0.17						20.52	8640.36			
298	3.42	0.14						24.97	15568.82			

APPENDIX

Blast No	Extreme Rupture: Charge Depth d_c	Δ	Depth of Extreme Rupture D_e, ft	Extreme Rupture Radius, ft r_e	Slant Distance to Limit, ft	Volume ft^3 V_e	V_e/W	Critical Depth, W ft	N-Scaled Extreme Rupture: $W^{1/3}$	$d_c/W^{1/3}$ Depth	$r_e/W^{1/3}$ Radius	$V_e/W^{1/3}$ Volume
5	4.86	0.81	6.22		4.15	52	52.45	6.00	216	1.84		0.24
6	6.00	1.00	7.29		4.7	74	74.45	6.00	216	1.21		0.34
12	6.76	0.68	9.72	5.99	9.03	683	261.20	9.98	979	0.98	0.60	0.67
19	15.10	0.96	18.53		11.3	2.715	271.40	15.70	3,870	1.19		0.70
20	22.60	1.44	26.4		11.65			15.70	3,870	1.60		
25	20.57	0.82	27.04	12.81	24.23	8.401	210.02	24.97	15,569	1.09	0.51	0.54
29	24.07	0.96	30.22		24.4	10,630	265.95	24.97	15,569	1.21		0.68
548	7.28	0.90	9.55		5.9	123	49.24	8.16	543	1.17		0.23
591/2	21.23	1.31	25.90		10.2	2.124	106.20	16.26	4,299	1.60		0.49
727	6.86	0.81	8.94	5.96	9.09	621	248.59	8.43	599	1.06	0.71	1.03
757	9.51	1.13	11.84		6.22	239	135.75	8.43	599	1.40		0.57
947	8.18	1.25	10.62		6.6	287	114.73	6.53	278	1.63		1.03

II-11

Blast No	CANOUFLET									N-Scaled Cavity			
	Charge Depth d_c ft	Δ	Radius ft (Vertical) r_v	Radius at d_c ft (Horizontal) r_h	Volume, V_c ft^3	V_c/W	Maximum Width W_c	Critical Depth, N ft	N^3	Vert. Radius r_v/N	Horiz. Radius r_h/N	Cavity Vol. V/N^3	Ratio Max. Height to Max. Width
1	1.00	0.17	1.12					6.00	216.00	0.19			
2	2.00	0.33	0.90					6.00	216.00	0.15			
2A	2.00	0.33	0.90					6.00	216.00	0.15			
3	3.00	0.50	1.00					6.00	216.00	0.17			
4	3.95	0.66	1.45					6.00	216.00	0.24			
5	4.85	0.81	1.13	1.01	23.39	23.39	4.10	6.00	216.00	0.19	0.17	0.88	0.80
6	6.00	1.00	1.30	1.78	48.93	48.93	4.16	6.00	216.00	0.22	0.30	0.23	1.02
7	0.00	0.00	1.00					6.00	216.00	0.17			
8	+1.00	+0.17	1.24					6.00	216.00	0.21			
9	1.36	0.14	2.00					9.93	979.15	0.20			
9 1/2	0.00	0.00	2.02					9.93	979.15	0.20			
10	2.80	0.28	1.60					9.93	979.15	0.16			
11	5.30	0.53	1.40					9.93	979.15	0.14			
12	6.76	0.68	1.60					9.93	979.15	0.16			

I-1

Blast No	CANOUFLET									N-Scaled Cavity			
	Charge Depth d_c ft	Δ	Radius ft (Vertical) r_v	Radius at d_c ft (Horizontal) r_h	Volume, V_c ft^3	V_c/W	Maximum Width W_c	Critical Depth, N ft	N^3	Vert. Radius r_v/N	Horiz. Radius r_h/N	Cavity Vol. V/N^3	Ratio Max. Height to Max. Width
12 1/2	7.17	0.57	2.49					12.48	1943.76	0.20			
13	8.11	0.82	2.09	2.19	143.35	57.34	6.62	9.93	979.15	0.21	0.22	0.15	1.04
14	9.61	0.99	1.72	1.91	127.40	50.96	5.90	9.93	979.15	0.17	0.19	0.13	1.25
14 1/2	12.34	0.99						12.48	1943.76				
15	2.20	0.14						15.70	3869.89				
15 R	2.20	0.14	4.13					15.70	3869.89	0.26			
16	4.30	0.27						15.70	3869.89				
16 R	4.40	0.28	2.48					15.70	3869.89	0.16			
17	8.10	0.52	2.37					15.70	3869.89	0.15			
17 1/2	11.58	0.59						19.78	7738.89				
18	10.80	0.69	2.80	3.79	436.97	43.70	9.50	15.70	3869.89	0.18	0.24	0.11	1.00
18 1/2	12.90	0.82	2.31	3.57	376.29	37.62	9.36	15.70	3869.89	0.15	0.23	0.10	0.81
19	15.10	0.96	2.64	3.51	380.26	38.03	10.06	15.70	3869.89	0.17	0.22	0.10	0.84
19 1/2	19.48	0.98						19.78	7738.89				

I-2

Blast No	CANOUFLET									N-Scaled Cavity			
	Charge Depth d_c ft	Δ	Radius ft (Vertical) r_v	Radius at d_c ft (Horizontal) r_h	Volume, V_c ft^3	V_c/W	Maximum Width W_c	Critical Depth, W ft	W^3	Vert. Radius r_v/W	Horiz. Radius r_h/W	Cavity Vol. V_c/W^3	Ratio Max. Height to Max. Width
20	22.60	1.44	2.66	2.64	94.00	9.41	6.00	15.76	3969.09	0.17	0.17	0.02	1.12
21	3.32	0.14	4.10					24.97	15660.02	0.16			
21 1/2	0.00	0.00	4.02					24.97	15660.02	0.19			
22	6.00	0.27	3.35					24.97	15660.02	0.13			
23	12.47	0.50	4.02					24.97	15660.02	0.16			
23 1/2	23.00	0.58						39.64	62287.51				
26	20.57	0.82	6.51	4.49	833.15	20.83	11.40	24.97	15660.07	0.26	0.18	0.50	1.37
29	24.07	0.96	3.00	4.07	835.16	20.88	13.04	24.97	15660.07	0.15	0.20	0.50	0.83
30	1.30	0.15	2.00					8.43	599.00	0.23			
30 1/2	0.00	0.00	1.90					8.43	599.00	0.22			
31	2.70	0.32	1.20					8.43	599.00	0.15			
32	4.00	0.47	1.30					8.43	599.00	0.15			
33	5.30	0.63	0.85					8.43	599.00	0.10			
34	6.00	0.71	1.75					8.43	599.00	0.23			

I-3

Blast No	CANOUFLET									N-Scaled Cavity			
	Charge Depth d_c ft	Δ	Radius ft (Vertical) r_v	Radius at d_c ft (Horizontal) r_h	Volume, V_c ft^3	V_c/W	Maximum Width W_c	Critical Depth, W ft	W^3	Vert. Radius r_v/W	Horiz. Radius r_h/W	Cavity Vol. V_c/W^3	Ratio Max. Height to Max. Width
34 1/2	6.22	0.59	1.76					10.60	1191.02	0.17			
35	8.00	0.95	1.28	1.96	63.38	25.35	5.10	8.43	599.00	0.22	0.23	0.11	1.12
35 1/2	10.14	0.96						10.60	1191.02				
36	2.16	0.16	2.64					13.33	2360.59	0.20			
37	4.40	0.33	2.00					13.33	2360.59	0.15			
38	8.31	0.62	3.10					13.33	2360.59	0.23			
38 1/2	9.40	0.56						16.00	4741.63				
39	10.70	0.80	2.04	3.05	240.36	24.04	7.74	13.33	2360.59	0.21	0.29	0.50	1.06
40	12.71	0.95	2.02	3.25	171.19	17.19	7.50	13.33	2360.59	0.21	0.24	0.07	0.85
40 1/2	16.37	0.97	2.47	3.13	375.40	18.77	9.14	16.00	4741.63	0.15	0.19	0.08	1.01
42	3.37	0.16	3.05					21.20	9528.13	0.18			
42 1/2	0.00	0.00	5.00					21.20	9528.13	0.17			
43	6.02	0.32	2.78					21.20	9528.13	0.13			
44	11.37	0.54	2.66					21.20	9528.13	0.13			

I-4

Blast No	CAMOUFLET									N-Scaled Cavity			
	Charge Depth ft d_c	Δ	Radius ft (Vertical) r_v	Radius at d_c ft (Horizontal) r_h	Volume, V_c ft^3	V_c/W	Maximum Width w_c	Critical Depth, N ft	N^3	Vert. Radius r_v/N	Horiz. Radius r_h/N	Cavity Vol. V_c/N^3	Ratio Max. Height to Max. Width
441/2	19.55	0.50						33.67	38170.65				
46	20.67	0.90	3.90	5.74	408.27	10.00	11.60	21.20	9529.13	0.19	0.27	0.04	0.82
50	1.33	0.16	1.81					8.16	543.34	0.22			
51	2.40	0.30	1.70					8.16	543.34	0.22			
52	5.13	0.63	1.63					8.16	543.34	0.20			
521/2	5.65	0.55						10.26	1080.06				
54	6.33	0.78	1.45	2.43	197.84	79.14	7.02	8.16	543.34	0.18	0.30	0.36	0.90
54 B	7.30	0.90	1.62	2.13	77.09	31.16	5.54	8.16	543.34	0.20	0.26	0.14	0.92
541/2	9.47	0.92	2.02	2.65	92.63	18.53	6.06	10.26	1080.06	0.20	0.21	0.09	0.96
55	0.00	0.00	1.56					8.16	543.34	0.19			
56	2.20	0.17	2.32					12.90	2146.69	0.78			
57	4.45	0.24	1.27					12.90	2146.69	0.11			
58	8.14	0.63	2.36					12.90	2146.69	0.18			
581/2	9.33	0.57						16.26	4298.94				

DATA SHEET 1 I-6

Blast No	CAMOUFLET									N-Scaled Cavity			
	Charge Depth ft d_c	Δ	Radius ft (Vertical) r_v	Radius at d_c ft (Horizontal) r_h	Volume, V_c ft^3	V_c/W	Maximum Width w_c	Critical Depth, N ft	N^3	Vert. Radius r_v/N	Horiz. Radius r_h/N	Cavity Vol. V_c/N^3	Ratio Max. Height to Max. Width
59	12.54	0.97	1.89	2.37	163.24	16.32	7.76	12.90	2146.69	0.15	0.18	0.08	0.82
59 1/2	21.23	1.31	3.40	3.45	143.58	7.18	7.36	16.26	4298.94	0.21	0.23	0.03	0.93
60	10.84	0.84	2.17	2.83	170.71	17.07	6.28	12.90	2146.69	0.17	0.22	0.08	1.46
63	3.45	0.17	4.37					20.52	8640.36	0.21			
63 1/2	0.00	0.00	4.80					20.52	8640.36	0.23			
64	6.95	0.34	2.13					20.52	8640.36	0.10			
65	12.85	0.63	3.57					20.52	8640.36	0.17			
65 1/2	18.90	0.92						20.52	8640.36				
67	20.65	1.01	3.81	4.77	481.46	12.04	11.32	20.52	8640.36	0.19	0.23	0.06	0.88
70T	1.36	0.17	0.38					8.43	599.08	0.04			
71T	2.66	0.32	1.14					8.43	599.08	0.13			
72T	5.38	0.64	1.50					8.43	599.08	0.18			
73T	6.86	0.81	1.50	2.10	44.04	17.62	5.06	8.43	599.08	0.18	0.25	0.07	0.75
74T	8.11	0.97	2.26	1.74	20.85	8.34	3.52	8.43	599.08	0.27	0.21	0.03	1.13

I-6

Blast No	CANOUFLET									N-Scaled Cavity			
	Charge Depth d_c ft	Δ	Radius ft (Vertical) r_v	Radius at d_c ft (Horizontal) r_h	Volume, V_c ft^3	V_c/W	Maximum Width w_c	Critical Depth, W ft	W^3	Vert. Radius r_v/W	Horiz. Radius r_h/W	Cavity Vol. V_c/W	Ratio Max. Height to Max. Width
75 T	9.51	1.13	1.59	1.64	21.01	8.40	3.48	9.43	599.08	0.19	0.20	0.03	1.05
76 T	2.20	0.17	0.70					13.33	2368.59	0.05			
77 T	4.30	0.32	1.80					13.33	2368.59	0.14			
78 T	9.60	0.65	2.31					13.33	2368.59	0.17			
79 T	10.75	0.80	3.18	4.13	277.97	27.98	8.42	13.33	2368.59	0.24	0.31	0.11	0.94
80 T	12.95	0.97	2.87	2.84	130.59	13.06	4.78	13.33	2368.59	0.21	0.21	0.05	0.88
81 T	5.40	0.40	2.07					13.33	2368.59	0.16			
82 T	3.20	0.24	2.47					13.33	2368.59	0.19			
90 T	1.58	0.24	1.06					6.53	278.45	0.16			
91 T	2.88	0.38	0.88					6.53	278.45	0.09			
92 T	5.38	0.83	1.35	1.27	11.06	4.42	2.70	6.53	278.45	0.21	0.20	0.04	1.19
93 T	6.78	1.04	1.40	1.44	9.64	3.86	2.88	6.53	278.45	0.21	0.23	0.04	0.94
94 T	8.18	1.25	1.48	1.48	12.75	5.10	3.00	6.53	278.45	0.23	0.23	0.04	0.91
96 T	2.24	0.21	1.40					10.32	1099.10	0.14			

I-7

Blast No	CANOUFLET									N-Scaled Cavity			
	Charge Depth d_c ft	Δ	Radius ft (Vertical) r_v	Radius at d_c ft (Horizontal) r_h	Volume, V_c Ft^3	V_c/W	Maximum width w_c	Critical Depth, W ft	W^3	Vert. Radius r_v/W	Horiz. Radius r_h/W	Cavity V_c/W Vol.	Ratio Max. Height to Max. Width
97 T	4.34	0.43	1.68					10.32	1099.10	0.16			
98 T	8.64	0.86	2.07	3.00	182.46	18.25	7.30	10.32	1099.10	0.20	0.29	0.16	0.94
99 T	9.74	0.95	2.49	2.40	132.54	13.25	6.86	10.32	1099.10	0.24	0.24	0.12	0.95
100 T	5.44	0.53	2.22					10.32	1099.10	0.21			
101 T	3.29	0.33	1.51					10.32	1099.10	0.15			
200	4.08	0.41	1.36					9.93	979.15	0.14			
201	6.46	0.41	2.60					15.70	3869.89	0.17			
202	6.46	0.50	2.02					12.90	2146.69	0.16			
210	4.08	0.48						8.43	599.08				
211	6.46	0.48	1.90					13.33	2368.59	0.14			
212	10.26	0.48	2.92					21.20	9520.13	0.14			
220	4.08	0.50	1.68					8.16	599.08	0.21			
220 B	4.08	0.50						8.16	599.08				
222	10.26	0.50	4.58					20.52	8640.36	0.22			

I-8

Shot No	CARDUFLET									N-Scaled Cavity			
	Charge Depth d_c ft	Δ	Radius ft (Vertical) r_v	Radius at d_c ft (Horizontal) r_h	Volume, V_c ft^3	V_c/W	Maximum Width W_c	Critical Depth, W ft	W^3	Vert. Radius $r_v/\sqrt[3]{W}$	Horiz. Radius $r_h/\sqrt[3]{W}$	Cavity Vol. $V_c/\sqrt[3]{W}$	Ratio Max. Height to Max. Width
230 T	4.07	0.48	0.74					0.48	999.00	0.09			
231 T	6.46	0.48	2.20					13.33	2368.59	0.17			
232	10.26	0.41	3.24					24.97	15568.03	0.13			
240 T	4.07	0.63	1.14					6.53	278.45	0.17			
241 T	6.46	0.63	2.30					10.88	1099.10	0.28			
260	+2.15	+0.16						13.33	2368.59				
270	+1.00	+0.00	2.96					13.33	2368.59	0.22			
270 B	+1.00	+0.00						13.33	2368.59				
271	+1.00	+0.00	2.01					15.70	3869.00	0.13			
272	+1.00	+0.00	2.38					12.90	2146.60	0.18			
280	0.00	0.00						13.33	2368.59				
281	0.00	0.00	3.00					15.70	3869.00	0.24			
282	0.00	0.00	2.54					12.90	2146.60	0.20			
290	2.15	0.16	3.00					13.33	2368.59	0.23			

I-9

Shot No	CARDUFLET									N-Scaled Cavity			
	Charge Depth d_c ft	Δ	Radius ft (Vertical) r_v	Radius at d_c ft (Horizontal) r_h	Volume, V_c ft^3	V_c/W	Maximum Width W_c	Critical Depth, W ft	W^3	Vert. Radius $r_v/\sqrt[3]{W}$	Horiz. Radius $r_h/\sqrt[3]{W}$	Cavity Vol. $V_c/\sqrt[3]{W}$	Ratio Max. Height to Max. Width
291	2.15	0.17	2.31					12.90	2146.60	0.18			
292	2.15	0.14	2.40					15.70	3869.00	0.16			
293	1.71	0.16	2.63					10.60	1191.02	0.25			
294	1.71	0.17	2.60					10.36	1080.05	0.26			
295	1.71	0.14	3.25					12.40	1943.76	0.26			
296	3.42	0.16						21.20	9320.13				
297	3.42	0.17						20.52	8640.36				
298	3.42	0.14						24.97	15568.03				

I-10

1958 Surface

36 Lbs AAG

N 9.93

N^3 999.16

S 7.3 B C 1.0

Blast No.	Charge Depth d_c ft	Depth Ratio Δ	Apparent Crater V_a	Volume $\kappa_a = \frac{V_a}{N^3}$	Shape $\Lambda_a = \frac{V_a}{\pi r_a^2 h_a}$	Energy Utilization $\Lambda_e = \frac{V_a}{V_c}$	Apparent Crater Radius $\kappa_r = \frac{r_a}{N}$	Apparent Crater Depth $\kappa_h = \frac{h_a}{N}$	Apparent Crater Slant Distance $\kappa_c = \frac{c_a}{N}$				
	CRATER COEFFICIENTS--APPARENT CRATER												
9 1/2	0.90	0.08	8.48	0.022	0.45		0.30	0.17	0.30				
9	1.34	0.14	27.84	0.097	0.53		0.48	0.25	0.50				
10	2.80	0.28	20.70	0.052	0.67		0.51	0.11	0.58				
200	4.08	0.41	5.59	0.014	0.42		0.54	0.037	0.68				
11	5.30	0.53	12.91	0.033	0.41		0.48	0.11	0.71				
12	6.76	0.68											

J-1

1958 Surface

5.0 Lbs AAG

N 12.48

N^3 1943.76

S 7.3 B C1.0

Blast No.	Charge Depth d_c ft	Depth Ratio Δ	Apparent Crater V_a	Volume $\kappa_a = \frac{V_a}{N^3}$	Shape $\Lambda_a = \frac{V_a}{\pi r_a^2 h_a}$	Energy Utilization $\Lambda_e = \frac{V_a}{V_c}$	Apparent Crater Radius $\kappa_r = \frac{r_a}{N}$	Apparent Crater Depth $\kappa_h = \frac{h_a}{N}$	Apparent Crater Slant Distance $\kappa_c = \frac{c_a}{N}$				
	CRATER COEFFICIENTS--APPARENT CRATER												
295	1.71	0.14	23.55	0.041	0.62		0.41	0.19	0.43				
12 1/2	7.17	0.57	11.35	0.029	0.52		0.47	0.1 0	0.75				
14 1/2	12.34	0.99											

J-2

1950 Surface

10.0 Lbs AAO

N 15.70

N^3 3969.09

E 7.3 B C 1.0

Shot No.	Charge Depth d_c ft	Depth Ratio Δ	Apparent Crater V_a	Volume $V_a = \frac{V_a}{N^3}$	Shape $A_s = \frac{V_a}{\pi r_a^2 h_a}$	Energy Utilization $A_e = \frac{V_a}{E_c}$	Apparent Crater Radius $r_a = \frac{r_a}{N}$	Apparent Crater Depth $h_a = \frac{h_a}{N}$	Apparent Crater Slant Distance $E_c = \frac{c_a}{N}$				
	CRATER COEFFICIENTS--APPARENT CRATER												
271	+1.00	+0.07	3.69	0.010	0.32		0.28	0.12	0.29				
281	0.00	0.00	10.67	0.070	0.51		0.32	0.17	0.32				
292	2.15	0.14	21.28	0.081	0.52		0.50	0.20	0.52				
15	2.20	0.14											
152	2.20	0.14	25.26	0.066	0.51		0.46	0.19	0.48				
16	4.20	0.27											
162	4.40	0.28	25.02	0.067	0.44		0.54	0.15	0.62				
281	6.46	0.41	10.95	0.028	0.52		0.57	0.052	0.71				
17	8.10	0.52											
18	10.00	0.63											
181/2	12.90	0.82											
19	15.10	0.96											
20	22.60	1.44											

J-3

1950 Surface

20.0 Lbs AAO

N 19.70

N^3 7738.89

E 7.3 B C 1.0

Shot No.	Charge Depth d_c ft	Depth Ratio Δ	Apparent Crater V_a	Volume $V_a = \frac{V_a}{N^3}$	Shape $A_s = \frac{V_a}{\pi r_a^2 h_a}$	Energy Utilization $A_e = \frac{V_a}{E_c}$	Apparent Crater Radius $r_a = \frac{r_a}{N}$	Apparent Crater Depth $h_a = \frac{h_a}{N}$	Apparent Crater Slant Distance $E_c = \frac{c_a}{N}$				
	CRATER COEFFICIENTS--APPARENT CRATER												
17 1/2	11.50	0.59											
19 1/2	19.48	0.98											

J-4

1960 Surface

[illegible] lbs ANFO

E 7.2 N 24.97 N^B 15,[illegible] B C 1.0

Blast No.	Charge Depth ft d_c	Depth Ratio Δ	Apparent Crater V_a	Volume $K_v = \frac{V_a}{W}$	Shape $K_s = \frac{V_a}{\pi r_a^2 h_a}$	Energy Utilization $A_e = \frac{V_a}{V}$	Apparent Crater Radius $K_r = \frac{r_a}{W^{1/3}}$	Apparent Crater Depth $K_h = \frac{h_a}{W^{1/3}}$	Apparent Crater Slant Distance $K_c = \frac{c_a}{W^{1/3}}$				
	CRATER COEFFICIENTS--APPARENT CRATER												
21 1/2	0.00	0.00	0.91	0.053	0.41		0.22	0.17	0.32				
21	2.22	0.14	14.82	0.030	0.46		0.44	0.14	0.46				
298	3.42	0.14											
22	6.00	0.27	11.77	0.20	0.34		0.53	0.099	0.60				
222	10.24	0.41	18.67	0.027	0.41		0.47	0.098	0.62				
23	12.47	0.50	2.67	0.007	0.45		0.29	0.021	0.63				
24	20.57	0.82											
29	24.07	0.96											
													J-5

Trench Blasts

2.5 lbs ANFO

E 6.2 N 8.43 N^B 599.06 B C 1.0

Blast No.	Charge Depth ft d_c	Depth Ratio Δ	Apparent Crater V_a	Volume $K_v = \frac{V_a}{W}$	Shape $K_s = \frac{V_a}{\pi r_a^2 h_a}$	Energy Utilization $A_e = \frac{V_a}{V}$	Apparent Crater Radius $K_r = \frac{r_a}{W^{1/3}}$	Apparent Crater Depth $K_h = \frac{h_a}{W^{1/3}}$	Apparent Crater Slant Distance $K_c = \frac{c_a}{W^{1/3}}$				
	CRATER COEFFICIENTS--APPARENT CRATER												
707	1.26	0.17	9.06	0.037	0.20		0.53	0.21	0.58				
717	2.66	0.32	32.40	0.14	0.33		0.74	0.24	0.83				
2207	4.07	0.48	23.66	0.096	0.64		0.50	0.15	0.73				
727	5.28	0.64	33.56	0.14	0.37		0.74	0.22	0.98				
227	6.86	0.81											
747	8.11	0.97											
787	9.51	1.13											
													J-6

Trench Shots

N 13.33 10.6 lbs ANFO

E 6.2 N^3 3360.89 B C 1.0

Shot No.	Charge Depth d_c ft	Depth Ratio Δ	Apparent Crater $V_a^{1/3}$	Volume $\kappa_a = \frac{V_a^{1/3}}{W^{1/3}}$	Shape $\Delta_s = \frac{V_a}{\pi r_a^2 h_a}$	Energy Utilization $\Delta_e = \frac{V_a}{V_c}$	Apparent Crater Radius $\kappa_r = \frac{r_a^{1/3}}{W^{1/3}}$	Apparent Crater Depth $\kappa_h = \frac{h_a^{1/3}}{W^{1/3}}$	Apparent Crater Slant Distance $\kappa_c = \frac{c_a^{1/3}}{W^{1/3}}$				
	CRATER COEFFICIENTS--APPARENT CRATER												
762	2.30	0.17	17.73	0.075	0.80		0.44	0.15	0.47				
827	3.30	0.24	4.87	0.021	0.44		0.30	0.10	0.45				
772	4.30	0.32	10.19	0.042	0.44		0.50	0.13	0.59				
817	5.60	0.40	11.18	0.047	0.48		0.53	0.11	0.67				
2817	6.46	0.48	15.50	0.065	0.24		0.55	0.20	0.74				
782	8.60	0.65											
797	10.75	0.80											
807	12.95	0.97											
													J-7

1950 Surface

N 0.43 2.5 lbs Cm4

E 6.2 N^3 399.00 B C 1.0

Shot No.	Charge Depth d_c ft	Depth Ratio Δ	Apparent Crater $V_a^{1/3}$	Volume $\kappa_a = \frac{V_a^{1/3}}{W^{1/3}}$	Shape $\Delta_s = \frac{V_a}{\pi r_a^2 h_a}$	Energy Utilization $\Delta_e = \frac{V_a}{V_c}$	Apparent Crater Radius $\kappa_r = \frac{r_a^{1/3}}{W^{1/3}}$	Apparent Crater Depth $\kappa_h = \frac{h_a^{1/3}}{W^{1/3}}$	Apparent Crater Slant Distance $\kappa_c = \frac{c_a^{1/3}}{W^{1/3}}$				
	CRATER COEFFICIENTS--APPARENT CRATER												
20 1/2	0.00	0.00	9.37	0.039	0.47		0.34	0.23	0.34				
30	1.30	0.15	35.10	0.15	0.39		0.62	0.31	0.63				
31	2.70	0.33	12.96	0.054	0.43		0.60	0.11	0.69				
32	4.00	0.47	4.51	0.019	0.34		0.45	0.084	0.65				
210	4.00	0.40											
33	5.30	0.63	17.07	0.075	0.37		0.66	0.14	0.92				
34	6.00	0.71	3.47	0.014	0.60		0.33	0.071	0.79				
35	8.05	0.95											
													J-8

APPENDIX

1958 Surface

8.0 lbs C-4

N 10.60

N^3 1191.02

E 6.2 B C 1.0

Blast No.	Charge Depth d_c ft	Depth Ratio Δ	Apparent Crater V_a	Volume $K_v = \frac{V_a}{W^{3/2}}$	Shape $A_s = \frac{V_a}{\pi r_a^2 h_a}$	Energy Utilization $A_e = \frac{V_a d_c}{V_c}$	Apparent Crater Radius $K_r = \frac{r_a}{W^{1/3}}$	Apparent Crater Depth $K_h = \frac{h_a}{W^{1/3}}$	Apparent Crater Slant Distance $K_s = \frac{s_a}{W^{1/3}}$				
	CRATER COEFFICIENTS--APPARENT CRATER												
293	1.71	0.16	32.62	0.14	0.56		0.56	0.25	0.58				
34 1/2	6.22	0.59	9.90	0.042	0.57		0.42	0.13	0.72				
35 1/2	10.14	0.96											
													J-9

1958 Surface

10.0 Lbs C-4

N 13.33

N^3 2369.59

E 6.2 B C 1.0

Blast No.	Charge Depth d_c ft	Depth Ratio Δ	Apparent Crater V_a	Volume $K_v = \frac{V_a}{W^{3/2}}$	Shape $A_s = \frac{V_a}{\pi r_a^2 h_a}$	Energy Utilization $A_e = \frac{V_a d_c}{V_c}$	Apparent Crater Radius $K_r = \frac{r_a}{W^{1/3}}$	Apparent Crater Depth $K_h = \frac{h_a}{W^{1/3}}$	Apparent Crater Slant Distance $K_s = \frac{s_a}{W^{1/3}}$				
	CRATER COEFFICIENTS--APPARENT CRATER												
260	+2.15	+0.16											
270	+1.08	+0.08	4.95	0.021	0.45		0.32	0.14	0.33				
270R	+1.08	+0.08											
280	0.00	0.00											
290	2.15	0.16	23.[illegible]	0.099	0.55		0.52	0.21	0.55				
36	2.16	0.16	19.33	0.082	0.62		0.47	0.19	0.50				
37	4.40	0.33	9.77	0.041	0.47		0.56	0.090	0.65				
211	6.46	0.48	11.12	0.047	0.38		0.50	0.16	0.70				
38	8.31	0.62	11.22	0.047	0.51		0.47	0.14	0.79				
39	10.70	0.80											
40	12.70	0.95											
													J-10

1960 Surface

20.0 lbs C-4

N 16.00
N^3 4741.63

E 6.2 B C 1.0

Shot No.	Charge Depth ft d_c	Depth Ratio Δ	Apparent Crater r_a	Volume $V_a = \frac{V_a}{W}$	Shape $h_a = \frac{V_a}{\pi r_a^2 h_a}$	Energy Utilization $A_a = \frac{V_a}{V_c}$	Apparent Crater Radius $r_r = \frac{r_a}{W^{1/3}}$	Apparent Crater Depth $h_r = \frac{h_a}{W^{1/3}}$	Apparent Crater Slant Distance $R_c = \frac{R_c}{W^{1/3}}$				
	CRATER COEFFICIENTS--APPARENT CRATER												
20 1/2	9.48	0.56											
40 1/2	16.27	0.97											
													J-11

1960 Surface

40.0 lbs C-4

N 21.20
N^3 9880.13

E 6.2 B C 1.0

Shot No.	Charge Depth ft d_c	Depth Ratio Δ	Apparent Crater r_a	Volume $V_a = \frac{V_a}{W}$	Shape $h_a = \frac{V_a}{\pi r_a^2 h_a}$	Energy Utilization $A_a = \frac{V_a}{V_c}$	Apparent Crater Radius $r_r = \frac{r_a}{W^{1/3}}$	Apparent Crater Depth $h_r = \frac{h_a}{W^{1/3}}$	Apparent Crater Slant Distance $R_c = \frac{R_c}{W^{1/3}}$				
	CRATER COEFFICIENTS--APPARENT CRATER												
42 1/2	0.00	0.00	9.41	0.040	0.40		0.30	0.10	0.30				
42	3.37	0.16	12.91	0.080	0.84		0.40	0.15	0.51				
294	3.42	0.16											
43	6.03	0.32	13.04	0.066	0.75		0.37	0.072	0.65				
212	10.26	0.48	11.34	0.040	0.60		0.33	0.000	0.71				
44	11.37	0.54	4.66	0.020	0.51		0.33	0.043	0.75				
46	20.67	0.98											
													J-12

1950 Surface

1.0 Lbs TNT

N 6.0

E 6.0 N^3 216.00 B C 1.0

Blast No.	Charge Depth d_c ft	Depth Ratio Δ	Apparent Crater $V^{1/3}$	Volume $K_a = \frac{V^{1/3}}{W^{1/3}}$	Shape $A_a = \frac{V}{\pi r_a^2 h_a}$	Energy Utilization $A_e = \frac{V^{1/3}}{E^{1/3}}$	Apparent Crater Radius $A_r = \frac{r^{1/3}}{W^{1/3}}$	Apparent Crater Depth $A_h = \frac{h^{1/3}}{W^{1/3}}$	Apparent Crater Slant Distance $K_c = \frac{c^{1/3}}{W^{1/3}}$				
	CRATER COEFFICIENTS--APPARENT CRATER												
8	+1.04	+0.17	4.61	0.021	0.50		0.60	0.033	0.62				
7	0.00	0.00	3.48	0.016	0.50		0.29	0.12	0.29				
1	1.00	0.17	23.64	0.11	0.58		0.51	0.23	0.62				
2	2.00	0.33	12.82	0.059	0.60		0.47	0.15	0.49				
2A	2.00	0.33	7.20	0.033	0.51		0.50	0.083	0.61				
3	3.00	0.50	7.11	0.033	0.42		0.47	0.11	0.68				
4	3.95	0.66	2.97	0.014	0.35		0.24	0.21	0.73				
5	4.85	0.81											
6	6.00	1.00											

J-13

1950 Surface

2.5 Lbs TNT

N 8.16

E 6.0 N^3 543.34 B C 1.0

Blast No.	Charge Depth d_c ft	Depth Ratio Δ	Apparent Crater $V^{1/3}$	Volume $K_a = \frac{V^{1/3}}{W^{1/3}}$	Shape $A_a = \frac{V}{\pi r_a^2 h_a}$	Energy Utilization $A_e = \frac{V^{1/3}}{E^{1/3}}$	Apparent Crater Radius $A_r = \frac{r^{1/3}}{W^{1/3}}$	Apparent Crater Depth $A_h = \frac{h^{1/3}}{W^{1/3}}$	Apparent Crater Slant Distance $A_c = \frac{c^{1/3}}{W^{1/3}}$
	CRATER COEFFICIENTS--APPARENT CRATER								
55	0.00	0.00	4.30	0.020	0.45		0.31	0.14	0.31
50	1.33	0.16	23.35	0.11	0.43		0.56	0.25	0.59
51	2.48	0.30	13.20	0.061	0.62		0.55	0.11	0.62
220	4.08	0.50							
220R	4.08	0.50							
52	5.13	0.63	11.87	0.055	0.49		0.38	0.25	0.74
54	6.33	0.78							
54B	7.38	0.90							

J-14

1958 Surface

5.0 Lbs TS

N 10.56

N^3 1000.06

E 6.0 B C 1.0

CRATER COEFFICIENTS--APPARENT CRATER

Blast No.	Charge Depth ft d_c	Depth Ratio Δ	Apparent Crater V_a	Volume $A_v = \frac{V_a}{N^3}$	Shape $A_s = \frac{V_a}{\pi r_a^2 h_a}$	Energy Utilization $A_e =$	Apparent Crater Radius $A_r = \frac{r_a}{N}$	Apparent Crater Depth $A_h = \frac{h_a}{N}$	Apparent Crater Slant Distance $A_c = \frac{c_a}{N}$
294	1.71	0.17	20.89	0.097	0.56		0.51	0.21	0.53
82 1/2	5.65	0.55							
84 1/2	9.47	0.92							

J-15

1958 Surface

10.0 Lbs TS

N 12.90

N^3 2146.59

E 6.0 B C 1.0

CRATER COEFFICIENTS--APPARENT CRATER

Blast No.	Charge Depth ft d_c	Depth Ratio Δ	Apparent Crater V_a	Volume $A_v = \frac{V_a}{N^3}$	Shape $A_s = \frac{V_a}{\pi r_a^2 h_a}$	Energy Utilization $A_e =$	Apparent Crater Radius $A_r = \frac{r_a}{N}$	Apparent Crater Depth $A_h = \frac{h_a}{N}$	Apparent Crater Slant Distance $A_c = \frac{c_a}{N}$
272	+ 1.08	+0.08	1.82	0.008	0.37		0.27	0.093	0.29
282	0.00	0.00	8.00	0.037	0.48		0.38	0.17	0.38
291	2.15	0.17	19.41	0.090	0.56		0.51	0.20	0.54
56	2.20	0.17	19.00	0.089	0.62		0.47	0.20	0.50
57	4.45	0.34	14.65	0.068	0.57		0.63	0.10	0.71
202	6.46	0.50	8.30	0.039	0.64		0.41	0.11	0.74
58	8.14	0.63	11.23	0.052	0.53		0.55	0.10	0.84
60	10.84	0.84							
59	12.54	0.97							

J-16

1958 Surface

20.0 Lbs TR

N 16.26

N^3 4298.94

E 6.0 B C 1.0

CRATER COEFFICIENTS--APPARENT CRATER

Blast No.	Charge Depth d_c ft	Depth Ratio Δ	Apparent Crater V_a	Volume $\Delta_v = \frac{V_a^{1/3}}{N}$	Shape $\Delta_s = \frac{V_a}{\pi r_a^2 h_a}$	Energy Utilization $A_e = \frac{V_a}{V_c}$	Apparent Crater Radius $\Delta_r = \frac{r_a}{N}$	Apparent Crater Depth $\Delta_h = \frac{h_a}{N}$	Apparent Crater Slant Distance $\Delta_c = \frac{c_a}{N}$
58 1/2	9.23	0.57							
59 1/2	21.22	1.31							

J-17

1958 Surface

40.0 Lbs TR

N 20.52

N^3 8640.36

E 6.0 B C 1.0

CRATER COEFFICIENTS--APPARENT CRATER

Blast No.	Charge Depth d_c ft	Depth Ratio Δ	Apparent Crater V_a	Volume $\Delta_v = \frac{V_a^{1/3}}{N}$	Shape $\Delta_s = \frac{V_a}{\pi r_a^2 h_a}$	Energy Utilization $A_e = \frac{V_a}{V_c}$	Apparent Crater Radius $\Delta_r = \frac{r_a}{N}$	Apparent Crater Depth $\Delta_h = \frac{h_a}{N}$	Apparent Crater Slant Distance $\Delta_c = \frac{c_a}{N}$
63 1/2	0.00	0.00	7.28	0.034	0.42		0.37	0.16	0.37
297	3.42	0.17							
63	3.45	0.17	12.77	0.059	0.46		0.48	0.19	0.51
64	6.95	0.34	9.44	0.044	0.44		0.60	0.090	0.68
222	10.26	0.50	4.31	0.020	0.52		0.48	0.052	0.70
65	12.85	0.63	5.77	0.027	0.31		0.48	0.12	0.79
67	20.65	1.01							

J-18

APPENDIX

Trench Blasts

2.5 Lbs TE

N 6.53

N^3 270.45

E 4.0 B C 1.0

Blast No.	Charge Depth d_c ft	Depth Ratio Δ	Apparent Crater $V_a^{1/3}/W$	Volume $V_a^{1/3}/N = A_v$	Shape $A_s = \frac{V_a^{1/3}}{\pi r_a^2 h_a}$	Energy Utilization $V_a^{1/3}/E = A_e$	Apparent Crater Radius $r_a^{1/3}/N = A_r$	Apparent Crater Depth $h_a^{1/3}/N = A_h$	Apparent Crater Slant Distance $c_a^{1/3}/N = A_c$
CRATER COEFFICIENTS--APPARENT CRATER									
90T	1.50	0.24	25.52	0.23	0.50		0.76	0.24	0.85
91T	2.48	0.38	28.71	0.12	0.42		0.66	0.31	0.79
260T	4.07	0.63	39.23	0.35	0.34		0.55	0.11	0.84
92T	5.30	0.83							
93T	6.70	1.04							
94T	8.18	1.25							

J-19

Trench Blasts

10.0 Lbs TE

N 10.32

N^3 1099.10

E 4.0 B C 1.0

Blast No.	Charge Depth d_c ft	Depth Ratio Δ	Apparent Crater $V_a^{1/3}/W$	Volume $V_a^{1/3}/N = A_v$	Shape $A_s = \frac{V_a^{1/3}}{\pi r_a^2 h_a}$	Energy Utilization $V_a^{1/3}/E = A_e$	Apparent Crater Radius $r_a^{1/3}/N = A_r$	Apparent Crater Depth $h_a^{1/3}/N = A_h$	Apparent Crater Slant Distance $c_a^{1/3}/N = A_c$
CRATER COEFFICIENTS--APPARENT CRATER									
96T	2.24	0.21	8.30	0.076	0.63		0.53	0.14	0.56
101T	2.29	0.22	4.44	0.042	0.44		0.44	0.16	0.54
97T	4.34	0.42	14.74	0.13	0.60		0.50	0.21	0.71
100T	5.44	0.52	7.97	0.072	0.61		0.51	0.14	0.74
261T	6.46	0.63	10.60	0.090	0.62		0.73	0.14	0.96
98T	8.64	0.84							
99T	9.74	0.95							

J-20

2.5 Lbs A60

N^3 979.15
λ 9.93

E 7.3 — 1958 Surface — B — C 1.0

Blast No.	Charge Depth d_c ft	Depth Ratio Δ	True Crater $V_t^{1/3}$	Volume $K_t = \frac{V_t^{1/3}}{\lambda}$	Shape $K_s = \frac{V_t^{1/3}}{\pi r_t^2 h_t}$	Energy Utilization $A_t = \frac{V_t^{1/3}}{N^{1/3}}$	True Crater Radius $K_r = \frac{r_t}{\lambda}$	True Crater Depth $K_h = \frac{h_t}{\lambda}$	True Crater Slant Distance $K_c = \frac{c_t}{\lambda}$	Vertical Camouflet $K_{cv} = \frac{c_v}{\lambda}$	Horizontal Camouflet $K_{ch} = \frac{c_h}{\lambda}$	N-Scaled Max. Cavity Span $K_w = \frac{w}{\lambda}$	Cavity Shape Height to Span Ratio $S_c = \frac{h_c}{w}$
CRATER COEFFICIENTS--TRUE CRATER AND CAMOUFLET													
9 1/2	0.00	0.00	14.44	0.04	0.51		0.24	0.20	0.49	0.20			
9	1.24	0.14	49.20	0.13	0.50		0.40	0.24	0.89	0.20			
10	2.00	0.20	90.46	0.23	0.63		0.51	0.44	0.69	0.16			
200	4.00	0.41	74 78	0.19	0.46		0.49	0.55	0.74	0.14			
11	5.20	0.53	96.18	0.24	0.50		0.40	0.47	0.82	0.14			
12	6.76	0.60	294.51	0.74	0.85		0.50	0.84	1.07	0.16			
13	8.11	0.82	57.34	0.15						0.21	0.22	0.67	1.04
14	9.61	0.92	50.96	0.13						0.17	0.19	0.59	1.25

K-1

5.0 Lbs A60

N^3 1943.76
λ 12.48

E 7.3 — 1958 Surface — B — C 1.0

Blast No.	Charge Depth d_c ft	Depth Ratio Δ	True Crater $V_t^{1/3}$	Volume $K_t = \frac{V_t^{1/3}}{\lambda}$	Shape $K_s = \frac{V_t^{1/3}}{\pi r_t^2 h_t}$	Energy Utilization $A_t = \frac{V_t^{1/3}}{N^{1/3}}$	True Crater Radius $K_r = \frac{r_t}{\lambda}$	True Crater Depth $K_h = \frac{h_t}{\lambda}$	True Crater Slant Distance $K_c = \frac{c_t}{\lambda}$	Vertical Camouflet $K_{cv} = \frac{c_v}{\lambda}$	Horizontal Camouflet $K_{ch} = \frac{c_h}{\lambda}$	N-Scaled Max. Cavity Span $K_w = \frac{w}{\lambda}$	Cavity Shape Height to Span Ratio $S_c = \frac{h_c}{w}$
CRATER COEFFICIENTS--TRUE CRATER AND CAMOUFLET													
295	1.71	0.14	51.04	0.13	0.56		0.44	0.40	0.59	0.26			
12 1/2	7.17	0.57	122.33	0.31	0.55		0.49	0.77	0.91	0.20			
14 1/2	12.34	0.99											

K-2

10.0 Lbs AAA

N^3 3869.89

7.3 19.70 1958 Surface B C1.0

CRATER COEFFICIENTS--TRUE CRATER AND CAMOUFLET

Blast No.	Charge Depth d_c ft	Depth Ratio Δ	True Crater $V^{1/3}$	Volume V_t =	Shape V_s = $V/r_t^2 h_t$	Energy Utilization V_t =	True Crater Radius r_t =	True Crater Depth h_t =	True Crater Slant Distance h_c =	Vertical Camouflet r_c =	Horizontal Camouflet h_c =	Scaled Max. Cavity Span h_w =	Cavity Shape Height to Span Ratio h_c/w_c
271	1.08	0.07	3.69	0.01	0.62		0.29	0.059	0.29	0.13			
281	0.00	0.00	16.03	0.04	0.40		0.37	0.24	0.44	0.24			
292	2.15	0.14	52.72	0.14	0.52		0.53	0.29	0.61	0.16			
15	2.20	0.14											
152	2.20	0.14	55.66	0.14	0.47		0.49	0.40	0.64	0.26			
16	4.30	0.27											
162	4.40	0.28	89.00	0.23	0.53		0.56	0.44	0.71	0.16			
201	6.46	0.41	83.96	0.22	0.52		0.48	0.58	0.75	0.17			
17	8.10	0.52	99.24	0.26	0.44		0.53	0.67	0.85	0.15			
18	10.80	0.69	43.70	0.11						0.15	0.24	0.61	1.00
18 1/2	12.90	0.87	37.63	0.10						0.15	0.23	0.60	0.81
19	15.10	0.96	38.03	0.10						0.17	0.22	0.64	0.84
20	22.60	1.44	9.41	0.02						0.17	0.17	0.39	1.12

.3

10.0 Lbs AAA

N^3 7780.89

7.3 19.70 1958 Surface B C 1.0

CRATER COEFFICIENTS--TRUE CRATER AND CAMOUFLET

Blast No.	Charge Depth d_c ft	Depth Ratio Δ	True Crater $V^{1/3}$	Volume V_t =	Shape V_s = $V/r_t^2 h_t$	Energy Utilization V_t =	True Crater Radius r_t =	True Crater Depth h_t =	True Crater Slant Distance h_c =	Vertical Camouflet r_c =	Horizontal Camouflet h_c =	Scaled Max. Cavity Span h_w =	Cavity Shape Height to Span Ratio h_c/w_c
17 1/2	11.50	0.59											
19 1/2	19.48	0.98											

[illegible] ANO

$W^{\frac{1}{3}}$ 15,960.08

E 7.2 Y 24.97 1980 Surface B C 1.0

Blast No.	Charge Depth d_c ft	Depth Ratio Δ	True Crater r_t ft	Volume $V_t = \frac{r_t^3}{3}$	Shape $h_s = \frac{V_t}{\pi r_t^2 h_t}$	Energy Utilization $\Lambda_t = \frac{r_t}{W^{1/3}}$	True Crater Radius $\lambda_r = \frac{r_t}{d_c}$	True Crater Depth $\lambda_h = \frac{h_t}{d_c}$	True Crater Slant Distance $\lambda_c = \frac{c_t}{d_c}$	Vertical Cavouflet $\lambda_{cv} = \frac{c_v}{d_c}$	Horizontal Cavouflet $\lambda_{ch} = \frac{c_h}{d_c}$	Scaled Max. Cavity Span $\lambda_s = \frac{s_t}{d_c}$	Cavity Slope Height to Span Ratio $S_c = \frac{h_s}{s_t}$
CRATER COEFFICIENTS--TRUE CRATER AND CAVOUFLET													
21 1/2	9.00	0.00	11.06	0.03	0.44		0.24	0.19	0.60	0.12			
21	2.22	0.14	27.90	0.10	0.51		0.48	0.30	0.54	0.14			
298	3.42	0.14											
22	6.00	0.27	54.14	0.14	0.29		0.53	0.41	0.81	0.13			
222	10.24	0.41	71.18	0.18	0.49		0.47	0.54	0.72	0.13			
23	12.47	0.50	71.09	0.18	0.52		0.41	0.44	0.78	0.16			
24	20.57	0.82	20.83	0.05						0.24	0.18	0.46	1.37
29	24.07	0.96	20.83	0.05						0.15	0.20	0.53	0.84
													K-5

2.5 Lbs ANO

$W^{\frac{1}{3}}$ 599.08

0.42 Trench Blasts

E 4.2 B C 1.0

Blast No.	Charge Depth d_c ft	Depth Ratio Δ	True Crater r_t ft	Volume $V_t = \frac{r_t^3}{3}$	Shape $h_s = \frac{V_t}{\pi r_t^2 h_t}$	Energy Utilization $\Lambda_t = \frac{r_t}{W^{1/3}}$	True Crater Radius $\lambda_r = \frac{r_t}{d_c}$	True Crater Depth $\lambda_h = \frac{h_t}{d_c}$	True Crater Slant Distance $\lambda_c = \frac{c_t}{d_c}$	Vertical Cavouflet $\lambda_{cv} = \frac{c_v}{d_c}$	Horizontal Cavouflet $\lambda_{ch} = \frac{c_h}{d_c}$	Scaled Max. Cavity Span $\lambda_s = \frac{s_t}{d_c}$	Cavity Slope Height to Span Ratio $S_c = \frac{h_s}{s_t}$
CRATER COEFFICIENTS--TRUE CRATER AND CAVOUFLET													
70T	1.24	0.17	19.84	0.08	0.49		0.52	0.20	0.55	0.04			
71T	2.64	0.32	45.12	0.20	0.27		0.71	0.45	0.84	0.13			
230T	4.07	0.48	61.90	0.24	0.47		0.55	0.57	0.74	0.09			
72T	5.38	0.64	98.59	0.41	0.34		0.68	0.82	1.06	0.18			
73T	6.84	0.81	17.62	0.07						0.18	0.28	0.60	0.75
74T	8.11	0.97	8.24	0.03						0.27	0.21	0.41	1.13
75T	9.51	1.12	8.40	0.03						0.19	0.20	0.41	1.05
													K-6

APPENDIX

10.0 Lbs AA8

N^3 2360.89

E 6.9 — 13.22 — Trench Blasts — B — C 1.0

Blast No.	Charge Depth d_c ft	Depth Ratio Δ	True Crater $V_{1/3}$	Volume A_t =	Shape $A_s = \frac{V}{\pi r_t^2 h_t}$	Energy Utilization A_t =	True Crater Radius A_r =	True Crater Depth A_h =	True Crater Slant Distance A_c =	Vertical Camouflet A_{cv} =	Horizontal Camouflet A_{ch} =	Scaled Max. Cavity Span A_w =	Cavity Shape Height to Span Ratio S_c =
	CRATER COEFFICIENTS--TRUE CRATER AND CAMOUFLET												
76T	2.20	0.17	22.05	0.19	0.72		0.44	0.22	0.60	0.05			
82T	3.20	0.24	44.66	0.20	0.55		0.51	0.42	0.66	0.19			
77T	4.20	0.32	29.27	0.16	0.34		0.50	0.46	0.73	0.14			
81T	5.40	0.40	47.62	0.20	0.29		0.53	0.56	0.78	0.16			
221T	6.46	0.48	74.18	0.21	0.47		0.58	0.65	0.87	0.17			
78T	8.60	0.65	106.93	0.46	0.92		0.44	0.92	0.92	0.17			
79T	10.75	0.80	27.98	0.11						0.24	0.31	0.64	0.94
80T	12.95	0.97	13.04	0.05						0.21	0.21	0.51	0.88

K-7

2.5 Lbs C4

N^3 599.08

E 6.2 — 8.43 — 1958 Surface — B — C 1.0

Blast No.	Charge Depth d_c ft	Depth Ratio Δ	True Crater $V_{1/3}$	Volume A_t =	Shape $A_s = \frac{V}{\pi r_t^2 h_t}$	Energy Utilization A_t =	True Crater Radius A_r =	True Crater Depth A_h =	True Crater Slant Distance A_c =	Vertical Camouflet A_{cv} =	Horizontal Camouflet A_{ch} =	Scaled Max. Cavity Span A_w =	Cavity Shape Height to Span Ratio S_c =
	CRATER COEFFICIENTS--TRUE CRATER AND CAMOUFLET												
30 1/2	0.00	0.00	9.37	0.04	0.44		0.35	0.23	0.42	0.23			
30	1.20	0.15	53.56	0.22	0.40		0.62	0.49	0.77	0.33			
31	2.70	0.33	65.09	0.27	0.48		0.60	0.46	0.90	0.14			
32	4.00	0.47	86.18	0.36	0.73		0.50	0.63	0.80	0.15			
210	4.08	0.48											
33	5.30	0.63	69.84	0.29	0.35		0.60	0.73	0.95	0.10			
34	6.00	0.71	71.00	0.30	0.82		0.35	0.93	1.00	0.21			
35	8.00	0.95	25.35	0.11						0.22	0.23	0.60	1.12

K-8

5.0 Lbs C4

W^3 1191.02

E 6.2 10.60 1580 Surface B C 1.0

Blast No.	Charge Depth d_c ft	Depth Ratio Δ	True Crater $\sqrt{V_t}$	Volume $\sqrt{V_t}$	Shape $\sqrt{V_t}/\pi r_t^2 h_t$	Tracer Fillization $\sqrt{A_t}$	True Crater Radius $\sqrt{r_t}$	True Crater Depth $\sqrt{h_t}$	True Crater Slant Distance $\sqrt{c_t}$	Vertical Camouflet $\sqrt{K_{cv}}$	Horizontal Camouflet $\sqrt{K_{ch}}$	Scaled Max. Cavity Span $\sqrt{A_w}$	Cavity Shape Height to Span Ratio S_c
CRATER COEFFICIENTS--TRUE CRATER AND CAMOUFLET													
293	1.71	0.16	51.00	0.22	0.84		0.56	0.41	0.69	0.25			
34 1/2	6.22	0.59	48.92	0.21	0.46		0.42	0.78	0.87	0.17			
35 1/2	10.14	0.96											

K-9

10.0 Lbs C4

W^3 2360.59

E 6.2 13.22 1960 Surface B C 1.0

Blast No.	Charge Depth d_c ft	Depth Ratio Δ	True Crater $\sqrt{V_t}$	Volume $\sqrt{V_t}$	Shape $\sqrt{V_t}/\pi r_t^2 h_t$	Tracer Fillization $\sqrt{A_t}$	True Crater Radius $\sqrt{r_t}$	True Crater Depth $\sqrt{h_t}$	True Crater Slant Distance $\sqrt{c_t}$	Vertical Camouflet $\sqrt{K_{cv}}$	Horizontal Camouflet $\sqrt{K_{ch}}$	Scaled Max. Cavity Span $\sqrt{A_w}$	Cavity Shape Height to Span Ratio S_c
CRATER COEFFICIENTS--TRUE CRATER AND CAMOUFLET													
260	2.15	0.16											
270	1.00	0.08	4.95	0.02	0.45		0.32	0.14	0.35	0.22			
270B	1.00	0.08											
280	0.00	0.00											
290	2.15	0.16	46.04	0.19	0.56		0.53	0.39	0.66	0.23			
36	2.16	0.16	31.72	0.13	0.50		0.49	0.36	0.61	0.20			
37	4.40	0.33	60.69	0.26	0.54		0.56	0.48	0.74	0.15			
211	6.46	0.48	98.38	0.42	0.66		0.57	0.63	0.85	0.14			
38	8.31	0.62	75.38	0.32	0.55		0.47	0.86	0.98	0.23			
39	10.70	0.80	24.04	0.10						0.21	0.29	0.58	1.06
40	12.70	0.95	17.19	0.07						0.21	0.24	0.57	0.85

K-10

20.0 Lbs C4

W^3 4741.63

E 6.2 16.60 1980 Surface B C 1.0

Blast No.	Charge Depth d_c ft	Depth Ratio Δ	True Crater $\sqrt{V_t}$	Volume $\sqrt{V_t}$	Shape $\sqrt{V_t}/\pi r_t^2 h_t$	Tracer Fillization $\sqrt{A_t}$	True Crater Radius $\sqrt{r_t}$	True Crater Depth $\sqrt{h_t}$	True Crater Slant Distance $\sqrt{c_t}$	Vertical Camouflet $\sqrt{K_{cv}}$	Horizontal Camouflet $\sqrt{K_{ch}}$	Scaled Max. Cavity Span $\sqrt{A_w}$	Cavity Shape Height to Span Ratio S_c
CRATER COEFFICIENTS--TRUE CRATER AND CAMOUFLET													
38 1/2	9.48	0.56											
40 1/2	16.27	0.97	19.77	0.08						0.18	0.19	0.56	1.01

K-11

40.0 Lbs C4

W^{3} 9620.13

t 6.2 51.30 1950 Surface B C 1.0

Shot No.	Charge Depth d_c ft	Depth Ratio Δ	True Crater r_m	Volume V_t	Shape V_s	Height Utilization h_t	True Crater Radius r_t	True Crater Depth h_t	True Crater Slant Distance s_t	Vertical Camouflet h_{cv}	Horizontal Camouflet h_{ch}	Scaled Max. Cavity Span h_w	Cavity Shape Height to Span Ratio S_c
CRATER COEFFICIENTS--TRUE CRATER AND CAMOUFLET													
43 1/2	0.00	0.00	14.24	0.06	0.46		0.39	0.27	0.50	0.27			
43	2.37	0.16	30.51	0.13	0.50		0.49	0.34	0.60	0.18			
29½	2.42	0.16											
43	6.82	0.32	43.61	0.18	0.46		0.57	0.45	0.73	0.13			
212	10.24	0.48	44.35	0.19	0.34		0.53	0.62	0.82	0.14			
44	11.37	0.54	43.42	0.18	0.19		0.62	0.66	0.99	0.13			
46	20.67	0.98	10.08	0.04						0.19	0.27	0.55	0.82

K-12

1.0 Lbs 75

W^{3} 216.00

t 6.0 6.0 1950 Surface B C 1.0

Shot No.	Charge Depth d_c ft	Depth Ratio Δ	True Crater r_m	Volume V_t	Shape V_s	Height Utilization h_t	True Crater Radius r_t	True Crater Depth h_t	True Crater Slant Distance s_t	Vertical Camouflet h_{cv}	Horizontal Camouflet h_{ch}	Scaled Max. Cavity Span h_w	Cavity Shape Height to Span Ratio S_c
CRATER COEFFICIENTS--TRUE CRATER AND CAMOUFLET													
8	1.00	0.17	4.61	0.02	0.49		0.62	0.04	0.62	0.21			
7	0.00	0.00	4.04	0.03	0.51		0.37	0.17	0.36	0.17			
1	1.00	0.17	32.99	0.15	0.39		0.61	0.35	0.65	0.19			
2	2.00	0.33	47.11	0.22	0.66		0.47	0.48	0.57	0.15			
2A	2.00	0.33	44.31	0.21	0.55		0.50	0.48	0.61	0.15			
3	3.00	0.50	62.58	0.29	0.64		0.47	0.67	0.82	0.17			
4	3.95	0.66	73.32	0.34	0.98		0.35	0.90	0.98	0.24			
5	4.85	0.81	23.39	0.11						0.19	0.17	0.68	0.80
6	6.00	1.00	48.93	0.23						0.22	0.30	0.69	1.02

K-13

2.5 [illegible] TS

N^3 543.34

6.0 8.16 1958 Surface B C 1.9

CRATER COEFFICIENTS--TRUE CRATER AND CANOUFLET

Blast No.	Charge Depth d_c ft	Depth Ratio Δ	True Crater $V^{1/3}$	Volume A_t	Shape A_s	Energy Utilization A_u	True Crater Radius A_r	True Crater Depth A_h	True Crater Slant Distance A_c	Vertical Canouflet k_{cv}	Horizontal Canouflet k_{ch}	Scaled Max. Cavity Span k_w	Cavity Stage Height to Span Ratio Δ_c
55	0.00	0.00	8.02	0.04	0.39		0.39	0.19	0.44	0.19			
50	1.33	0.16	26.11	0.17	0.44		0.56	0.28	0.68	0.22			
51	2.48	0.30	49.44	0.23	0.47		0.58	0.51	0.75	0.21			
220	4.08	0.50	78.56	0.26	0.43		0.61	0.71	0.94	0.21			
220B	4.08	0.50											
52	5.13	0.63	66.66	0.31	0.81		0.38	0.83	0.91	0.20			
54	6.33	0.78	79.14	0.36						0.18	0.30	0.96	0.90
54B	7.38	0.90	31.16	0.14						0.20	0.26	0.68	0.92

K-14

5.0 [illegible] TS

N^3 1080.05

6.0 10.26 1958 Surface B C 1.0

CRATER COEFFICIENTS--TRUE CRATER AND CANOUFLET

Blast No.	Charge Depth d_c ft	Depth Ratio Δ	True Crater $V^{1/3}$	Volume A_t	Shape A_s	Energy Utilization A_u	True Crater Radius A_r	True Crater Depth A_h	True Crater Slant Distance A_c	Vertical Canouflet k_{cv}	Horizontal Canouflet k_{ch}	Scaled Max. Cavity Span k_w	Cavity Stage Height to Span Ratio Δ_c
294	1.71	0.17	40.86	0.19	0.53		0.52	0.33	0.67	0.26			
521/2	5.65	0.55											
541/2	9.47	0.92	18.53	0.09						0.20	0.21	0.62	0.96

K-15

APPENDIX

10.0 Lbs TS

W^{3} 2146.69

t 6.0 ; 12.90 1950 Surface B C 1.0

CRATER COEFFICIENTS--TRUE CRATER AND CANOUFLET

Blast No.	Charge Depth d_c ft	Depth Ratio Δ	True Crater $r_{tc}/W^{1/3}$	Volume V_t/W	Shape $A_s/W^{2/3}$	Energy Utilization A_t/W	True Crater Radius $r_t/W^{1/3}$	True Crater Depth $h_t/W^{1/3}$	True Crater Slant Distance $s_t/W^{1/3}$	Vertical Canouflet $h_{cv}/W^{1/3}$	Horizontal Canouflet $h_{ch}/W^{1/3}$	Scaled Max. Cavity Span $h_w/W^{1/3}$	Cavity Shape Height to Span Ratio h_c/h_w
272	1.00	0.08	1.02	0.01	0.48		0.24	0.10	0.26	0.18			
282	0.09	0.09	8.86	0.04	0.46		0.38	0.20	0.43	0.20			
291	2.15	0.17	28.27	0.18	0.63		0.52	0.35	0.62	0.18			
56	2.20	0.17	45.73	0.21	0.67		0.54	0.35	0.64	0.18			
57	4.45	0.34	50.14	0.23	0.42		0.63	0.45	0.77	0.11			
292	6.46	0.50	92.70	0.39	0.61		0.55	0.66	0.86	0.16			
58	8.14	0.62	80.52	0.30	0.44		0.48	0.81	0.94	0.18			
60	10.84	0.84	17.07	0.08						0.17	0.22	0.49	1.46
59	12.54	0.97	16.22	0.08						0.15	0.18	0.60	0.82

K-16

20.0 Lbs TS

W^{3} 4298.94

t 6.0 ; 16.26 1950 Surface B C 1.0

CRATER COEFFICIENTS--TRUE CRATER AND CANOUFLET

Blast No.	Charge Depth d_c ft	Depth Ratio Δ	True Crater $r_{tc}/W^{1/3}$	Volume V_t/W	Shape $A_s/W^{2/3}$	Energy Utilization A_t/W	True Crater Radius $r_t/W^{1/3}$	True Crater Depth $h_t/W^{1/3}$	True Crater Slant Distance $s_t/W^{1/3}$	Vertical Canouflet $h_{cv}/W^{1/3}$	Horizontal Canouflet $h_{ch}/W^{1/3}$	Scaled Max. Cavity Span $h_w/W^{1/3}$	Cavity Shape Height to Span Ratio h_c/h_w
68 1/2	0.38	0.57											
69 1/2	21.23	1.21	7.18	0.02						0.21	0.21	0.45	0.93

K-17

40.0 Lbs TS

W^{3} 8640.36

t 6.0 ; 20.52 1950 Surface B C 1.0

CRATER COEFFICIENTS--TRUE CRATER AND CANOUFLET

Blast No.	Charge Depth d_c ft	Depth Ratio Δ	True Crater $r_{tc}/W^{1/3}$	Volume V_t/W	Shape $A_s/W^{2/3}$	Energy Utilization A_t/W	True Crater Radius $r_t/W^{1/3}$	True Crater Depth $h_t/W^{1/3}$	True Crater Slant Distance $s_t/W^{1/3}$	Vertical Canouflet $h_{cv}/W^{1/3}$	Horizontal Canouflet $h_{ch}/W^{1/3}$	Scaled Max. Cavity Span $h_w/W^{1/3}$	Cavity Shape Height to Span Ratio h_c/h_w
63 1/2	0.60	0.00	10.87	0.02	0.47		0.37	0.23	0.44	0.23			
297	2.42	0.17											
62	2.45	0.17	29.53	0.14	0.49		0.48	0.38	0.61	0.21			
64	4.95	0.34	54.71	0.25	0.51		0.60	0.44	0.74	0.10			
222	10.24	0.50	61.87	0.29	0.29		0.66	0.72	0.98	0.22			
65	12.95	0.63	75.45	0.35	0.28		0.70	0.80	1.07	0.17			
67	20.05	1.01	12.04	0.04						0.19	0.23	0.55	0.08

K-16

2.5 Lbs TS

N^3 278.45

E 4.0 — $\sqrt[3]{N}$ 6.53 — Trench Blasts — B — C 1.0

Blast No.	Charge Depth d_c ft	Depth Ratio Δ	True Crater $\sqrt[3]{N}$	Volume $K_t = \frac{V_t}{N}$	Shape $A_s = \frac{V_t}{\pi r_t^2 h_t}$	Energy Utilization $A_t = \frac{V_t}{N}$	True Crater Radius $A_r = \frac{r_t}{\sqrt[3]{N}}$	True Crater Depth $A_h = \frac{h_t}{\sqrt[3]{N}}$	True Crater Slant Distance $K_c = \frac{c_t}{\sqrt[3]{N}}$	Vertical Camouflet $K_{cv} = \frac{r_v}{\sqrt[3]{N}}$	Horizontal Camouflet $A_{ch} = \frac{r_h}{\sqrt[3]{N}}$	V-Scaled Max. Cavity Span $A_w = \frac{w_c}{\sqrt[3]{N}}$	Cavity Shape Height to Span Ratio $S_c = \frac{h_c}{w_c}$
CRATER COEFFICIENTS--TRUE CRATER AND CAMOUFLET													
90T	1.50	0.24	42.15	0.37	0.42		0.84	0.40	0.94	0.16			
91T	2.48	0.38	41.30	0.39	0.50		0.68	0.47	0.85	0.09			
240T	4.07	0.63	58.27	0.53	0.39		0.74	0.80	1.09	0.17			
92T	5.38	0.83	4.42	0.04						0.21	0.20	0.41	1.19
93T	6.78	1.04	3.86	0.04						0.21	0.28	0.46	0.94
94T	8.18	1.25	5.10	0.04						0.22	0.32	0.46	0.91

K-19

10.0 Lbs TS

N^3 1099.10

E 4.0 — $\sqrt[3]{N}$ 10.32 — Trench Blasts — B — C 1.0

Blast No.	Charge Depth d_c ft	Depth Ratio Δ	True Crater $\sqrt[3]{N}$	Volume $K_t = \frac{V_t}{N}$	Shape $A_s = \frac{V_t}{\pi r_t^2 h_t}$	Energy Utilization $A_t = \frac{V_t}{N}$	True Crater Radius $A_r = \frac{r_t}{\sqrt[3]{N}}$	True Crater Depth $A_h = \frac{h_t}{\sqrt[3]{N}}$	True Crater Slant Distance $K_c = \frac{c_t}{\sqrt[3]{N}}$	Vertical Camouflet $K_{cv} = \frac{r_v}{\sqrt[3]{N}}$	Horizontal Camouflet $A_{ch} = \frac{r_h}{\sqrt[3]{N}}$	V-Scaled Max. Cavity Span $A_w = \frac{w_c}{\sqrt[3]{N}}$	Cavity Shape Height to Span Ratio $S_c = \frac{h_c}{w_c}$
CRATER COEFFICIENTS--TRUE CRATER AND CAMOUFLET													
96T	2.24	0.21	18.54	0.18	0.46		0.58	0.35	0.68	0.14			
101T	3.29	0.32	34.77	0.31	0.57		0.61	0.47	0.78	0.15			
97T	4.34	0.42	40.79	0.37	0.48		0.65	0.59	0.88	0.16			
100T	5.44	0.53	41.20	0.37	0.46		0.59	0.74	0.95	0.21			
241T	6.46	0.62	76.76	0.70	0.49		0.73	0.85	1.13	0.22			
98T	8.64	0.86	18.25	0.16						0.20	0.29	0.71	0.94
99T	9.74	0.95	13.25	0.12						0.24	0.24	0.66	0.95

K-20

2.5 Lbs A60

N^3 979.15

E 7.3 N 9.93 1958 Surface B C 1.0

Shot No.	Charge Depth ft d_c	Depth Ratio Δ	Complete Rupture V_r	Volume $K = \frac{V_r}{N}$	Shape $h_s = \frac{V_r}{\pi r_r^2 h_r}$	Energy Utilization $A = \frac{V_r}{V_o}$	Complete Rupture Radius $r_r = \frac{r_r}{N}$	Complete Rupture Depth $h_r = \frac{h_r}{N}$	Complete Rupture Slant Distance $h_c = \frac{c_r}{N}$	Scaled Charge Depth $\lambda_c = d_c/\sqrt[3]{W}$	Scaled Slant Distance $C_r/\sqrt[3]{W}$		
	CRATER COEFFICIENTS--COMPLETE RUPTURE												
9 1/2	0.00	0.00	44.95	0.11	0.65	0.19	0.42	0.22	0.42	0.00	3.07		
9	1.26	0.14	81.42	0.21	0.49	0.34	0.56	0.44	0.57	1.00	4.16		
10	2.80	0.28	170.99	0.44	0.77	0.72	0.58	0.54	0.64	2.06	4.67		
200	4.08	0.41	141.64	0.36	0.64	0.60	0.54	0.62	0.68	3.00	4.96		
11	5.30	0.54	214.92	0.55	0.53	0.91	0.62	0.87	0.81	3.93	5.91		
12	6.76	0.68	261.28	0.67	0.60	1.10	0.60	0.98	0.91	4.97	6.64		
13	8.11	0.82	231.99	0.59	0.72	0.98	0.49	1.10	0.95	5.98	6.94		
14	9.61	0.99								7.08			
													L-1

5.0 Lbs A60

N^3 1943.76

E 7.3 N 12.48 1958 Surface B C 1.0

Shot No.	Charge Depth ft d_c	Depth Ratio Δ	Complete Rupture V_r	Volume $K = \frac{V_r}{N}$	Shape $h_s = \frac{V_r}{\pi r_r^2 h_r}$	Energy Utilization $A = \frac{V_r}{V_o}$	Complete Rupture Radius $r_r = \frac{r_r}{N}$	Complete Rupture Depth $h_r = \frac{h_r}{N}$	Complete Rupture Slant Distance $h_c = \frac{c_r}{N}$	Scaled Charge Depth $\lambda_c = d_c/\sqrt[3]{W}$	Scaled Slant Distance $C_r/\sqrt[3]{W}$		
	CRATER COEFFICIENTS--COMPLETE RUPTURE												
295	1.71	0.14	84.89	0.22	0.64	0.43	0.50	0.43	0.52	1.00	3.80		
12 1/2	7.17	0.57	224.35	0.58	0.59	1.13	0.60	0.86	0.82	4.20	4.04		
14 1/2	12.34	0.99								7.23			
													L-2

18.0 Lb AAD

W^3 3069.09

A 7.3 N 18.70 1950 Surface B C 1.0

CRATER COEFFICIENTS--COMPLETE RUPTURE

Blast No.	Charge Depth d_c ft	Depth Ratio Δ	Complete Rupture V_r	Volume $K = \frac{V_r}{W}$	Shape $h_o = \frac{V_r}{W r_r^3}$	Energy Utilization $A = \frac{V_r}{V_o}$	Complete Rupture Radius $r_r = \frac{r_r}{W}$	Complete Rupture Depth $h_r = \frac{h_r}{W}$	Complete Rupture Slant Distance $R_r = \frac{S_r}{W}$	Scaled Charge Depth $\lambda_o = d_c/\sqrt[3]{W}$	Scaled Slant Distance $C_r = S_r/\sqrt[3]{W}$
271	1.00	0.07								0.50	
301	0.00	0.00	37.27	0.10	0.50	0.22	0.42	0.30	0.42	0.00	2.06
292	2.15	0.14	112.44	0.29	0.56	0.69	0.61	0.66	0.62	1.00	4.60
15	2.20	0.14								1.03	
152	2.20	0.14	96.06	0.35	0.56	0.50	0.55	0.60	0.56	1.06	4.09
16	4.20	0.27								2.00	
162	4.40	0.28	146.59	0.28	0.63	0.90	0.50	0.57	0.64	2.05	4.67
201	6.46	0.41	160.69	0.36	0.57	0.86	0.57	0.63	0.70	3.00	5.11
17	8.10	0.52	164.52	0.42	0.59	1.06	0.56	0.72	0.76	3.77	5.55
18	10.00	0.69	166.55	0.43	0.74	1.01	0.48	0.91	0.82	5.01	5.99
18 1/2	12.90	0.82								6.00	

L-3

22.0 Lb AAD

W^3 7720.09

A 7.3 N 19.70 1950 Surface B C 1.0

CRATER COEFFICIENTS--COMPLETE RUPTURE

Blast No.	Charge Depth d_c ft	Depth Ratio Δ	Complete Rupture V_r	Volume $K = \frac{V_r}{W}$	Shape $h_o = \frac{V_r}{W r_r^3}$	Energy Utilization $A = \frac{V_r}{V_o}$	Complete Rupture Radius $r_r = \frac{r_r}{W}$	Complete Rupture Depth $h_r = \frac{h_r}{W}$	Complete Rupture Slant Distance $R_r = \frac{S_r}{W}$	Scaled Charge Depth $\lambda_o = d_c/\sqrt[3]{W}$	Scaled Slant Distance $C_r = S_r/\sqrt[3]{W}$
17 1/2	11.00	0.59								4.26	
19 1/2	19.40	0.98								7.16	

L-4

40.0 Lbs A60

N^3 15,560.82

L 7.3 N 24.97 1950 Surface B C 1.0

CRATER COEFFICIENTS--COMPLETE RUPTURE

Blast No.	Charge Depth d_c ft	Depth Ratio Δ	Complete Rupture V_c/W	Volume $\lambda = V/W^{3/2}$	Shape $\lambda_s = V_r/\pi r_r^2 h_r$	Energy Utilization $A = V_r/V_o$	Complete Rupture Radius $r_r/W^{1/3}$	Complete Rupture Depth $h_r/W^{1/3}$	Complete Rupture Slant Distance $\Delta_c = c_r/W^{1/3}$	Scaled Charge Depth $\lambda_o = d_o/\sqrt[3]{W}$	Scaled Slant Distance $c_r/\sqrt[3]{W}$
21 1/2	0.00	0.00	22.34	0.06	0.53	0.19	0.39	0.24	0.39	0.00	2.85
21	3.32	0.14	69.93	0.10	0.65	0.58	0.48	0.30	0.50	0.97	3.65
298	3.42	0.14								1.00	
22	6.00	0.27	111.42	0.29	0.59	0.93	0.54	0.53	0.61	1.99	4.45
232	10.26	0.41	97.09	0.25	0.55		0.48	0.63	0.63	3.00	4.60
23	12.47	0.50	112.02	0.29	0.55	0.93	0.48	0.71	0.70	3.67	5.11

L-5

2.5 Lbs A60

N^3 599.08

L 6.2 N 8.43 Trench Blasts B C 1.0

CRATER COEFFICIENTS--COMPLETE RUPTURE

Blast No.	Charge Depth d_c ft	Depth Ratio Δ	Complete Rupture V_c/W	Volume $\lambda = V/W^{3/2}$	Shape $\lambda_s = V_r/\pi r_r^2 h_r$	Energy Utilization $A = V_r/V_o$	Complete Rupture Radius $r_r/W^{1/3}$	Complete Rupture Depth $h_r/W^{1/3}$	Complete Rupture Slant Distance $\Delta_c = c_r/W^{1/3}$	Scaled Charge Depth $\lambda_o = d_o/\sqrt[3]{W}$	Scaled Slant Distance $c_r/\sqrt[3]{W}$
70T	1.36	0.17	42.53	0.78	0.51	0.31	0.48	0.48	0.52	1.00	3.22
71T	2.66	0.32	81.16	0.34	0.33	0.59	0.71	0.67	0.77	1.95	4.77
230T	4.07	0.48	86.91	0.26	0.56	0.63	0.57	0.66	0.74	3.00	4.59
72T	5.38	0.64	130.86	0.57	0.37	0.99	0.76	0.97	0.99	3.95	6.16
74T	8.11	0.97								5.97	

L-6

10.0 Lbs ANFO

N^3 2360.89

E 6.2 N 13.33 Trench Blasts B C 1.0

CRATER COEFFICIENTS--COMPLETE RUPTURE

Blast No.	Charge Depth d_c ft	Depth Ratio Δ	Complete Rupture V_r ft³	Volume $A = \frac{V_r}{W}$	Shape $A_s = \frac{V_r}{W \cdot h_r}$	Energy Utilization $A = \frac{V_r}{h_o}$	Complete Rupture Radius $r_r = \frac{r_r}{W}$	Complete Rupture Depth $\Delta_h = \frac{h_r}{W}$	Complete Rupture Slant Distance $\Delta_c = \frac{c_r}{W}$	Scaled Charge Depth $\lambda_o = d_o/\sqrt[3]{W}$	Scaled Slant Distance $C_r/\sqrt[3]{W}$
76Y	2.20	0.17	44.24	0.28	0.53	0.37	0.50	0.40	0.60	1.02	3.72
82Y	3.30	0.24	112.47	0.47	0.66	0.65	0.63	0.59	0.67	1.49	4.15
77Y	4.30	0.32	71.22	0.29	0.47	0.41	0.50	0.63	0.66	2.02	4.09
81Y	5.40	0.40	79.17	0.33	0.44	0.45	0.59	0.70	0.72	2.50	4.46
221Y	6.46	0.48	122.40	0.55	0.45	0.76	0.73	0.74	0.87	3.02	5.39
78Y	8.60	0.65	178.12	0.75	0.49	1.02	0.76	0.87	0.99	4.00	6.14

L-7

2.5 Lbs C4

N^3 599.08

E 6.2 N 8.43 1968 Surface B C 1.0

CRATER COEFFICIENTS--COMPLETE RUPTURE

Blast No.	Charge Depth d_c ft	Depth Ratio Δ	Complete Rupture V_r ft³	Volume $A = \frac{V_r}{W}$	Shape $A_s = \frac{V_r}{W \cdot h_r}$	Energy Utilization $A = \frac{V_r}{h_o}$	Complete Rupture Radius $r_r = \frac{r_r}{W}$	Complete Rupture Depth $\Delta_h = \frac{h_r}{W}$	Complete Rupture Slant Distance $\Delta_c = \frac{c_r}{W}$	Scaled Charge Depth $\lambda_o = d_o/\sqrt[3]{W}$	Scaled Slant Distance $C_r/\sqrt[3]{W}$
30 1/2	0.00	0.00	28.37	0.12	0.61	0.30	0.48	0.26	0.48	0.00	2.90
30	1.30	0.15	81.30	0.34	0.52	0.50	0.66	0.48	0.68	0.96	4.22
31	2.70	0.33	114.15	0.48	0.66	0.81	0.63	0.57	0.71	2.03	4.40
32	4.00	0.47	118.93	0.50	0.80	0.85	0.51	0.74	0.79	2.94	4.24
310	4.00	0.48								3.00	
33	5.30	0.63	153.90	0.64	0.42	1.10	0.74	0.80	0.90	3.90	6.00
34	6.00	0.71	145.07	0.61	0.81	1.03	0.48	1.02	0.86	4.42	5.33
35	8.00	0.95								5.87	

L-8

5.0 LBS C4

N^3 1191.02
N 10.60 1958 Surface

E 6.2 B 1.0

CRATER COEFFICIENTS--COMPLETE RUPTURE

Blast No.	Charge Depth d_c ft	Depth Ratio Δ	Complete Rupture $\lambda_r = \frac{r_r}{W}$	Volume $\lambda = \frac{V_r^{1/3}}{W}$	Shape $\lambda_s = \frac{V_r}{W \cdot r_r^3}$	Energy Utilization $\lambda = \frac{V_r}{V_o}$	Complete Rupture Radius $\lambda_r = \frac{r_r}{W}$	Complete Rupture Depth $\lambda_h = \frac{h_r}{W}$	Complete Rupture Slant Distance $\lambda_c = \frac{c_r}{W}$	Scaled Charge Depth $\lambda_d = d_c/\sqrt[3]{W}$	Scaled Slant Distance $c_r/\sqrt[3]{W}$
293	1.71	0.16	102.20	0.43	0.59	0.77	0.60	0.81	0.70	1.00	4.34
341/2	6.22	0.59	133.51	0.56	0.73	1.01	0.52	0.87	0.70	3.64	4.90
351/2	10.14	0.96								5.94	

10.0 LBS C4

N^3 2368.59
N 13.33 1958 Surface

E 6.2 B C1.0

CRATER COEFFICIENTS--COMPLETE RUPTURE

Blast No.	Charge Depth d_c ft	Depth Ratio Δ	Complete Rupture $\lambda_r = \frac{r_r}{W}$	Volume $\lambda = \frac{V_r^{1/3}}{W}$	Shape $\lambda_s = \frac{V_r}{W \cdot r_r^3}$	Energy Utilization $\lambda = \frac{V_r}{V_o}$	Complete Rupture Radius $\lambda_r = \frac{r_r}{W}$	Complete Rupture Depth $\lambda_h = \frac{h_r}{W}$	Complete Rupture Slant Distance $\lambda_c = \frac{c_r}{W}$	Scaled Charge Depth $\lambda_d = d_c/\sqrt[3]{W}$	Scaled Slant Distance $c_r/\sqrt[3]{W}$
260	2.15	0.16								1.00	
270	1.08	0.08	20.19	0.09	0.57	0.16	0.44	0.25	0.45	0.50	2.79
270R	1.08	0.08								0.50	
289	0.00	0.00								0.00	
290	2.15	0.16	65.71	0.28	0.60	0.53	0.54	0.51	0.56	1.00	3.47
36	2.14	0.16	58.12	0.25	0.73	0.47	0.50	0.43	0.52	1.00	3.29
37	4.40	0.33	83.52	0.35	0.61	0.67	0.56	0.58	0.65	2.05	4.03
211	6.46	0.48	111.61	0.47	0.59	0.90	0.60	0.70	0.77	3.00	4.77
39	8.31	0.62	96.47	0.37	0.56	0.70	0.47	0.95	0.78	3.86	4.84
40	12.70	0.95									

20.0 Lbs C4

W^3 4741.63
E 6.2 N 16.00 1950 Surface B C 1.0

Blast No.	Charge Depth ft d_c	Depth Ratio Δ	Complete Rupture $V_r/W^{1/3}$	Volume $K = V_r/W^{1/3}$	Shape $h_s = V_r/(\pi r_r^2 h_r)$	Energy Utilization $A = V_r/V_o$	Complete Rupture Radius $r_r/W^{1/3}$	Complete Rupture Depth $h_r/W^{1/3}$	Complete Rupture Slant Distance $h_c = c_r/W^{1/3}$	Scaled Charge Depth $\lambda_o = d_o/\sqrt[3]{W}$	Scaled Slant Distance $c_r/\sqrt[3]{W}$		
	CRATER COEFFICIENTS--COMPLETE RUPTURE												
201/2	7.60	0.56								2.42			
401/2	16.27	0.97								6.01			
													L-11

40.0 Lbs C4

W^3 9630.13
E 6.2 N 21.30 1950 Surface B C 1.0

Blast No.	Charge Depth ft d_c	Depth Ratio Δ	Complete Rupture $V_r/W^{1/3}$	Volume $K = V_r/W^{1/3}$	Shape $h_s = V_r/(\pi r_r^2 h_r)$	Energy Utilization $A = V_r/V_o$	Complete Rupture Radius $r_r/W^{1/3}$	Complete Rupture Depth $h_r/W^{1/3}$	Complete Rupture Slant Distance $h_c = c_r/W^{1/3}$	Scaled Charge Depth $\lambda_o = d_o/\sqrt[3]{W}$	Scaled Slant Distance $c_r/\sqrt[3]{W}$		
	CRATER COEFFICIENTS--COMPLETE RUPTURE												
421/2	0.80	0.08	21.12	0.09	0.56	0.21	0.41	0.29	0.41	0.08	2.54		
62	2.27	0.16	73.84	0.31	0.70	0.72	0.56	0.44	0.58	0.98	3.60		
296	3.42	0.16								1.00			
48	6.32	0.32	87.90	0.27	0.58	0.87	0.57	0.62	0.66	1.99	4.09		
212	10.36	0.48	101.68	0.43	0.67	1.01	0.54	0.69	0.86	3.00	3.47		
44	11.27	0.54	99.29	0.38	0.51	0.89	0.53	0.83	0.74	3.32	4.71		
46	20.67	0.98								6.06			
													L-12

1.0 Lbs TX

W^3 216.00
E 6.0 N 6.0 1950 Surface B C 1.0

Blast No.	Charge Depth ft d_c	Depth Ratio Δ	Complete Rupture $V_r/W^{1/3}$	Volume $K = V_r/W^{1/3}$	Shape $h_s = V_r/(\pi r_r^2 h_r)$	Energy Utilization $A = V_r/V_o$	Complete Rupture Radius $r_r/W^{1/3}$	Complete Rupture Depth $h_r/W^{1/3}$	Complete Rupture Slant Distance $h_c = c_r/W^{1/3}$	Scaled Charge Depth $\lambda_o = d_o/\sqrt[3]{W}$	Scaled Slant Distance $c_r/\sqrt[3]{W}$		
	CRATER COEFFICIENTS--COMPLETE RUPTURE												
8	1.00	0.17								1.00			
7	0.00	0.00	9.10	0.04	0.15	0.10	0.33	0.30	0.33	0.00	1.98		
1	1.00	0.17	50.72	0.23	0.37	0.53	0.61	0.54	0.63	1.00	3.78		
2	2.00	0.33	62.00	0.29	0.55	0.65	0.50	0.67	0.60	2.00	3.60		
2A	2.00	0.33	84.45	0.39	0.73	0.89	0.53	0.61	0.63	2.00	3.78		
3	3.00	0.50	85.63	0.40	0.83	0.90	0.47	0.70	0.68	3.00	4.08		
4	3.95	0.66	92.69	0.43	0.57	0.98	0.51	0.91	0.83	3.95	4.98		
													L-13

W^3 543.34 2.5 Lbs TE

E 6.0 N 8.16 1950 Surface B C 1.0

Blast No.	Charge Depth d_c ft	Depth Ratio Δ	Complete Rupture $V_r^{1/3}$	Volume $K = \frac{V_r^{1/3}}{W^{1/3}}$	Shape $K_s = \frac{V_r^{1/3}}{\pi r_r^2 h_r}$	Energy Utilization $A = \frac{V_r^{1/3}}{V_o}$	Complete Rupture Radius $\Delta_r = \frac{r_r^{1/3}}{W^{1/3}}$	Complete Rupture Depth $\Delta_h = \frac{h_r^{1/3}}{W^{1/3}}$	Complete Rupture Slant Distance $\Delta_c = \frac{c_r^{1/3}}{W^{1/3}}$	Scaled Charge Depth $\lambda_o = d_c/\sqrt[3]{W}$	Scaled Slant Distance $C_r/\sqrt[3]{W}$		
CRATER COEFFICIENTS--COMPLETE RUPTURE													
55	0.00	0.00	18.46	0.06	0.53	0.11	0.41	0.22	0.41	0.00	2.46		
50	1.33	0.14	64.60	0.20	0.51	0.54	0.57	0.56	0.60	0.97	3.60		
51	2.48	0.20	85.44	0.29	0.65	0.72	0.55	0.65	0.63	1.83	3.78		
220	4.00	0.50	118.22	0.54	0.59	0.99	0.61	0.78	0.79	3.00	4.74		
220B	4.00	0.50								3.00			
52	5.13	0.63								3.78			
54	6.33	0.79								4.67			

L-14

W^3 1080.05 5.0 Lbs TE

E 6.0 N 10.26 1950 Surface B C 1.0

Blast No.	Charge Depth d_c ft	Depth Ratio Δ	Complete Rupture $V_r^{1/3}$	Volume $K = \frac{V_r^{1/3}}{W^{1/3}}$	Shape $K_s = \frac{V_r^{1/3}}{\pi r_r^2 h_r}$	Energy Utilization $A = \frac{V_r^{1/3}}{V_o}$	Complete Rupture Radius $\Delta_r = \frac{r_r^{1/3}}{W^{1/3}}$	Complete Rupture Depth $\Delta_h = \frac{h_r^{1/3}}{W^{1/3}}$	Complete Rupture Slant Distance $\Delta_c = \frac{c_r^{1/3}}{W^{1/3}}$	Scaled Charge Depth $\lambda_o = d_c/\sqrt[3]{W}$	Scaled Slant Distance $C_r/\sqrt[3]{W}$		
CRATER COEFFICIENTS--COMPLETE RUPTURE													
294	1.71	0.17	65.04	0.30	0.65		0.54	0.51	0.56	1.00	3.36		
521/2	5.65	0.55								3.30			

L-15

10.0 Lbs TR

W^3 2146.69

E 6.0 W 12.90 1988 Surface B C 1.0

Blast No.	Charge Depth ft d_c	Depth Ratio Δ	Complete Rupture V_r/W	Volume $K = \frac{V_r}{W}$	Shape $K_s = \frac{V_r}{W r_r^2 h_r}$	Energy Utilization $A = \frac{V_r}{V_o}$	Complete Rupture Radius $r_r = \frac{r_r}{W}$	Complete Rupture Depth $h_r = \frac{h_r}{W}$	Complete Rupture Slant Distance $h_c = \frac{c_r}{W}$	Scaled Charge Depth $\lambda_o = d_o/\sqrt[3]{W}$	Scaled Slant Distance $C_r/\sqrt[3]{W}$		
272	1.08	0.08	6.66	0.03	0.40	0.86	0.35	0.20	0.36	0.50	2.16		
282	0.00	0.00	21.25	0.10	0.69	0.28	0.28	0.31	0.28	0.00	2.28		
291	2.15	0.17	66.59	0.31	0.62	0.63	0.55	0.52	0.58	1.00	3.40		
56	2.20	0.17	68.37	0.32	0.70	0.64	0.54	0.50	0.57	1.02	3.42		
57	4.45	0.34	99.10	0.46	0.61	0.92	0.52	0.72	0.71	2.07	4.24		
202	6.46	0.50	104.58	0.49	0.65	0.99	0.56	0.75	0.75	3.00	4.50		
58	8.14	0.62	100.05	0.47	0.58	0.94	0.53	0.89	0.83	3.78	4.98		
60	10.84	0.84	123.50	0.58	0.84	1.16	0.44	1.13	0.95	5.03	5.70		
59	12.54	0.97								5.82			
													L-16

20.0 Lbs TR

W^3 4290.94

E 6.0 W 16.26 1988 Surface B C 1.0

Blast No.	Charge Depth ft d_c	Depth Ratio Δ	Complete Rupture V_r/W	Volume $K = \frac{V_r}{W}$	Shape $K_s = \frac{V_r}{W r_r^2 h_r}$	Energy Utilization $A = \frac{V_r}{V_o}$	Complete Rupture Radius $r_r = \frac{r_r}{W}$	Complete Rupture Depth $h_r = \frac{h_r}{W}$	Complete Rupture Slant Distance $h_c = \frac{c_r}{W}$	Scaled Charge Depth $\lambda_o = d_o/\sqrt[3]{W}$	Scaled Slant Distance $C_r/\sqrt[3]{W}$		
501/2	9.29	0.57											
													L-17

CRATER COEFFICIENTS--COMPLETE RUPTURE

N^3 8440.26 40.0 Lbs TE

E 6.0 R 20.32 1958 Surface B C 1.0

CRATER COEFFICIENTS--COMPLETE RUPTURE

Blast No.	Charge Depth ft d_c	Depth Ratio Δ	Complete Rupture V_r/W	Volume $K = V_r/W^{1/3}$	Shape $\Delta_s = V_r/(\pi r_r^2 h_r)$	Energy Utilization $A = V_r/V_o$	Complete Rupture Radius $\Delta_r = r_r/W^{1/3}$	Complete Rupture Depth $\Delta_h = h_r/W^{1/3}$	Complete Rupture Slant Distance $\Delta_c = C_r/W^{1/3}$	Scaled Charge Depth $\lambda_o = d_o/\sqrt[3]{W}$	Scaled Slant Distance $C_r/\sqrt[3]{W}$		
481/2	0.00	0.00	17.47	0.08	0.64	0.19	0.38	0.28	0.38	0.00	2.28		
297	3.42	0.17								1.00			
48	3.45	0.17	63.76	0.30	0.63	0.69	0.57	0.47	0.59	3.75	3.54		
64	6.95	0.34	79.89	0.37	0.56	0.86	0.60	0.58	0.69	2.02	4.14		
322	10.26	0.50	88.64	0.41	0.65	0.94	0.54	0.70	0.73	3.00	4.38		
65	12.85	0.63	90.15	0.42	0.58	0.98	0.51	0.87	0.81	3.75	4.84		
67	20.65	1.01								6.05			

L-18

N^3 278.45 2.5 Lbs TE

E 4.0 R 6.53 Trench Blasts B C 1.0

CRATER COEFFICIENTS--COMPLETE RUPTURE

Blast No.	Charge Depth ft d_c	Depth Ratio Δ	Complete Rupture V_r/W	Volume $K = V_r/W^{1/3}$	Shape $\Delta_s = V_r/(\pi r_r^2 h_r)$	Energy Utilization $A = V_r/V_o$	Complete Rupture Radius $\Delta_r = r_r/W^{1/3}$	Complete Rupture Depth $\Delta_h = h_r/W^{1/3}$	Complete Rupture Slant Distance $\Delta_c = C_r/W^{1/3}$	Scaled Charge Depth $\lambda_o = d_o/\sqrt[3]{W}$	Scaled Slant Distance $C_r/\sqrt[3]{W}$	
90T	1.50	0.24	57.13	0.51	0.35	0.71	0.84	0.66	0.83	1.16	4.22	
91T	2.48	0.38	53.24	0.47	0.39	0.66	0.71	0.76	0.81	1.82	3.89	
240T	4.07	0.63	72.65	0.64	0.38	0.91	0.76	0.94	0.99	3.00	4.75	

L-19

N^3 1099.10 10.0 Lbs TE

E 4.0 R 10.32 Trench Blasts B C 1.0

CRATER COEFFICIENTS--COMPLETE RUPTURE

Blast No.	Charge Depth ft d_c	Depth Ratio Δ	Complete Rupture V_r/W	Volume $K = V_r/W^{1/3}$	Shape $\Delta_s = V_r/(\pi r_r^2 h_r)$	Energy Utilization $A = V_r/V_o$	Complete Rupture Radius $\Delta_r = r_r/W^{1/3}$	Complete Rupture Depth $\Delta_h = h_r/W^{1/3}$	Complete Rupture Slant Distance $\Delta_c = C_r/W^{1/3}$	Scaled Charge Depth $\lambda_o = d_o/\sqrt[3]{W}$	Scaled Slant Distance $C_r/\sqrt[3]{W}$	
96T	2.24	0.21	45.88	0.41	0.68	0.48	0.58	0.59	0.61	1.04	2.93	
101T	3.39	0.33	62.14	0.57	0.58	0.65	0.70	0.64	0.76	1.53	3.65	
97T	4.34	0.42	51.57	0.47	0.46	0.54	0.65	0.75	0.78	2.01	3.74	
100T	5.44	0.53	86.97	0.80	0.55	0.91	0.73	0.88	0.90	2.52	4.32	
241T	6.46	0.63	83.06	0.76	0.48	0.87	0.73	0.96	0.96	3.00	4.61	

L-20

N^3 979.15 2.5 Lbs A 60

ε 7.3 N 9.93 1958 Surface B ~ 4.0

Blast No.	Charge Depth, ft d_c	Depth Ratio Δ	Extreme Rupture $V_e^{1/3}$	Volume $V_e^{1/3}/N$ A_v =	Shape $V_e/\pi r_e^2 d_e$ A_s =	Energy Utilization V_e/A_e A_u =	Extreme Rupture Radius $r_e^{1/3}/N$ A_r =	Extreme Rupture Depth $d_e^{1/3}/N$ A_d =	Extreme Rupture Slant Distance $c_e^{1/3}/N$ A_c =	Scaled Charge Depth $\lambda_c = d_c/\sqrt[3]{W}$	Scaled Slant Distance $C_e/\sqrt[3]{W}$	Cracking Radius Ft	N-Scaled Cracking Radius
CRATER COEFFICIENTS--EXTREME RUPTURE													
9 1/2	0.00	0.00								0.00			
9	1.36	0.14								1.00			
10	2.00	0.20								2.06		6.67	0.67
200	4.08	0.41								3.00		7.00	0.70
11	5.30	0.53								3.95		6.50	0.65
12	6.76	0.68	261.28	0.67	0.60		0.60	0.98	0.91	4.97	6.64	6.80	0.68
13	8.11	0.82	221.99	0.59	0.71		0.49	1.10	0.95	5.96	6.94	6.80	0.68
14	9.61	0.99	258.86	0.92	0.82		0.54	1.24	1.11	7.06	8.10	8.95	0.60
													M-1

N^3 1943.76 5.0 Lbs A 60

ε 7.3 N 12.48 1958 Surface B C 1.0

Blast No.	Charge Depth, ft d_c	Depth Ratio Δ	Extreme Rupture $V_e^{1/3}$	Volume $V_e^{1/3}/N$ A_v =	Shape $V_e/\pi r_e^2 d_e$ A_s =	Energy Utilization V_e/A_e A_u =	Extreme Rupture Radius $r_e^{1/3}/N$ A_r =	Extreme Rupture Depth $d_e^{1/3}/N$ A_d =	Extreme Rupture Slant Distance $c_e^{1/3}/N$ A_c =	Scaled Charge Depth $\lambda_c = d_c/\sqrt[3]{W}$	Scaled Slant Distance $C_e/\sqrt[3]{W}$	Cracking Radius Ft	N-Scaled Cracking Radius
CRATER COEFFICIENTS--EXTREME RUPTURE													
295	1.71	0.14								1.0		6.42	0.51
12 1/2	7.17	0.57	311.80	0.80	0.66		0.66	0.39	0.88	4.18	6.67	7.90	0.63
14 1/2	12.34	0.99								7.23			
													M-2

N^3 3809.89 10.0 Lbs A60

E 7.3 N 15.70 1958 Surface B C 1.0

CRATER COEFFICIENTS--EXTREME RUPTURE

Blast No.	Charge Depth, ft d_e	Depth Ratio Δ	Extreme Rupture $\frac{V_c}{W}$	Volume $\frac{V_e}{W}$ λ_e =	Shape $\frac{V_e}{\pi r_e^2 h_e}$ λ_s =	Energy Utilization $\frac{V_e}{E_o}$ λ_u =	Extreme Rupture Radius $\frac{r_e}{W}$ λ_r =	Extreme Rupture Depth $\frac{h_e}{W}$ λ_h =	Extreme Rupture Slant Distance $\frac{c_e}{W}$ λ_c =	Scaled Charge Depth $\lambda_c = d_e/\sqrt[3]{W}$	Scaled Slant Distance $C_o/\sqrt[3]{W}$	Cracking Radius Ft	N-Scaled Cracking Radius
271	1.08	0.07	22.79	0.06	0.37		0.42	0.29	0.43	0.50	2.58		
281	0.00	0.00	70.72	0.18	0.55		0.55	0.35	0.55	0.00	4.09		
292	2.15	0.14								1.00			
15	2.20	0.14								1.02			
15R	2.20	0.14	150.90	0.39	0.74		0.54	0.57	0.56	1.06	4.90		
16	4.30	0.27								2.00			
16R	4.40	0.28	216.78	0.56	0.77		0.64	0.57	0.69	2.05	5.15		
201	6.46	0.41								3.00		8.55	0.56
17	8.10	0.52								3.77		9.65	0.61
18	10.80	0.69	269.85	0.70	0.70		0.56	1.01	0.89	5.01	6.10	10.27	0.65
18 1/2	12.90	0.82	378.60	0.98	0.76		0.62	1.06	1.03	6.00	7.52	9.75	0.62
19	15.10	0.96	271.48	0.70				1.18	0.72	7.02	5.25		
20	22.60	1.44						1.68	0.74	10.50	5.41		

N-3

N^3 7738.89 20.0 Lbs A60

E 7.3 N 19.78 1958 Surface B C 1.0

CRATER COEFFICIENTS--EXTREME RUPTURE

Blast No.	Charge Depth, ft d_e	Depth Ratio Δ	Extreme Rupture $\frac{V_c}{W}$	Volume $\frac{V_e}{W}$ λ_e =	Shape $\frac{V_e}{\pi r_e^2 h_e}$ λ_s =	Energy Utilization $\frac{V_e}{E_o}$ λ_u =	Extreme Rupture Radius $\frac{r_e}{W}$ λ_r =	Extreme Rupture Depth $\frac{h_e}{W}$ λ_h =	Extreme Rupture Slant Distance $\frac{c_e}{W}$ λ_c =	Scaled Charge Depth $\lambda_c = d_e/\sqrt[3]{W}$	Scaled Slant Distance $C_o/\sqrt[3]{W}$	Cracking Radius Ft	N-Scaled Cracking Radius
17 1/2	11.58	0.59								4.26			
19 1/2	19.48	0.98								7.16			

M-4

40.0 Lbs AAO

N^3 15,560.02

N 24.97

1958 Surface

E 7.3 B C 1.0

Shot No.	Charge Depth, ft d_e	Depth Ratio Δ	Extreme Rupture $V_e^{1/3}$	Volume $V_e^{1/3}/W$ K_v =	Shape $V_e/\pi r_e^2 h_e$ K_s =	Energy Utilization V_e/V_c A_e =	Extreme Rupture Radius r_e/W K_r =	Extreme Rupture Depth h_e/W K_h =	Extreme Rupture Slant Distance s_e/W K_s =	Scaled Charge Depth $d_e/W^{1/3}$ λ_e =	Scaled Slant Distance $s_e/W^{1/3}$	Cracking Radius Ft	N-Scaled Cracking Radius
CRATER COEFFICIENTS--EXTREME RUPTURE													
21 1/2	0.00	0.00	44.16	0.11	0.79		0.42	0.25	0.42	0.00	2.27		
21	2.22	0.14								0.97			
22B	2.42	0.14								1.00			
22	4.80	0.27								1.99		12.45	0.54
22C	10.26	0.41	172.81	0.44	0.69		0.50	0.70	0.71	2.00	5.41		
23	12.47	0.50								2.67		13.50	0.54
26	20.57	0.82	210.02	0.54	0.60		0.51	1.08	0.97	4.02	7.02		
29	24.07	0.96	245.98	0.68				1.21	0.98	7.04	7.12	15.10	0.60
													M-5

2.5 Lbs AAO

N^3 599.08

N 8.43

Trench Blasts

E 6.2 B C 1.0

Shot No.	Charge Depth, ft d_e	Depth Ratio Δ	Extreme Rupture $V_e^{1/3}$	Volume $V_e^{1/3}/W$ K_v =	Shape $V_e/\pi r_e^2 h_e$ K_s =	Energy Utilization V_e/V_c A_e =	Extreme Rupture Radius r_e/W K_r =	Extreme Rupture Depth h_e/W K_h =	Extreme Rupture Slant Distance s_e/W K_s =	Scaled Charge Depth $d_e/W^{1/3}$ λ_e =	Scaled Slant Distance $s_e/W^{1/3}$	Cracking Radius Ft	N-Scaled Cracking Radius
CRATER COEFFICIENTS--EXTREME RUPTURE													
70T	1.26	0.17								1.00		5.40	0.64
71T	2.46	0.32								1.95		4.95	0.59
2B0T	4.07	0.48	157.24	0.65	0.70		0.67	0.66	0.83	3.00	5.20	4.80	0.57
72T	5.38	0.64								3.95			
73T	6.84	0.81	248.59	1.03	0.62		0.71	1.06		5.05		8.40	1.00
74T	8.11	0.97	342.29	1.42	0.78		0.66	1.33	1.17	6.97	5.[illegible]	7.15	0.85
75T	9.51	1.13	135.75	0.57				1.40	0.74	7.00	4.58	5.70	0.68
													M-6

$W^{1/3}$ 2968.89 10.8 lbs AN

A 6.2 R 13.33 Trench Blasts B C 1.0

Shot No.	Charge Depth, ft d_o	Depth Ratio Δ	Extreme Rupture $V_e^{1/3}$	Volume $V_e^{1/3}/W = \Lambda_o$	Shape $\Lambda_s = \frac{V_e}{W r_o h_o}$	Energy Utilization $A_o = \frac{V_e}{V_o}$	Extreme Rupture Radius $r_e/W^{1/3} = \Lambda_r$	Extreme Rupture Depth $h_e/W^{1/3} = \Lambda_h$	Extreme Rupture Slant Distance $s_e/W^{1/3} = \Lambda_s$	Scaled Charge Depth $\lambda_o = d_o/W^{1/3}$	Scaled Slant Distance $s_o/W^{1/3}$	Cracking Radius Ft	N-Scaled Cracking Radius
CRATER COEFFICIENTS--EXTREME RUPTURE													
76T	2.20	0.17	107.52	0.46	0.66		0.65	0.52	0.67	1.02	4.22		
82T	3.20	0.24	251.72	1.06	0.84		0.81	0.61	0.85	1.49	5.95	6.50	0.49
77T	4.30	0.32								2.00		7.22	0.54
81T	5.60	0.40	280.78	1.06	0.68		0.84	0.71	0.93	2.50	4.65	8.00	0.60
231T	6.44	0.48	286.13	1.08	0.67		0.83	0.77	0.94	3.00	5.33		
78T	8.60	0.65	338.17	1.42	0.50		0.94	0.89	1.14	4.00	7.24	10.42	0.78
79T	10.75	0.80	419.70	1.76	0.62		0.90	1.13	1.20	4.99	7.50	9.70	0.73
80T	12.95	0.97	505.57	2.14	0.72		0.87	1.24	1.31	6.00	8.30	15.0	1.12

M-7

$W^{1/3}$ 599.00 2.2 Lbs C4

A 6.2 R 8.43 1950 Surface B C 1.0

Shot No.	Charge Depth, ft d_o	Depth Ratio Δ	Extreme Rupture $V_e^{1/3}$	Volume $V_e^{1/3}/W = \Lambda_o$	Shape $\Lambda_s = \frac{V_e}{W r_o h_o}$	Energy Utilization $A_o = \frac{V_e}{V_o}$	Extreme Rupture Radius $r_e/W^{1/3} = \Lambda_r$	Extreme Rupture Depth $h_e/W^{1/3} = \Lambda_h$	Extreme Rupture Slant Distance $s_e/W^{1/3} = \Lambda_s$	Scaled Charge Depth $\lambda_o = d_o/W^{1/3}$	Scaled Slant Distance $s_o/W^{1/3}$	Cracking Radius Ft	N-Scaled Cracking Radius
CRATER COEFFICIENTS--EXTREME RUPTURE													
20 1/2	0.80	0.09	80.47	0.34	0.50		0.71	0.37	0.71	0.00	4.35		
20	1.20	0.15								0.96			
21	2.70	0.33								2.03		4.90	0.50
22	4.00	0.47								2.94			
210	4.00	0.48								2.00			
23	5.20	0.63								3.90		5.35	0.63
24	6.00	0.71								4.42			
25	8.00	0.95	165.09	0.69	0.79		0.48	1.23	1.66	5.87	6.57	5.60	0.66

M-8

8.0 Lbs C4

N^3 1191.02
N 10.60

L 0.4 — 1950 Surface — B — C 1.0

CRATER COEFFICIENTS--E TWENE RUPTURE

Blast No.	Charge Depth, ft d_e	Depth Ratio Δ	Extreme Rupture V_e/N	Volume $V_e/N = A_e$	Shape $\frac{V_e}{\pi r_e^2 h_e} = A_s$	Energy Utilization $V_e/V_o = A_e$	Extreme Rupture Radius $r_e/N = A_r$	Extreme Rupture Depth $h_e/N = A_h$	Extreme Rupture Slant Distance $c_e/N = A_c$	Scaled Charge Depth $\lambda_c = d_c/\sqrt[3]{W}$	Scaled Slant Distance $C_o/\sqrt[3]{W}$	Cracking Radius Ft	N-Scaled Cracking Radius
293	1.71	0.16								1.00			
34 1/2	6.22	0.59	211.41	0.89	0.57		0.72	0.95	0.93	3.64	5.85	7.35	0.69
35 1/2	10.14	0.96								5.94			

M-9

10.0 Lbs C4

N^3 2360.59
N 13.35

E 6.2 — 1950 Surface — B — C 1.0

CRATER COEFFICIENTS--E TWENE RUPTURE

Blast No.	Charge Depth, ft d_e	Depth Ratio Δ	Extreme Rupture V_e/N	Volume $V_e/N = A_e$	Shape $\frac{V_e}{\pi r_e^2 h_e} = A_s$	Energy Utilization $V_e/V_o = A_e$	Extreme Rupture Radius $r_e/N = A_r$	Extreme Rupture Depth $h_e/N = A_h$	Extreme Rupture Slant Distance $c_e/N = A_c$	Scaled Charge Depth $\lambda_c = d_c/\sqrt[3]{W}$	Scaled Slant Distance $C_o/\sqrt[3]{W}$	Cracking Radius Ft	N-Scaled Cracking Radius
260	2.15	0.16								1.00			
270	1.00	0.00	53.91	0.22	0.52		0.70	0.29	0.70	0.50	4.46		
270B	1.00	0.00								0.50			
280	0.00	0.00								0.00			
290	2.15	0.16	110.15	0.50	0.71		0.64	0.55	0.66	1.00	4.09		
36	2.16	0.16	110.12	0.44	0.75		0.65	0.47	0.67	1.00	4.36	6.60	0.68
37	4.40	0.32	124.35	0.53	0.56		0.66	0.50	0.74	2.06	4.60	0.22	0.62
211	6.66	0.48	156.68	0.66	0.69		0.64	0.74	0.80	3.00	5.01	7.10	0.53
38	8.21	0.62	127.81	0.54	0.74		0.69	0.95	0.80	3.86	4.87	7.65	0.57
39	10.70	0.80	293.74	1.24	0.92		0.60	1.17	1.00	4.97	4.27	8.40	0.63
40	12.79	0.95	102.65	0.77	0.81		0.50	1.22	1.00	5.90	4.59	8.30	0.62

M-10

80.0 Lbs C4

W^3 4741.63

E 6.2 N 16.00 1950 Surface B C 1.0

CRATER COEFFICIENTS--EXTREME RUPTURE

Blast No.	Charge Depth, ft d_e	Depth Ratio Δ	Extreme Rupture $V_e^{1/3}$	Volume $V_e^{1/3}/W = \lambda_e$	Shape $V_e/\pi r_e^2 h_e = \lambda_s$	Energy Utilization $A_e = V_e/V_o$	Extreme Rupture Radius $r_e^{1/3}/W = \lambda_r$	Extreme Rupture Depth $h_e^{1/3}/W = \lambda_h$	Extreme Rupture Slant Distance $c_e^{1/3}/W = \lambda_c$	Scaled Charge Depth $\lambda_o = d_e/\sqrt[3]{W}$	Scaled Slant Distance $C_o/\sqrt[3]{W}$	Cracking Radius Ft	N-Scaled Cracking Radius
20 1/2	9.68	0.56								3.49			
40 1/2	16.27	0.97	289.26	0.80	0.09		0.52	1.16	1.10	6.01	6.52	11.60	0.60
													M-11

80.0 Lbs C4

W^3 9520.13

E 6.2 N 21.20 1950 Surface B C 1.0

CRATER COEFFICIENTS--EXTREME RUPTURE

Blast No.	Charge Depth, ft d_e	Depth Ratio Δ	Extreme Rupture $V_e^{1/3}$	Volume $V_e^{1/3}/W = \lambda_e$	Shape $V_e/\pi r_e^2 h_e = \lambda_s$	Energy Utilization $A_e = V_e/V_o$	Extreme Rupture Radius $r_e^{1/3}/W = \lambda_r$	Extreme Rupture Depth $h_e^{1/3}/W = \lambda_h$	Extreme Rupture Slant Distance $c_e^{1/3}/W = \lambda_c$	Scaled Charge Depth $\lambda_o = d_e/\sqrt[3]{W}$	Scaled Slant Distance $C_o/\sqrt[3]{W}$	Cracking Radius Ft	N-Scaled Cracking Radius
42 1/2	0.00	0.00	32.21	0.14	0.53		0.49	0.34	0.49	0.00	2.04		
42	2.37	0.16								0.98			
296	2.42	0.16								1.00			
43	6.82	0.32	153.42	0.64	0.78		0.63	0.67	0.71	1.99	4.44	13.05	0.62
212	10.26	0.48	187.61	0.79	1.50		0.66	0.38	0.82	3.00	4.65	11.90	0.56
44	11.27	0.54								3.32		13.10	0.62
46	20.67	0.98	277.96	1.17	0.76		0.63	1.22	1.16	6.05	6.05	13.05	0.62
													M-12

18.0 Lbs RX

W^3 216.00

E 6.0 N 6.0 1950 Surface B C 1.0

CRATER COEFFICIENTS--EXTREME RUPTURE

Blast No.	Charge Depth, ft d_e	Depth Ratio Δ	Extreme Rupture $V_e^{1/3}$	Volume $V_e^{1/3}/W = \lambda_e$	Shape $V_e/\pi r_e^2 h_e = \lambda_s$	Energy Utilization $A_e = V_e/V_o$	Extreme Rupture Radius $r_e^{1/3}/W = \lambda_r$	Extreme Rupture Depth $h_e^{1/3}/W = \lambda_h$	Extreme Rupture Slant Distance $c_e^{1/3}/W = \lambda_c$	Scaled Charge Depth $\lambda_o = d_e/\sqrt[3]{W}$	Scaled Slant Distance $C_o/\sqrt[3]{W}$	Cracking Radius Ft	N-Scaled Cracking Radius
8	1.00	0.17								1.00			
7	0.00	0.00								0.00			
1	1.00	0.17								1.00			
2	2.00	0.33								2.00		1.30	0.22
2A	2.00	0.33								2.00			
3	3.00	0.50								3.00			
4	3.95	0.66								3.95			
5	4.85	0.81	52.45	0.24				1.04	0.69	4.85	4.15	3.15	0.52
6	6.00	1.00	74.45	0.34				1.21	0.78	6.00	4.70	4.40	0.73
													M-13

2.5 Lbs TR

W^3 543.34

W 8.16

E 6.0 1988 Surface B C 1.0

Shot No.	Charge Depth, ft d_e	Depth Ratio Δ	Extreme Rupture V_r^e/W	Volume V_e^e/W $\lambda_e =$	Shape $\lambda_s = \frac{V_e^e}{\pi r_e^2 h_e}$	Energy Utilization $\lambda_u = \frac{V_e^e}{V_o^e}$	Extreme Rupture Radius r_r^e/W $\lambda_r =$	Extreme Rupture Depth h_h^e/W $\lambda_h =$	Extreme Rupture Slant Distance c_c^e/W $\lambda_c =$	Scaled Charge Depth $\lambda_c = d_e/\sqrt[3]{W}$	Scaled Slant Distance $C_c/\sqrt[3]{W}$	Cracking Radius Ft	N-Scaled Cracking Radius
CRATER COEFFICIENTS--EXTREME RUPTURE													
55	0.00	0.00								0.00			
50	1.33	0.16								0.97			
51	2.48	0.30								1.83			
330	4.08	0.50								3.00		6.10	0.75
330B	4.08	0.50								3.00			
52	5.13	0.63								3.78			
54	6.33	0.78								4.67		4.05	0.50
548	7.38	0.90	49.34	0.22				1.17	0.72	5.44	4.26	5.00	0.61
													M-14

5.0 Lbs TR

W^3 1000.05

W 10.26

E 6.0 1988 Surface B C1.0

Shot No.	Charge Depth, ft d_e	Depth Ratio Δ	Extreme Rupture V_r^e/W	Volume V_e^e/W $\lambda_e =$	Shape $\lambda_s = \frac{V_e^e}{\pi r_e^2 h_e}$	Energy Utilization $\lambda_u = \frac{V_e^e}{V_o^e}$	Extreme Rupture Radius r_r^e/W $\lambda_r =$	Extreme Rupture Depth h_h^e/W $\lambda_h =$	Extreme Rupture Slant Distance c_c^e/W $\lambda_c =$	Scaled Charge Depth $\lambda_c = d_e/\sqrt[3]{W}$	Scaled Slant Distance $C_c/\sqrt[3]{W}$	Cracking Radius Ft	N-Scaled Cracking Radius
CRATER COEFFICIENTS--EXTREME RUPTURE													
294	1.71	0.17								1.00		6.30	0.61
521/2	5.45	0.55								3.30			
541/2	9.47	0.92	277.62	1.29	1.00		0.57	1.25	1.09	5.54	6.49	6.10	0.59
													M-15

N^3 2166.69 — 10.0 Lbs TN

L 6.0 — N 12.90 — 1920 Surface — B — C 1.0

CRATER COEFFICIENTS--EXTREME RUPTURE

Blast No.	Charge Depth, ft d_o	Depth Ratio Δ	Extreme Rupture $\lambda_e = \frac{\lambda_e}{W^{1/3}}$	Volume $\lambda_v = \frac{V}{W}$	Shape $\lambda_s = \frac{V}{\pi r_e^2 d_e}$	Energy Utilization $\lambda_u = \frac{V}{d_e}$	Extreme Rupture Radius $\lambda_r = \frac{r_e}{W^{1/3}}$	Extreme Rupture Depth $\lambda_h = \frac{h_e}{W^{1/3}}$	Extreme Rupture Slant Distance $\lambda_c = \frac{c_e}{W^{1/3}}$	Scaled Charge Depth $\lambda_o = \frac{d_o}{W^{1/3}}$	Scaled Slant Distance $C_o = \frac{c_o}{W^{1/3}}$	Cracking Radius Ft	N-Scaled Cracking Radius
272	1.00	0.00	22.42	0.10	0.60		0.49	0.23	0.50	0.50	2.78		
202	0.00	0.00								0.00			
291	2.15	0.17								1.00			
86	3.20	0.17								1.02		7.25	0.86
87	4.45	0.34								2.07			
202	6.46												
88	8.14	0.62								3.78		6.99	0.83
60	10.84	0.84								5.02			
89	12.54	0.97	219.79	1.02	0.79		0.50	1.23	1.12	5.84	6.73	7.00	0.60

M-16

20.0 Lbs TN

N^3 4290.94
N 16.26 — 1920 Surface — B — C 1.0

CRATER COEFFICIENTS--EXTREME RUPTURE

Blast No.	Charge Depth, ft d_o	Depth Ratio Δ	Extreme Rupture $\lambda_e = \frac{\lambda_e}{W^{1/3}}$	Volume $\lambda_v = \frac{V}{W}$	Shape $\lambda_s = \frac{V}{\pi r_e^2 d_e}$	Energy Utilization $\lambda_u = \frac{V}{d_e}$	Extreme Rupture Radius $\lambda_r = \frac{r_e}{W^{1/3}}$	Extreme Rupture Depth $\lambda_h = \frac{h_e}{W^{1/3}}$	Extreme Rupture Slant Distance $\lambda_c = \frac{c_e}{W^{1/3}}$	Scaled Charge Depth $\lambda_o = \frac{d_o}{W^{1/3}}$	Scaled Slant Distance $C_o = \frac{c_o}{W^{1/3}}$	Cracking Radius Ft	N-Scaled Cracking Radius
50 1/2	9.33	0.57								2.43			
59 1/2	21.23	1.31	186.20	0.49				1.60	0.62	7.85	3.76		

M-17

40.0 Lbs TN

N^3 8640.26
N 20.52 — 1920 Surface — B — C 1.0

CRATER COEFFICIENTS--EXTREME RUPTURE

Blast No.	Charge Depth, ft d_o	Depth Ratio Δ	Extreme Rupture $\lambda_e = \frac{\lambda_e}{W^{1/3}}$	Volume $\lambda_v = \frac{V}{W}$	Shape $\lambda_s = \frac{V}{\pi r_e^2 d_e}$	Energy Utilization $\lambda_u = \frac{V}{d_e}$	Extreme Rupture Radius $\lambda_r = \frac{r_e}{W^{1/3}}$	Extreme Rupture Depth $\lambda_h = \frac{h_e}{W^{1/3}}$	Extreme Rupture Slant Distance $\lambda_c = \frac{c_e}{W^{1/3}}$	Scaled Charge Depth $\lambda_o = \frac{d_o}{W^{1/3}}$	Scaled Slant Distance $C_o = \frac{c_o}{W^{1/3}}$	Cracking Radius Ft	N-Scaled Cracking Radius
63 1/2	0.00	0.00	37.19	0.17	0.71		0.51	0.29	0.51	0.00	3.19		
297	3.42	0.17								1.00			
63	3.45	0.17								1.01			
64	6.95	0.34	146.37	0.68	0.69		0.69	0.67	0.77	2.03	4.59	13.95	0.68
232	10.26	0.50	141.85	0.66	0.66		0.58	0.70	0.85	3.00	4.59	11.15	0.54
65	12.85	0.63	153.57	0.71	0.62		0.64	0.88	0.90	3.75	5.15	12.47	0.61
67	20.65	1.01	228.36	1.06	1.25		0.46	1.25	1.11	6.05	5.99	14.10	0.69

M-18

2.5 Lbs 7%

N^3 278.48

N 6.53

S 4.8 Trench Blasts B C 1.0

Blast No.	Charge Depth, ft d_c	Depth Ratio Δ	Extreme Rupture $V_r^{1/3}$	Volume $V_r^{1/3}/N$ λ_v =	Shape $V_r/\pi r_o^2 h_o$ λ_s =	Energy Utilization V_r/V_o A_p =	Extreme Rupture Radius $r_r^{1/3}/N$ λ_r =	Extreme Rupture Depth $h_r^{1/3}/N$ λ_h =	Extreme Rupture Slant Distance $c_r^{1/3}/N$ λ_c =	Scaled Charge Depth $\lambda_d = d_c/\sqrt[3]{N}$	Scaled Slant Distance $c_o/\sqrt[3]{N}$	Cracking Radius Ft	N-Scaled Cracking Radius
	CRATER COEFFICIENTS--EXTREME RUPTURE												
90T	1.50	0.24								1.16		3.75	0.57
91T	2.48	0.38								1.82		5.20	0.80
240T	4.07	0.63	200.06	2.69	0.65		1.18	0.96	1.36	3.00	6.11	6.18	0.63
98T	5.20	0.80	200.50	1.79	0.62		0.88	1.21	1.20	3.95	6.04	6.80	1.04
95T	6.78	1.04	279.81	2.59	0.80		0.85	1.38	1.34	4.97	5.40	1.10	0.17
94T	8.18	1.25	314.73	1.93				1.63	1.01	6.02	4.86		
													M-19

10.0 Lbs 7%

N^3 1099.10

N 10.32

S 4.8 Trench Blasts B C 1.0

Blast No.	Charge Depth, ft d_c	Depth Ratio Δ	Extreme Rupture $V_r^{1/3}$	Volume $V_r^{1/3}/N$ λ_v =	Shape $V_r/\pi r_o^2 h_o$ λ_s =	Energy Utilization V_r/V_o A_p =	Extreme Rupture Radius $r_r^{1/3}/N$ λ_r =	Extreme Rupture Depth $h_r^{1/3}/N$ λ_h =	Extreme Rupture Slant Distance $c_r^{1/3}/N$ λ_c =	Scaled Charge Depth $\lambda_d = d_c/\sqrt[3]{N}$	Scaled Slant Distance $c_o/\sqrt[3]{N}$	Cracking Radius Ft	N-Scaled Cracking Radius
	CRATER COEFFICIENTS--EXTREME RUPTURE												
96T	2.24	0.21	86.80	0.78	0.80		0.70	0.64	0.74	1.04	3.64		
101T	2.29	0.22	249.95	2.26	0.78		1.08	0.80	1.13	1.53	5.76		
97T	4.34	0.42	114.36	1.03	0.55		0.88	0.80	0.96	2.01	4.46	6.45	0.62
100T	5.44	0.53	270.59	2.46	1.00		0.94	0.89	1.06	2.52	5.29	6.05	0.59
241T	6.46	0.62	180.00	1.64	0.73		0.85	1.00	1.05	3.00	5.04		
99T	8.64	0.84	212.09	1.93	0.48		1.05	1.16	1.34	4.01	6.59	9.87	0.96
93T	9.74	0.95	361.00	3.28	1.01		0.90	1.29	1.30	4.52	6.64	9.50	0.92
													M-20

Unclassified
Security Classification

DOCUMENT CONTROL DATA - R & D

(Security classification of title, body of abstract and indexing annotation must be entered when the overall report is classified)

1. ORIGINATING ACTIVITY (Corporate author) U.S. Army Cold Regions Research and Engineering Laboratory, Hanover, N.H.	2a. REPORT SECURITY CLASSIFICATION Unclassified 2b. GROUP

3. REPORT TITLE

EXPLOSIONS IN SNOW

4. DESCRIPTIVE NOTES (Type of report and inclusive dates)

Technical Report

5. AUTHOR(S) (First name, middle initial, last name)

Clifton W. Livingston

6. REPORT DATE May 1968	7a. TOTAL NO. OF PAGES 131	7b. NO. OF REFS 9
8a. CONTRACT OR GRANT NO. DA-11-190-ENG-33 b. PROJECT NO. c. d.	9a. ORIGINATOR'S REPORT NUMBER(S) Technical Report 85 9b. OTHER REPORT NO(S) (Any other numbers that may be assigned this report)	

10. DISTRIBUTION STATEMENT

This document has been approved for public release and sale; its distribution is unlimited.

11. SUPPLEMENTARY NOTES	12. SPONSORING MILITARY ACTIVITY U.S. Army Snow, Ice and Permafrost Research Establishment (now U.S. Army Cold Regions Research and Engineering Laboratory)

13. ABSTRACT

Studies were made to establish means of predicting and optimizing the results of blasts in snow of the Greenland Ice Cap. A total of 141 test blasts were fired above and below the snow surface using three types of explosives. Seismic measurements were made of all shots, and 32 were instrumented for measurement of air-blast and/or undersnow shock pressure. Crater cross sections were then mapped to beyond the limits of complete rupture. All crater data are presented in an Appendix. The change in texture of the snow was studied. Density samples of the disturbed and undisturbed snow were taken.

The failure process in snow differs from that in glacier ice, frozen ground, rock, and certain types of soil. Characteristic features of this failure (referred to here as "viscous-damping failure") are: 1) damping of the disturbance during the rise to peak pressure, and 2) substantial recovery of stored potential energy during unloading. Both features result because air is trapped within the voids in snow. The snow is first compacted and driven outward as the gas bubble expands, and a primary cavity is formed. Melting at the cavity wall converts the skin of the compacted, fractured, and expanding zone to ice. The next event is implosion and disturbance of the original cavity. The walls of the primary cavity are displaced inward, and both the zone of skin-surface melting and the zone of compaction are destroyed. A sensitively balanced transition condition appears to exist at critical depth. The balance determines under what conditions fractures during the rise of pressure and the outward expansion of the gas bubble predominate over fractures formed as a result

(Cont'd)

DD FORM 1 NOV 65 1473 REPLACES DD FORM 1473, 1 JAN 64, WHICH IS OBSOLETE FOR ARMY USE.

Unclassified
Security Classification

Unclassified

Security Classification

14 KEY WORDS	LINK A ROLE	LINK A WT	LINK B ROLE	LINK B WT	LINK C ROLE	LINK C WT
Greenland-ice cap Snow-failure						

Abstract (Cont'd)

of implosion. Implosion is closely followed by a vortex motion within the snow and scouring action as the gas bubble emerges from the rising column defined by the vortex. This scouring motion largely determines the final shape of the apparent crater.

Viscous-damping failure differs markedly from shock-type failure, which is characteristic of brittle materials, and from shear-type failure, which is characteristic of more plastic materials. During loading of the snow, a substantial proportion of the energy of the explosion is expended to compact and deform the material; during unloading, much of the energy expended to compress air in the void is recovered and re-expended in both fracture and flow.

Tables, curves, equations, and example problems presented in the report make it possible, within the range of the experiments, to accurately predict any desired dimensions of the limit of complete rupture. Limits of complete rupture and limits of extreme rupture in snow are correlated empirically using cube-root scaling as a first approximation. Ranges of similar behavior and transition limits between ranges for blasts with small HE charges in 1958 surface snow are discussed.

Unclassified

Security Classification